

macro-and
micro-**mechanics** of
cemented total
hip **arthroplasty**

dennis janssen

Copyright

©2009 Dennis Janssen

All rights reserved.

No part of this book may be reproduced in any form without written permission of the author.

ISBN

978-90-9023405-2

NUR

954 Biomedische technologie

Printing

PrintPartners Ipskamp BV, Enschede, The Netherlands.

Design

Dennis Janssen

Sponsors

Nederlandse Orthopaedische Vereniging

Biomet Nederland BV

Link Nederland BV

RMS Foundation, Bettlach, Switzerland

Stichting Anna Fonds

B.Braun Medical

Heraeus Medical

Johnson & Johnson Medical BV

Prothese- en Orthese-Makerij Nijmegen POM BV

Stryker Nederland BV

aap bio implants Netherlands BV

Macro- and micro- mechanics of cemented total hip arthroplasty

**Een wetenschappelijke proeve op het gebied
van de Medische Wetenschappen**

Proefschrift

Ter verkrijging van de graad van doctor
aan de Radboud Universiteit Nijmegen
op gezag van de rector magnificus prof. mr. S.C.J.J. Kortmann,
volgens besluit van het College van Decanen
in het openbaar te verdedigen op dinsdag 14 april 2009
om 15.30 uur precies

Door

Dennis Wilhelm Janssen
geboren op 7 april 1977
te 's-Hertogenbosch

Promotor

Prof. dr. ir. N. Verdonschot (Universiteit Twente)

Copromotores

Dr. ir. J. Stolk (DSM Research)

K.A. Mann, PhD (SUNY Upstate Medical University)

Manuscriptcommissie

Prof. dr. C. Gielen

Prof. dr. S. Bergé

Prof. dr. R.G.T. Geesink (Academisch Ziekenhuis Maastricht)

Dr. ir. T. Meinders (Universiteit Twente)

Prof. dr. ir. D.F. Stegeman

Contents

Chapter 1	Introduction	9
Chapter 2	Finite element analysis of failure of the Capital Hip designs	25
Chapter 3	Finite element analysis of the effect of cementing concepts on implant stability and cement fatigue failure	37
Chapter 4	Why would cement porosity reduction be clinically irrelevant, while experimental data show the contrary?	49
Chapter 5	The contradictory effects of pores on fatigue cracking of bone cement	63
Chapter 6	Experimental micro-mechanics of the cement-bone interface	75
Chapter 7	Finite element simulation of cement-bone interface micro-mechanics; a comparison to experimental results	91
Chapter 8	Micro-mechanical modeling of the cement-bone interface: the effect of friction, morphology and material properties	107
Chapter 9	Summary and general discussion	121
Chapter 10	Samenvatting en algemene discussie	129
Chapter 11	Computational modeling of total hip arthroplasty: past, present and future	137
Acknowledgements		149
About the author		153

mac

micro-mech

Chapter 1

Introduction

Total hip arthroplasty (THA) is one of the most successful surgical interventions in orthopaedics. The procedure offers immediate pain relief, and restores hip function. Hence, the operation substantially improves the quality of life, and allows patients to resume activities of daily living and even sports. THA is also very successful in terms of clinical success rates, with implant survival rates between 90 and 95% at ten years post-operatively.^{18,48,59} Due to this success, THA has become a very popular procedure. In the United States alone, approximately 234,000 operations were performed in 2004.⁵⁵ Worldwide, more than a million procedures are performed annually, and the number of operations is increasing every year.

In THA, a diseased hip joint is replaced by a stem that is implanted in the femur and a cup that is implanted in the acetabulum (Figure 1). The femoral stem is provided with a metal or ceramic head that articulates against the cup, forming the new artificial joint. The stem is usually made of forged metal (stainless steel, cobalt-chrome, titanium), while the cup is most often made of polyethylene (PE) with or without metal backing, although other materials such as ceramics or metal are also being used for the bearing surface. During the operation, the femoral head is resected and the intramedullary canal is reamed, after which the stem is inserted. On the acetabular side the cartilage is removed, after which the cup is placed. Hip implants can be fixated in the bone with acrylic bone cement or without cement, in which case the long-term implant stability relies on on- and ingrowth of bone. This thesis focuses on cemented THA only.

Acrylic bone cement is prepared in the operating theatre by mixing polymethylmethacrylate powder (PMMA) with monomethylmethacrylate (MMA) fluid. By mixing these two components, a viscous mixture

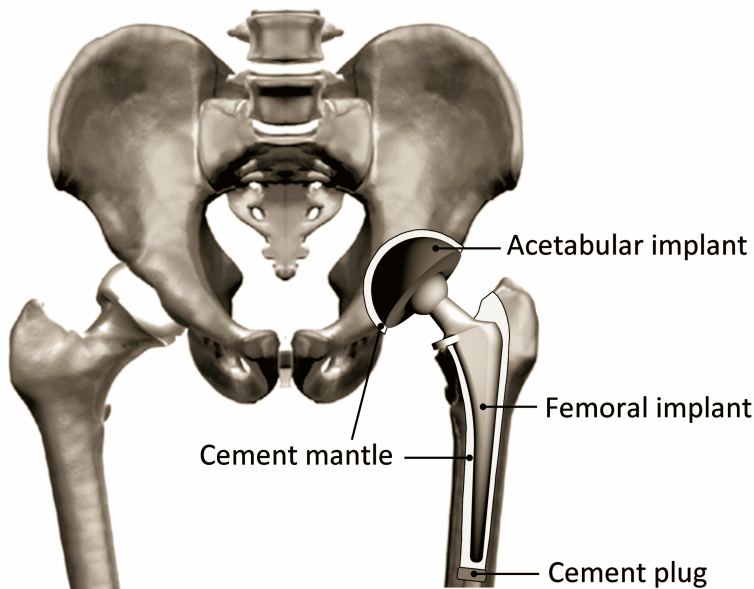


Figure 1: Healthy human hip joint (left) and a hip joint with a cemented total hip arthroplasty (THA, right).

is formed that further polymerizes until it becomes solid after a few minutes. The bone cement is injected in the femoral or acetabular cavity, after which the implant is inserted and held in place until the cement has solidified. This technique was developed in 1960 by sir John Charnley.⁷

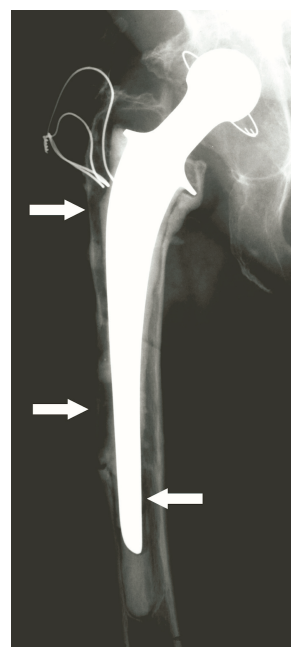
Although THA is a very successful operation, in time a fair number of patients require revision surgery. There are several indications for revision such as aseptic loosening of the implant, infection, bone fracture, recurrent hip dislocations and thigh pain. Revision THA is an elaborate and time consuming operation involving removal of the implants and cement remnants, and subsequent insertion of revision implants. Failure of a primary THA is often accompanied by severe loss of bone stock, which adversely affects the stability of the revision THA. As a result the survival of revision THA is much lower than that of the primary procedure (about 72% to 75% at ten years postoperatively^{42,59}). Due to the success of primary THA, the procedure is now being performed on younger patients. For these patients the chance to require revision is much higher than average, not only because of their more active lifestyle, but also because the implant service life is (and needs to be) longer.

In order to improve the clinical outcome of cemented THA it is important to know what mechanisms are responsible for failure of hip reconstructions. The most important reason for revision of cemented femoral components is aseptic loosening.^{38,48,59} Aseptic loosening can be identified clinically from radiographs by radiolucent areas around the cement mantle (Figure 2), indicating that the bone has been resorbed and replaced by soft tissue. Small PE and PMMA particles have been found in soft tissue surrounding clinical retrievals, suggesting that the soft tissue layer formation is a result of an inflammatory reaction to these

particles.^{29,52,82,83} This indicates that clinical failure is actually preceded by mechanical failure processes of the acetabular cup and the PMMA cement mantle.

The mechanical process responsible for failure of cemented THA has previously been identified as the “accumulated damage scenario”.^{23,67} This scenario describes a series of mechanical events eventually leading to clinical failure of the cemented reconstruction. According to the scenario, failure is often initiated by debonding at the implant-cement interface due to repetitive loading of the reconstruction. Subsequently, the implant subsides, which is enhanced by cement creep.^{46,76} Radiographic studies in which the migration of femoral stems was followed in time have shown that debonding and subsequent subsidence of the stem actually occur in a relative early stage of the lifespan of the reconstruction.³¹ Following stem-cement debonding, repetitive loading of the reconstruction causes the formation of fatigue cracks in the cement mantle.^{30,32,34,73} Fatigue cracking is governed by the local stress distribution, which is affected by several factors, such as the presence of pores,^{11,13,40,54} cement defects, mantle thickness,^{30,32,50} the shape and material properties of the implant^{22,72} and morphological and mechanical aspects of the cement-bone interface.⁶⁰ Fatigue cracks affect the mechanical integrity of the cement mantle, enhancing micromotion of the implant within the cement mantle. These micromotions cause cement abrasion at the implant-cement interface, leading to PMMA debris.^{2,29} Simultaneously, PE debris is formed in the acetabular part of the reconstruction, resulting from wear of the cup. These PMMA and PE particles can reach the intracapsular periprosthetic bone, causing osteolytic reactions and bone resorption. Furthermore,

Figure 2: Failed cemented reconstruction. The white arrows indicate osteolytic regions.



the particles can migrate along the cement-implant interface, due to the pumping mechanism of the dynamically loaded reconstruction. Thus, the particles can also reach the periprosthetic bone through defects in the cement mantle and through pathways created by full thickness fatigue cracks. This cascade of events triggers periprosthetic bone lysis, thereby adversely affecting the mechanical integrity of the cement-bone interface and causing gross failure of the reconstruction. In summary, failure of cemented total hip reconstructions is a complex interaction of various processes affected by implant, patient and surgeon-related factors, of which some are further analyzed in this thesis.

In the past, finite element analysis (FEA) techniques have been used to simulate various mechanical processes affecting survival of THA. FEA has been used to investigate periprosthetic stress patterns,^{22,85} femoral implant migration and its effect on bone stresses,^{26,71} the debonding process of the implant-cement interface^{27,57,77} and how debonding affects the cement stresses.¹⁶ As such, FEA has proven to be a valuable tool for investigation of orthopaedic issues.

In the current thesis several fundamental and clinical aspects of cemented THA reconstructions and their effect on failure are investigated, using FEA and experimental techniques. The particular subjects of investigation described in this thesis are elucidated below.

Implant design (Chapter 2)

The first aspect that was investigated is the design of the femoral hip implant. An example that illustrates the possible effects of changes in implant design is the Capital Hip system (3M Health Care Ltd, Loughborough, UK). The Capital Hip was a cemented hip implant that was introduced on the orthopaedic market in the United Kingdom in 1991. The implant was very similar to the original Charnley implant (DePuy, Leeds, UK), which is considered to be the 'gold standard' in THA, with an excellent survival of 93.9% at 22 years post-operatively.⁸⁴ The differences between the Capital Hip and the Charnley implants were considered to be small. Like the Charnley system, the Capital Hip system included a flanged and a roundback design, although the flange of the Capital Hip differed somewhat from the Charnley design due to patent restrictions. Another difference was that the Capital Hip was not only available in stainless-steel, like the Charnley, but also in titanium alloy. The latter was assumed to provide a more favorable stress transfer to the cement. Unfortunately, the apparently minor design changes had a catastrophic effect on the survival of the Capital Hip stems. Loosening rates of up to 16% after 26 months⁵¹ and 20% after 34 months⁶¹ were reported in the literature. Due to these alarming reports, the Capital Hip system was taken off the market and an investigation was started by the Royal College of Surgeons of England.⁷² This investigation showed distinct differences between the clinical outcome of the various Capital Hip designs. The stainless steel stems were superior to titanium-alloy stems, and the roundback stems performed better than the flanged designs. In a separate study, McGrath et al.⁵² studied retrievals and determined the sequence of events leading failure of the Capital Hip implants. They reported that failure involved debonding, cement fracture and osteolysis, and found bone cement debris in surrounding soft tissue. They were, however, unable to

identify what factor initiated failure of the Capital Hip. As the proposed failure mechanisms suggests that failure occurred along the 'accumulated damage' scenario, our creep-damage FEA algorithm provides an excellent tool to answer this question. Therefore the underlying mechanisms involved in failure of the Capital Hip designs were investigated in Chapter 2.

Cementing philosophy (Chapter 3)

Since the development of cemented THA, the cementing technique has evolved dramatically. The first generation cementing technique, developed by sir John Charnley⁷⁻⁹ involved mixing the cement in a bowl at room temperature and atmospheric pressure. The doughy cement was manually inserted into the cavity by so-called finger packing. The second generation technique included the use of a distal cement plug, water lavage of the intramedullary canal, retrograde filling using a cement gun and pressurization of the cement during insertion to enhance penetration of the cement into the cancellous bone.⁵⁶ Vacuum mixing⁴³ and cement centrifugation⁶ were introduced as additional features of the third generation cementing technique, to reduce air inclusions in the bone cement. Furthermore, centralizers and cement spacers were introduced for alignment of the implant within the cavity to ensure optimal thickness of the cement mantle without defects.

According to Charnley's philosophy, the function of bone cement in cemented THA was to uniformly transfer the joint loads to the femoral bone.⁸ Following this philosophy a minimal mantle thickness of 2 mm is generally advised to minimize stress concentrations in the cement. This is achieved by inserting a femoral implant that is undersized with respect to the broach or rap used to prepare the femoral cavity. With this technique, thin cement mantles or cement mantle defects, which have been shown to lead to early failure,^{62,66} are avoided. Excellent survival rates have been reported for THA's prepared with this technique.^{18,48,59}

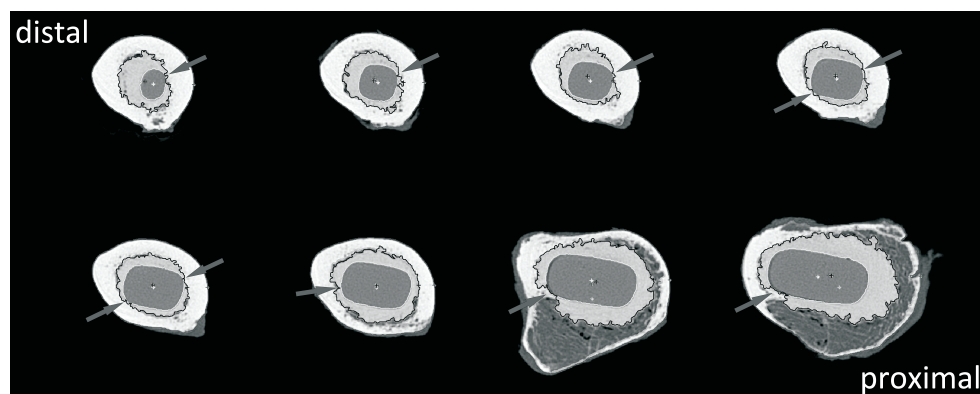


Figure 3: Cement mantle defects indicated by gray arrows after a line-to-line implantation (taken from Scheerlinck et al.⁶³).

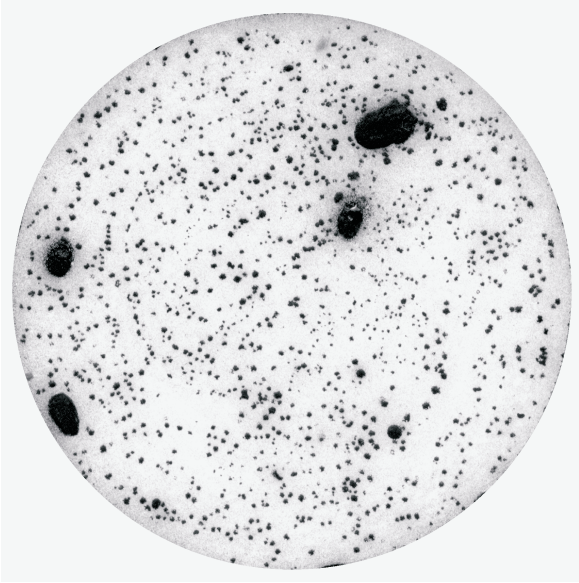


Figure 4: Cylindrical piece of bone cement with pores stained with black paint.

In contradiction with Charnley's philosophy, in the early 1970's a French orthopaedic surgeon named Marcel Kerboull developed a cementing technique that was based on an entirely different philosophy. In his technique the femoral cavity was fitted with the largest possible stem size, equal to the broach size.^{58,64} The function of the bone cement was to fill small gaps on the bone-implant interface resulting from imprecise fit of the implant in the reamed cavity. Because of the direct load transfer from implant to bone the cement was thought to be subjected to low stresses. This line-to-line technique results in a very thin cement mantle, with multiple cement mantle defects (Figure 3).⁶³ Surprisingly, however, excellent clinical results have been achieved with this technique.^{15,33}

Apparently there is more than one way to successfully perform a cemented THA. This phenomenon of two seemingly contradicting cementing philosophies has been referred to as the "French paradox".^{36,37,64} To further elucidate how these two cementing techniques perform relative to the 'accumulated damage' failure scenario, reconstructions prepared with both techniques were analyzed by FEA simulations in Chapter 3.

Cement porosity (Chapters 4 and 5)

Another aspect that was investigated in this thesis is the effect of cement porosity (Figure 4) on fatigue crack formation in the cement mantle. Pores in the mantle can originate from the mixing process of the bone cement. During mixing air can be introduced to the doughy cement that forms pores in the cement after polymerization.^{13,28,81} Furthermore, pores can be a result of the polymerization process itself.^{5,10,14}

Cement polymerization is an exothermic process, which means that heat is generated during curing. When the cement cools down again, it shrinks due to temperature reduction. In addition, the cement volume decreases due to the polymerization process itself, as polymerization of the viscous mixture increases its density. These two processes cause shrinkage voids to appear in the cement.

Air inclusions in the cement can be reduced by preparing the bone cement in a vacuum container,^{40,81} but also centrifuging has been applied in operating theatres.¹¹ These techniques remove air from the cement mixture prior to cement insertion, thereby effectively reducing porosity. Experimental studies have shown that these preparation methods improve the fatigue lifetime of the bone cement.^{11,39,54}

Pores originating from polymerization shrinkage cannot be prevented, but the distribution of pores in the cement mantle can be regulated to some extent. The initiation of the polymerization process is governed by the local temperature of the cement. Since the temperature of the intramedullary canal (body temperature, 37°C) usually is higher than the temperature of the implant (room temperature, 22°C), the polymerization process starts at the cement-bone interface. As shrinkage pores are formed in the regions that polymerize last, pore formation localizes at the implant-cement interface, causing so-called interface porosity. The polymerization process can, however, be manipulated by pre-heating of the femoral implant,^{5,27} or by pre-cooling of the intramedullary canal.²⁰ This will cause pores to be formed away from the implant-cement interface.

The effect of porosity on the strength of bone cement has been demonstrated in simple experiments, in which dog-bone shaped specimens with various levels of porosity are subjected to mechanical loads.^{11,13,40,54} Results of such experiments have clearly shown that the strength of acrylic bone cement is reduced by porosity. Clinically, however, the effect of porosity on the long term survival was reported to be irrelevant.⁴⁴ Chapter 4 of this thesis addresses this discrepancy between experimental and clinical findings.

The effect of pores on fatigue crack formation was further investigated by Topoleski et al.,⁷⁴ who analyzed cement fatigue fracture surfaces using scanning electron micrography. Based on their observations, they suggested that pores could have an ambiguous effect on fatigue crack formation and propagation. They found that pores acted as nucleation sites for cement fatigue cracks, and that these could accelerate fatigue crack propagation due to the stress concentrations around the pores. However, they suggested that pores could also have positive contributions to the fracture properties of bone cement. The idea behind this was that pores could disperse the crack propagating energy present at the tip of the crack, which drives crack propagation, thereby effectively decelerate crack propagation. These contradictory effects of pores on fatigue crack formation in bone cement were investigated using FEA, which is described in Chapter 5.

Cement-bone interface (Chapters 6 to 8)

The stability of a cemented THA depends on the anchorage of the cement in the femoral bone, and thus on the mechanical behavior of the cement-bone interface. The cement-bone interface is formed by complex structures of cement penetrating into the bone trabecular and lacunar spaces, creating an interlock

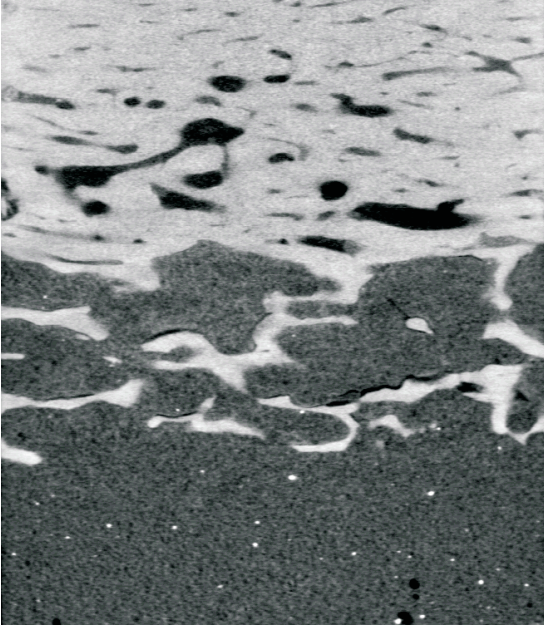


Figure 5: CT-image of the cement-bone interface
(top = bone; bottom = cement).

between the bone and bulk cement (Figure 5). Directly post-operatively, the cement-bone interface quality may be negatively affected by thermal necrosis due to cement polymerization heating,^{4,12,19} or by cement monomer toxicity.^{3,43,45} These processes may reduce the strength and the stiffness of the interface. Most research on the cement-bone interface has focused on the strength of the interface at an apparent, macroscopic level,^{3,35,49} but little is known about the mechanical behavior of the interface at the microlevel. For instance, it is unknown whether the cement or the bone is the weakest link in the cement-bone construct, and how the strength and stiffness of the cement-bone interface are affected by the level of interdigitation. Therefore, experiments were performed in which cement-bone interface specimens prepared from *in vitro* cemented THA's were subjected to quasistatic tensile and compressive loading. During the experiments the local deformations were monitored to investigate the separate contributions of the cement, bone and the cement-bone interface to the micro-mechanical response. Subsequently, the specimens were loaded to failure to investigate crack formation at the cement-bone interface, which should reveal what part of the interface is actually the weakest link. This research is described in Chapter 6.

In order to further study the micro-mechanics of the cement-bone interface, the experiments were simulated using FEA in Chapter 7. For this purpose, FEA models were created from the cement-bone interface based on micro computed tomography (μ CT) data. Subsequently, the FEA models were loaded according to the experimental protocol. It was investigated whether micro-mechanical FEA models of the

cement-bone interface were able to capture the micro-mechanical behavior of the specimens as observed experimentally in Chapter 6. These analyses also provided the local bone and cement stresses across the interface.

In Chapter 8 the micro-mechanical FEA model was used to study how the mechanical response of the cement-bone interface depends on the mechanical behavior of the individual constituents, their morphology, and their adhesion properties. Currently, it is not known to what degree the mechanical behavior of the cement-bone interface is governed by adhesion of cement to the bone and by shape-closed interlocking of the interdigitated cement-bone interface. Previously, authors have reported on the limited adhesive properties of PMMA to bone.^{47,65} Furthermore, cement-bone adhesion may be compromised by the presence of fluids in the bone (blood, fat, marrow) during cementation. The shape-closed interlock may be negatively affected by cement shrinkage, while on the other hand cement pressurization could improve its strength and stiffness. Another factor in the mechanical response of the cement-bone interface could be the material properties of the cement. For instance, the stiffness of commercially available cement has been shown to vary between 2.0 and 3.0 GPa,³⁸ which may have implications for the micro-mechanical response of the cement-bone interface. These issues were addressed by parametric variations in the FEA model.

In summary, this thesis addresses a number of aspects that are expected to affect the quality of cemented THA. The main goal of the thesis is to contribute to an improved understanding of the complex interactions of mechanical processes playing a role in failure of cemented femoral components.

References

1. Albrektsson T, Linder L (1984). Bone injury caused by curing bone cement. A vital microscopic study in the rabbit tibia. *Clin Orthop Relat Res* 183:280-287.
2. Anthony PP, Gie GA, Howie CR, Ling RS (1990). Localised endosteal bone lysis in relation to the femoral components of cemented total hip arthroplasties. *J Bone Joint Surg [Br]* 72(6):971-979.
3. Arola D, Stoffel KA, Yang DT (2006). Fatigue of the cement/bone interface: the surface texture of bone loosening. *J Biomed Mater Res B Appl Biomater* 76(2):287-297.
4. Berman AT, Reid JS, Yanicko DR, Jr, Sih GC, Zimmerman MR (1984). Thermally induced bone necrosis in rabbits. Relation to implant failure in humans. *Clin Orthop Relat Res* 186:284-292.
5. Bishop NE, Ferguson S, Tepic S (1996). Porosity reduction in bone cement at the cement-stem interface. *J Bone Joint Surg [Br]* 78(3):349-356.
6. Burke DW, Gates EI, Harris WH (1984). Centrifugation as a method of improving tensile fatigue properties of acrylic bone cement. *J Bone Joint Surg [Am]* 66(8):1265-1273.
7. Charnley J (1960). Anchorage of the femoral head prosthesis to the shaft of the femur. *J Bone Joint Surg [Br]* 42-B:28-30.
8. Charnley J (1961). Arthroplasty of the hip. A new operation. *Lancet* 1(7187):1129-1132.
9. Charnley J (1964). The bonding of prostheses to bone by cement. *J Bone Joint Surg [Br]* 46:518-529.
10. Davies JP, Harris WH (1995). Comparison of diametral shrinkage of centrifuged uncentrifuged Simplex P bone cement. *J Appl Biomater* 6(3):209-211.
11. Davies JP, Jasty M, O'Connor DO, Burke DW, Harrigan TP, Harris WH (1989). The effect of centrifuging bone cement. *J Bone Joint Surg [Br]* 71(1):39-42.
12. DiPisa JA, Sih GS, Berman AT (1976). The temperature problem at the bone-acrylic cement interface of the total hip replacement. *Clin Orthop Relat Res* 121:95-98.
13. Dunne NJ, Orr JF (2001). Influence of mixing techniques on the physical properties of acrylic bone cement. *Biomaterials* 22(13):1819-1826.
14. Gilbert JL, Hasenwinkel JM, Wixson RL, Lautenschlager EP (2000). A theoretical experimental analysis of polymerization shrinkage of bone cement: A potential major source of porosity. *J Biomed Mater Res* 52(1):210-218.
15. Hamadouche M, Boutin P, Daussange J, Bolander ME, Sedel L (2002). Alumina-on-alumina total hip arthroplasty: a minimum 18.5-year follow-up study. *J Bone Joint Surg [Am]* 84(1):69-77.
16. Harrigan TP, Harris WH (1991). A three-dimensional non-linear finite element study of the effect of cement-prosthesis debonding in cemented femoral total hip components. *J Biomech* 24(11):1047-1058.
17. Harrigan TP, Kareh JA, O'Connor DO, Burke DW, Harris WH (1992). A finite element study of the initiation of failure of fixation in cemented femoral total hip components. *J Orthop Res* 10(1):134-144.
18. Havelin LI, Engesaeter LB, Espehaug B, Furnes O, Lie SA, Vollset SE (2000). The Norwegian Arthroplasty Register: 11 years 73,000 arthroplasties. *Acta Orthop Scand* 71(4):337-353.
19. Homsy CA, Tullos HS, Anderson MS, Diferrante NM, King JW (1972). Some physiological aspects of prosthesis stabilization with acrylic polymer. *Clin Orthop Relat Res* 83:317-328.
20. Hsieh PH, Tai CL, Chang YH, Lee MS, Shih HN, Shih CH (2006). Precooling of the femoral canal enhances shear strength at the cement-prosthesis interface

- reduces the polymerization temperature. *J Orthop Res* 24(9):1809-1814.
21. Huiskes R (1980). Stress analyses of implanted orthopaedic joint prostheses for optimal design fixation. *Acta Orthop Belg* 46(6):711-727.
 22. Huiskes R (1990). The various stress patterns of press-fit, ingrown, cemented femoral stems. *Clin Orthop Relat Res* 261:27-38.
 23. Huiskes R (1993). Failed innovation in total hip replacement. Diagnosis proposals for a cure. *Acta Orthop Scand* 64(6):699-716.
 24. Huiskes R, Chao EY (1983). A survey of finite element analysis in orthopedic biomechanics: the first decade. *J Biomech* 16(6):385-409.
 25. Huiskes R, Nunamaker D (1984). Local stresses bone adaption around orthopedic implants. *Calcif Tissue Int* 36 Suppl 1:S110-S117.
 26. Huiskes R, Verdonchot N, Nivbrant B (1998). Migration, stem shape, surface finish in cemented total hip arthroplasty. *Clin Orthop Relat Res* 355:103-112.
 27. Ilesaka K, Jaffe WL, Kummer FJ (2003). Effects of preheating of hip prostheses on the stem-cement interface. *J Bone Joint Surg [Am]* 85(3):421-427.
 28. Jasty M, Davies JP, O'Connor DO, Burke D W, Harrigan TP, Harris WH (1990). Porosity of various preparations of acrylic bone cements. *Clin Orthop Relat Res* 259:122-129.
 29. Jasty M, Jiranek W, Harris WH (1992). Acrylic fragmentation in total hip replacements its biological consequences. *Clin Orthop Relat Res* 285:116-128.
 30. Jasty M, Maloney WJ, Bragdon CR, O'Connor DO, Haire T, Harris WH (1991). The initiation of failure in cemented femoral components of hip arthroplasties. *J Bone Joint Surg [Br]* 73(4):551-558.
 31. Karrholm J, Nivbrandt B, Thanner J, Anderberg C (2000). Radiostereometric evaluation of hip implant design surface finish - Micromotion of cemented femoral stems. Transactions of the 67th annual meeting of the American Academy of Orthopaedic Surgeons, Orlando, FL, USA .
 32. Kawate K, Maloney WJ, Bragdon CR, Biggs SA, Jasty M, Harris WH (1998). Importance of a thin cement mantle. Autopsy studies of eight hips. *Clin Orthop Relat Res* 355:70-76.
 33. Kerboul L, Hamadouche M, Courpied JP, Kerboul M (2004). Long-term results of Charnley-Kerboul hip arthroplasty in patients younger than 50 years. *Clin Orthop Relat Res* 418:112-118.
 34. Koster G, Willert H, Buchhorn GH (1999). Endoscopy of the femoral canal in revision arthroplasty of the hip. A new method for improving the operative technique analysis of implant failure. *Arch Orthop Trauma Surg* 119(5-6):245-252.
 35. Krause WR, Krug W, Miller J (1982). Strength of the cement-bone interface. *Clin Orthop Relat Res* 163:290-299.
 36. Langlais F, Howell JR, Lee AJ, Ling R. S (2002). The "French paradox". *Hip International* 12(2):166-168.
 37. Langlais F, Kerboul M, Sedel L, Ling RS (2003). The 'French paradox.'. *J Bone Joint Surg [Br]* 85(1):17-20.
 38. Lewis G (1997). Properties of acrylic bone cement: state of the art review. *J Biomed Mater Res* 38(2):155-182.
 39. Lewis G (1999). Effect of mixing method storage temperature of cement constituents on the fatigue porosity of acrylic bone cement. *J Biomed Mater Res* 48(2):143-149.
 40. Lewis G, Nyman JS, Trieu HH (1997). Effect of mixing method on selected properties of acrylic bone cement. *J Biomed Mater Res* 38(3):221-228.
 41. Lidgren L, Drar H, Moller J (1984). Strength of

- polymethylmethacrylate increased by vacuum mixing. *Acta Orthop Scand* 55(5):536-541.
42. Lie SA, Havelin LI, Furnes ON, Engesaeter LB, Vollset SE (2004). Failure rates for 4762 revision total hip arthroplasties in the Norwegian Arthroplasty Register. *J Bone Joint Surg [Br]* 86(4):504-509.
 43. Linder L (1977). Reaction of bone to the acute chemical trauma of bone cement. *J Bone Joint Surg [Am]* 59(1):82-87.
 44. Ling RS, Lee AJ (1998). Porosity reduction in acrylic cement is clinically irrelevant. *Clin Orthop Relat Res* 355:249-253.
 45. Lu JX, Huang ZW, Tropiano P, Clouet D'Orval B, Remusat M, Dejou J, Proust JP, Poitout D (2002). Human biological reactions at the interface between bone tissue polymethylmethacrylate cement. *J Mater Sci Mater Med* 13(8):803-809.
 46. Lu Z, McKellop H (1997). Effects of cement creep on stem subsidence stresses in the cement mantle of a total hip replacement. *J Biomed Mater Res* 34(2):221-226.
 47. Lucksanasomboon P, Higgs WA, Ignat M, Higgs RJ, Swain MV (2003). Comparison of failure characteristics of a range of cancellous bone-bone cement composites. *J Biomed Mater Res A* 64(1):93-104.
 48. Malchau H, Herberts P, Eisler T, Garellick G, Soderman P (2002). The Swedish Total Hip Replacement Register. *J Bone Joint Surg [Am]* 84 Suppl 2:2-20.
 49. Mann KA, Ayers DC, Werner FW, Nicoletta RJ, Fortino MD (1997). Tensile strength of the cement-bone interface depends on the amount of bone interdigitated with PMMA cement. *J Biomech* 30(4):339-346.
 50. Mann KA, Gupta S, Race A, Miller MA, Cleary RJ, Ayers DC (2004). Cement microcracks in thin-mantle regions after in vitro fatigue loading. *J Arthroplasty* 19(5):605-612.
 51. Massoud SN, Hunter JB, Holdsworth BJ, Wallace WA, Juliusson R (1997). Early femoral loosening in one design of cemented hip replacement. *J Bone Joint Surg [Br]* 79(4):603-608.
 52. McGrath LR, Shardlow DL, Ingham E, Andrews M, Ivory J, Stone MH, Fisher J (2001). A retrieval study of capital hip prostheses with titanium alloy femoral stems. *J Bone Joint Surg [Br]* 83(8):1195-1201.
 53. Murphy BP, Prendergast PJ (1999). Measurement of non-linear microcrack accumulation rates in polymethylmethacrylate bone cement under cyclic loading. *J Mater Sci Mater Med* 10(12):779-781.
 54. Murphy BP, Prendergast PJ (2002). The relationship between stress, porosity, nonlinear damage accumulation in acrylic bone cement. *J Biomed Mater Res* 59(4):646-654.
 55. National Center for Health Statistics (2008). National Hospital Discharge Survey, 1991 - 2004. Available from: <http://www.aaos.org> [Accessed date 7-5-2008].
 56. Oh I, Carlson CE, Tomford WW, Harris WH (1978). Improved fixation of the femoral component after total hip replacement using a methacrylate intramedullary plug. *J Bone Joint Surg [Am]* 60(5):608-613.
 57. Perez MA, Garcia-Aznar JM, Doblare M, Seral B, Seral F (2006). A comparative FEA of the debonding process in different concepts of cemented hip implants. *Med Eng Phys* 28(6):525-533.
 58. Postel M (1987). The routine operation. In: Postel M, Kerboul M, Evrard J, Courpied JP. Total hip replacement. Berlin, Germany: Springer Verlag; 26-33.
 59. Puolakka TJ, Pajamaki KJ, Halonen PJ, Pulkkinen PO, Paavolainen P, Nevalainen JK (2001). The Finnish Arthroplasty Register: report of the hip register. *Acta Orthop Scand* 72(5):433-441.

60. Race A, Miller MA, Ayers DC, Mann KA (2003). Early cement damage around a femoral stem is concentrated at the cement/bone interface. *J Biomech* 36(4):489-496.
61. Ramamohan N, Grigoris P, Schmolz W, Chapell AM, Hamblen DL (2000). Early failure of stainless steel 3M Capital femoral stem. *J Bone Joint Surg [Br]* 82 (Suppl. 1):71.
62. Ritter MA, Zhou H, Keating CM, Keating EM, Faris PM, Meding JB, Berend ME (1999). Radiological factors influencing femoral acetabular failure in cemented Charnley total hip arthroplasties. *J Bone Joint Surg [Br]* 81(6):982-986.
63. Scheerlinck T, de Mey J, Deklerck R, Noble PC (2006). CT analysis of defects of the cement mantle alignment of the stem: in vitro comparison of Charnley-Kerboul femoral hip implants inserted line-to-line undersized in paired femora. *J Bone Joint Surg [Br]* 88(1):19-25.
64. Scott G, Freeman MA, Kerboul M (2005). Femoral Components: The French Paradox. In: Breusch SJ, Malchau H. *The Well-Cemented Total Hip Arthroplasty - Theory Practice*. Heidelberg, Germany: Springer Medizin Verlag; 249-253.
65. Skripitz R, Aspenberg P (1999). Attachment of PMMA cement to bone: force measurements in rats. *Biomaterials* 20(4):351-356.
66. Star MJ, Colwell CW, Jr, Kelman GJ, Ballock RT, Walker RH (1994). Suboptimal (thin) distal cement mantle thickness as a contributory factor in total hip arthroplasty femoral component failure. A retrospective radiographic analysis favoring distal stem centralization. *J Arthroplasty* 9(2):143-149.
67. Stauffer RN (1982). Ten-year follow-up study of total hip replacement. *J Bone Joint Surg [Am]* 64(7):983-990.
68. Stolk J, Janssen D, Huiskes R, Verdonschot N (2007). Finite element-based preclinical testing of cemented total hip implants. *Clin Orthop Relat Res* 456:138-147.
69. Stolk J, Verdonschot N, Huiskes R (2002). Can finite element based pre-clinical tests differentiate between cemented hip replacement stems according to clinical survival rates? Transactions of the 49th annual meeting of the Orthopaedic Research Society, New Orleans, LA, USA.
70. Stolk J, Verdonschot N, Murphy BP, Prendergast PJ, Huiskes R (2004). Finite element simulation of anisotropic damage accumulation creep in acrylic bone cement. *Eng Fract Mech* 71:513-528.
71. Taylor M, Tanner KE, Freeman MA, Yettram AL (1995). Cancellous bone stresses surrounding the femoral component of a hip prosthesis: an elastic-plastic finite element analysis. *Med Eng Phys* 17(7):544-550.
72. The Royal College of Surgeons of England (2001). 3M Capital Hip system. The lessons learned from an investigation. The Royal College of Surgeons of England, London.
73. Topoleski LD, Ducheyne P, Cuckler JM (1990). A fractographic analysis of in vivo poly(methyl methacrylate) bone cement failure mechanisms. *J Biomed Mater Res* 24(2):135-154.
74. Topoleski LD, Ducheyne P, Cuckler JM (1993). Microstructural pathway of fracture in poly(methyl methacrylate) bone cement. *Biomaterials* 14(15):1165-1172.
75. Verdonschot N, Huiskes R (1995). Dynamic creep behavior of acrylic bone cement. *J Biomed Mater Res* 29(5):575-581.
76. Verdonschot N, Huiskes R (1996). Subsidence of THA stems due to acrylic cement creep is extremely sensitive to interface friction. *J Biomech* 29(12):1569-1575.
77. Verdonschot N, Huiskes R (1997). Cement debonding

- process of total hip arthroplasty stems. Clin Orthop Relat Res 336:297-307.
78. Verdonshot N, Huiskes R (1997). The effects of cement-stem debonding in THA on the long-term failure probability of cement. J Biomech 30(8):795-802.
79. Verdonshot N, Tanck E, Huiskes R (15-12-1998). Effects of prosthesis surface roughness on the failure process of cemented hip implants after stem-cement debonding. J Biomed Mater Res 42(4):554-559.
80. Verdonshot N, Huiskes R, Freeman MA (1993). Pre-clinical testing of hip prosthetic designs: a comparison of finite element calculations laboratory tests. Proc Inst Mech Eng [H] 207(3):149-154.
81. Wang JS, Toksvig-Larsen S, Muller-Wille P, Franzen H (1996). Is there any difference between vacuum mixing systems in reducing bone cement porosity? J Biomed Mater Res 33(2):115-119.
82. Willert HG, Bertram H, Buchhorn GH (1990). Osteolysis in alloarthroplasty of the hip. The role of bone cement fragmentation. Clin Orthop Relat Res 258:108-121.
83. Willert HG, Bertram H, Buchhorn GH (1990). Osteolysis in alloarthroplasty of the hip. The role of ultra-high molecular weight polyethylene wear particles. Clin Orthop Relat Res 258:95-107.
84. Wroblewski BM, Fleming PA, Siney PD (1999). Charnley low-frictional torque arthroplasty of the hip. 20-to-30 year results. J Bone Joint Surg [Br] 81(3):427-430.
85. Yettram AL, Wright KW (1980). Dependence of stem stress in total hip replacement on prosthesis cement stiffness. J Biomed Eng 2(1):54-59.

acro-

mechanic

Chapter 2

Finite element analysis of failure of the Capital Hip designs

Introduction

The Capital Hip (3M Health Care Ltd, Loughborough, UK) was introduced in the United Kingdom in 1991. The design was thought to be similar to that of the Charnley system (DePuy, Leeds, UK), which is considered to be the 'gold standard' in total hip arthroplasty. Like the Charnley, the Capital Hip system comprised a flanged and a roundback design, although the flange of the Capital Hip differed from that of the Charnley design because of patent restrictions. The former was shaped as a proximal wedge, while the Charnley system had an undercut flange. Both designs of the Capital Hip were available in either monobloc or modular versions. The monobloc stems were made of stainless steel, while the modular versions were made of titanium alloy (Ti6Al4V).

A few years after its introduction it became clear that the rate of revision of the Capital Hip was higher than expected. In response to this, the clinical protocol for the preparation of the femoral cavity was changed by the manufacturer to improve proximal and intramedullary rasping. However, in 1997, the Capital Hip system was withdrawn from the market for commercial reasons after which the Medical Devices Agency issued a hazard notice ordering the review of all patients who had had the system implanted.²⁰

After the withdrawal of the Capital Hip system, several studies were conducted to investigate its survival. A rate of loosening of up to 16% after 26 months was reported by Massoud et al.,⁴ while Ramamohan et al.¹¹ found a rate of failure of 20% after 34 months. Roy et al.¹⁴ reported a rate of failure of only 9% after follow-up for three years. There were, however, differences between these studies concerning the size

Table 1: Survival of the different Capital Hip designs as reported by the Royal College of Surgeons of England⁵

Hip Design	Stem material	Loosening rates* [%]
Modular - flanged	Titanium alloy	9.1
Modular - roundback	Titanium alloy	6.1
Monobloc - flanged	Stainless steel	4.4
Monobloc - roundback	Stainless steel	1.5

* These are given for the seven-year period before the release of the MDA hazard notice in 1998

and type of the rasp, the type of cement and the type of design of the Capital Hip which was used. In an investigation by the Royal College of Surgeons of England,¹⁹ a distinction was made between the various designs of the Capital Hip and their findings showed different rates of survival for the different designs. They reported that the stainless-steel stem had a better survival than the titanium-alloy stem, and also that the roundback performed better than the flanged stems (Table 1). This indicated that not all of the designs of the Capital Hip had an inferior performance. However, almost 50% of the patients had had the inferior titanium flanged stem, while only 9.4% had the superior stainless-steel roundback design.¹⁹

McGrath et al.⁵ analyzed titanium-alloy Capital Hip retrievals from failed reconstructions and investigated clinical and radiological data, as well as periprosthetic soft tissue. They described a sequence of events leading to the failure of the Capital Hip implant. First, lateral debonding was seen, followed by subsidence and calcar resorption. Subsequently, there was fragmentation of the cement mantle and osteolysis. Examination of the surface of the stem showed a typical pattern of wear in the anterolateral and posteromedial areas. This sequence of events corresponded to the damage-accumulation-failure scenario, as described by Huiskes.²

The Capital Hip disaster stresses the need for a reliable pre-clinical test to prevent inferior designs from entering the orthopaedic market. We have developed a simulation based on finite element analysis (FEA) for testing implants against the damage-accumulation-failure scenario.¹⁸ With this simulation, we have been able to differentiate between an inferior and a superior design, in accordance with clinical survival rates.¹⁶ In the current study, we simulated failure for the four designs of the Capital Hip stem. The aim was to investigate whether our finite element simulation was able to differentiate between stainless-steel and titanium-alloy stems, and secondarily between the roundback and flanged designs, in accordance with the findings of the Royal College of Surgeons of England.¹⁹ This would further validate our FEA-based simulation for use as a pre-clinical test.

Materials and methods

FEA models of reconstructions with the roundback and flanged Capital Hip stems were created. For this purpose, silicone moulds were made from two original implants obtained from the Medical Devices

Agency (one standard stainless-steel roundback and one standard titanium flanged stem (Figure 1a)). The silicone moulds were used to make casts of dental plaster, which were subsequently scanned by CT. Three-dimensional geometrical computer models were created from the CT data, using custom written software. Also a CT scan of a cadaver femur was made. Next, the geometrical models of the Capital Hip were virtually 'implanted' into the CT data of the cadaver femur in another custom-written program. The resulting three-dimensional models of the reconstructions were converted into FEA models of eight-node brick elements (Figure 1b). The cement mantle was defined by the geometry of the rasp, which was 2 mm oversized with respect to the implant, and by the geometry of the intramedullary canal. Hence, a minimum thickness of the cement mantle of 2 mm was obtained. The cortical bone was assumed to be transversely isotropic, while all other materials were assumed to be isotropic (Table 2). The material properties of the cortical and trabecular bone were taken from Stolk et al.¹⁷ and those of the bone cement from Murphy and Prendergast,^{7,8} representing Cemex RX bone cement (Tecres, Verona, Italy). The roundback and flanged designs were both analyzed using material properties of titanium alloy and stainless-steel to allow analysis of all four versions of the stem. The cement-bone interface was assumed to be bonded and the cement-stem interface to be debonded from the start of the simulations. The coefficient of friction for this interface was assumed to be 0.25 in all cases.

During the simulations, the models were fixed at the distal end of the femur while a loading history of 20

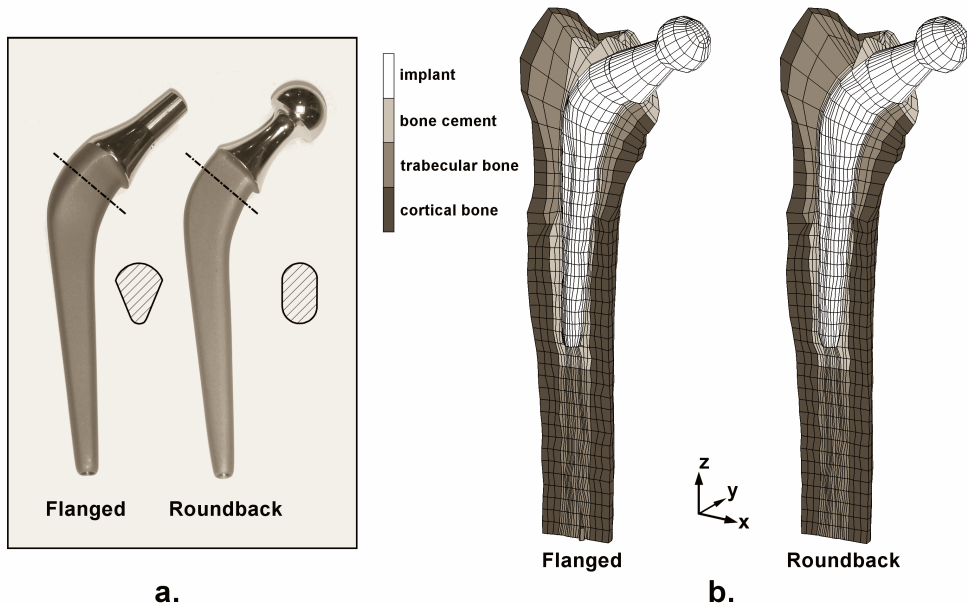


Figure 1: (a) Photograph showing the two Capital Hip stems with their typical cross-sectional shapes. (b) Longitudinal cross-sections of the FEA models which were used in the study.

Table 2: Material properties used in the FEA models.

Part of the model	Material	Elastic Modulus [GPa]	Poisson's ratio
Stem	Titanium alloy	110	0.3
	Stainless steel	210	0.3
Cement	Polymethylmethacrylate	2.4	0.3
Trabecular bone		0.4	0.3
Cortical bone		$E_x, E_y = 7.0; E_z = 11.5$ * $G_{yz}, G_{zx} = 3.5; G_{xy} = 2.6$ *	$\nu_{xy}, \nu_{yz}, \nu_{zx} = 0.4$

* The cortical bone was modeled as transversely isotropic. See Figure 1 for the definitions of the x, y and z directions.

million cycles was applied. The loading history consisted of an altering load of normal walking and stair-climbing. The stair-climbing and walking loads were applied in a ratio of 1:9 cycles, which is representative for active patients.⁶ The hip contact force and the muscle forces during these activities were taken from Heller et al.¹

Fatigue failure of the reconstructions with the Capital Hip stems was simulated using an algorithm which has previously been described by Stolk et al.¹⁸ Based on the local cement stresses and the number of loading cycles, the algorithm predicted cement creep and the formation of microcracks (also referred to as damage) in the cement mantle. For the calculation of creep, a relation was used which was derived by Verdonchot and Huiskes.²¹ The fatigue properties of bone cement were taken from Murphy and Prendergast.^{7,8} These were used to calculate the accumulation of damage in the cement. Once the damage had locally reached a critical level, a macrocrack was assumed to occur, which was accounted for by reducing the cement stiffness of the particular element almost to zero in the direction perpendicular to the crack. Subsequent failure of adjacent elements indicated that the macrocrack propagated through the cement mantle.

During the simulations, the crack formation process in the cement mantles surrounding the different Capital Hip designs was monitored, as well as the peak stresses in the cement. Furthermore, the migration of the stems with respect to the bone, as a result of creep and crack formation in the cement mantle, was calculated. Lastly, the contact between the stem and the cement mantle during the failure process was analyzed in order to locate areas where burnishing could be expected.

Results

There were distinct differences between the different Capital Hip designs regarding the formation of cracks in the cement mantle. At the onset of the simulation, the roundback titanium stem showed the largest amount of cement damage, but eventually the rates of crack formation around the two flanged designs were higher (Figure 2). After 20 million loading cycles, the largest amount of damage was found in the cement mantle surrounding the flanged titanium design, while the roundback stainless-steel stem

produced the least amount of cement damage. The development of damage around the flanged designs showed several stepwise increases during the simulations. These occurred at moments when stair-climbing loads were applied to the models, causing high concentrations of stress in the cement mantle (Figure 3). Not only the rate of crack formation, but also its pattern differed between the designs. In both the flanged and the roundback designs, cracks were initially formed in the proximomedial region below the collar and distally below the tip of the stem (Figure 4). In the reconstructions with the flanged designs, the proximal damage zone expanded from medial to lateral, via the posterior side. In the mid-part of the cement mantles, a crack was formed at the lateral side. This appeared in all cement mantles, except for that surrounding the roundback stainless-steel stem. The medial damage zone below the collar and the lateral crack at the level of the mid-stem propagated towards the tip of the stem. For the flanged designs, this effect was more pronounced than for the roundback designs.

Analysis of the migration of the prosthetic head also showed differences between the flanged and the roundback designs. The migration of the flanged designs in the posterior direction was much higher than that of the roundback designs, indicating increased rotation of the stem about its longitudinal axis (Figure 5). In the medial and distal directions, the differences between the type of design were very small. The titanium-alloy stems, however, seemed to migrate slightly more in these directions than the stainless steel stems.

The stem-cement interface was debonded from the start of the simulation and therefore the stem did not contact the cement mantle over the entire surface. During the loading history, the areas of contact varied in size and location. However, in both the flanged and the roundback designs, contact was mainly detected medially at the posterior side and laterally at the anterior side (Figure 6). The location and size of the area

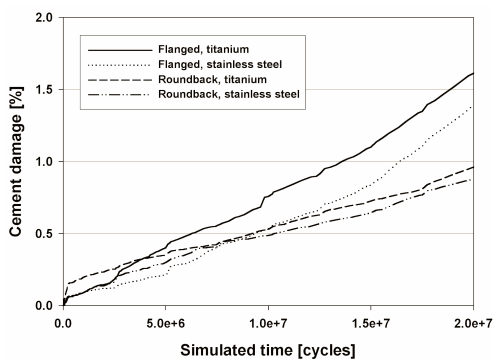


Figure 2: Graph showing the formation of cement cracks around the various Capital Hip stems. The total number of cracks was normalized by division by the total number of cement cracks ultimately possible.

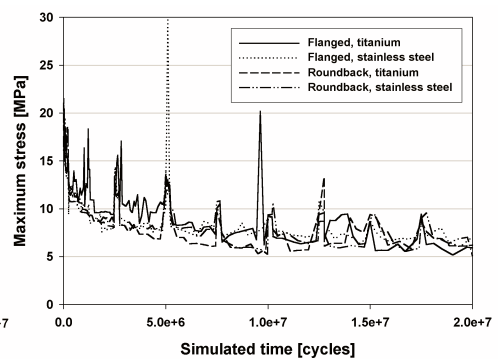


Figure 3: Graph showing the peak tensile stress in the cement mantles surrounding the various Capital Hip stems.

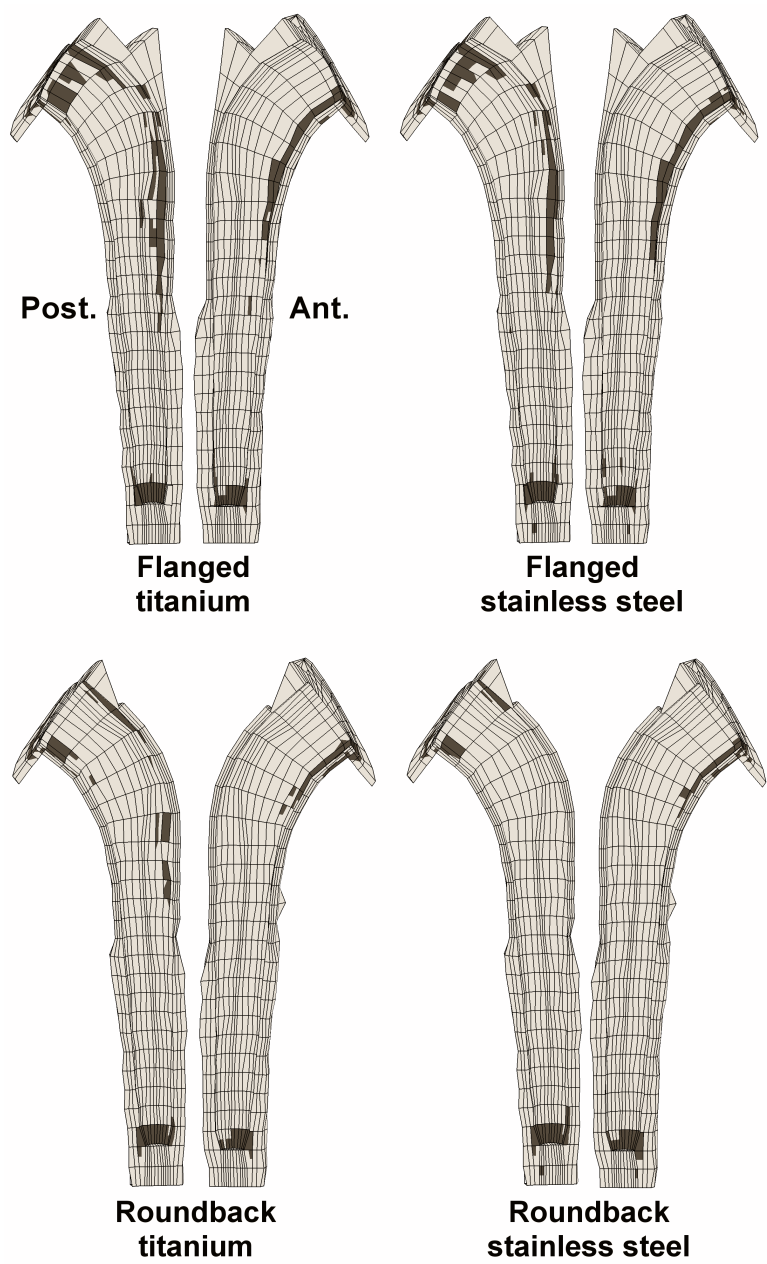


Figure 4: FEA models showing the distribution of cracks in the cement mantles surrounding the Capital Hip stems after 20 million loading cycles. The cement mantles are split open along the mid-frontal plane. The inside of the posterior part of the cement mantle is shown on the left, the inside of the anterior part is on the right in each model. The dark zones indicate the regions where cracks were formed.

of contact were virtually independent of the stem material and type of loading which had been applied to the models.

Discussion

In accordance with the study of the Royal College of Surgeons of England,²⁹ our simulation was able to demonstrate the detrimental effect of the flanged design and of the titanium-alloy stem material on the formation of cement fatigue cracks. However, in contrast with that study, our simulations showed that the effect of the design of stem was larger than that of the stem material. Hence, in comparison with the clinical data, in our model the effect of the change in the type of material was underestimated with respect to the effect of the change in geometry.

Obviously, our FEA models are limited in the extent to which the failure process of actual reconstructions with the Capital Hip system can be simulated, which is a possible explanation for the discrepancy between our results and the clinical scores. An important shortcoming in the models is that the formation of polymethylmethacrylate (PMMA) particles and their subsequent effect on failure of the implant cannot be predicted by our simulation. McGrath et al.⁵ studied periprosthetic soft tissue from retrieved Capital Hip implants and found large numbers of PMMA particles, which implied that biological reactions to PMMA particles were involved in the failure process of these implants. In addition, the Royal College of Surgeons of England²⁹ reported that the surface roughness of the titanium- alloy Capital Hip stems typically was higher than that of the stainless-steel Capital Hips. Since rougher stem surfaces have a higher abrasive potential, the titanium-alloy stems have caused more pronounced osteolytic reactions. This may explain why clinically the stem material was the primary design parameter involved in the failure of the Capital Hip, while it was secondary to the geometry of the stem in our simulation.

There were also limitations to our models which may have affected the correspondence to the survival rates found *in vivo*, regardless of the type of design or implant material. For instance, the cement mantle in our models had a minimum thickness of 2 mm, while in real reconstructions using the original Capital Hip rasps, a minimum cement thickness of 1 mm was obtained.²⁹ A thin cement mantle has been associated with earlier failure of cemented hip reconstructions.^{3,12,13} Furthermore, in our models the stems were implanted such that an optimum cement mantle was obtained, while the Royal College of Surgeons of England²⁹ reported that the cementing technique was 'doubtful' in 54% and 'unacceptable' in 33% of the 1899 cases which were studied. Obviously, with a thickness of the cement mantle of only 1 mm, a suboptimal positioning of the implant has significant consequences for the cement mantle surrounding the implant, which affects the rate of survival of the implant. Furthermore, in our simulation we used the fatigue characteristics of Cemex RX bone cement, while for the reconstructions with the Capital Hip mainly CMW (DePuy International Ltd, Leeds, UK) or Palacos (Schering Plough Ltd, Welwyn Garden City, UK) cement was used.^{4,24} However, we think that these effects are evenly distributed over the four types of stem, and would therefore not have affected the ranking which we found in this study.

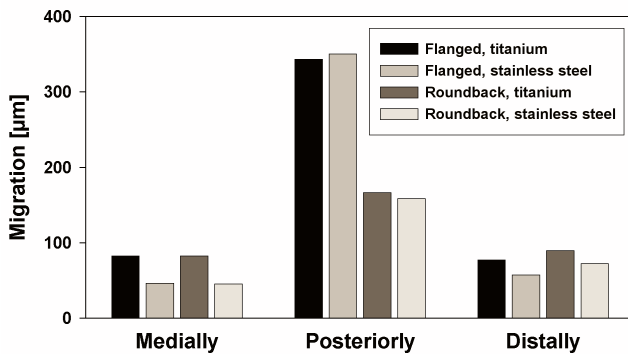


Figure 5: Bar chart showing migration of the various Capital Hip stems after 20 million loading cycles. The migration values represent the translation of the head centre in the medial, posterior and distal directions.

Despite the limitations of our simulations, some interesting findings which corresponded to the clinical data resulted from our study. In our models, initially, cracks were formed in the proximomedial region of the cement mantle. This was also observed by McGrath et al.,⁵ who studied post-operative radiographs of reconstructions with titanium Capital Hip implants. They also examined retrieved implants and noticed patterns of wear in the anterolateral and posteromedial regions due to burnishing of the stems against the cement mantles.⁵ Our simulations showed that these were the main regions where the stems contacted the cement mantle and therefore where loads were transferred between the stem and the cement. Furthermore, our simulations showed that the flanged designs displayed a high level of migration of the prosthetic head in the posterior direction. The major part of the migration in this direction was caused by rotation of the stem around its longitudinal axis, indicating torsional instability of this particular design. This was also reported by Ramamohan et al.,²¹ based on FEA.

The Capital Hip system was equipped with some new features compared with the Charnley system which were introduced to improve survival of the implant. Unfortunately, these features did not have the desired effect. Because of its low modulus of elasticity, titanium was thought to reduce cement stresses.^{9,15,22} However, our simulations indicated that the cement stresses increased with the titanium-alloy material. The titanium stems therefore produced more cement damage which was attributable to the decreased bending stiffness of the titanium with respect to the stainless-steel stems.¹⁰ The flanged design was introduced to provide a better proximal distribution of stress, while our simulations indicated that the flanged designs produced more cement damage in this region than the roundback stems. Additionally, the rotational instability of the flanged designs may have promoted abrasion of the cement mantle, further accelerated by the higher surface roughness of the titanium-alloy stems.

The aim of our study was to investigate whether our FEA simulation was able to differentiate between the different designs of the Capital Hip system, in accordance with the findings of the Royal College of Surgeons of England.¹⁹ Our study showed that the simulation was able to differentiate between stainless-steel and

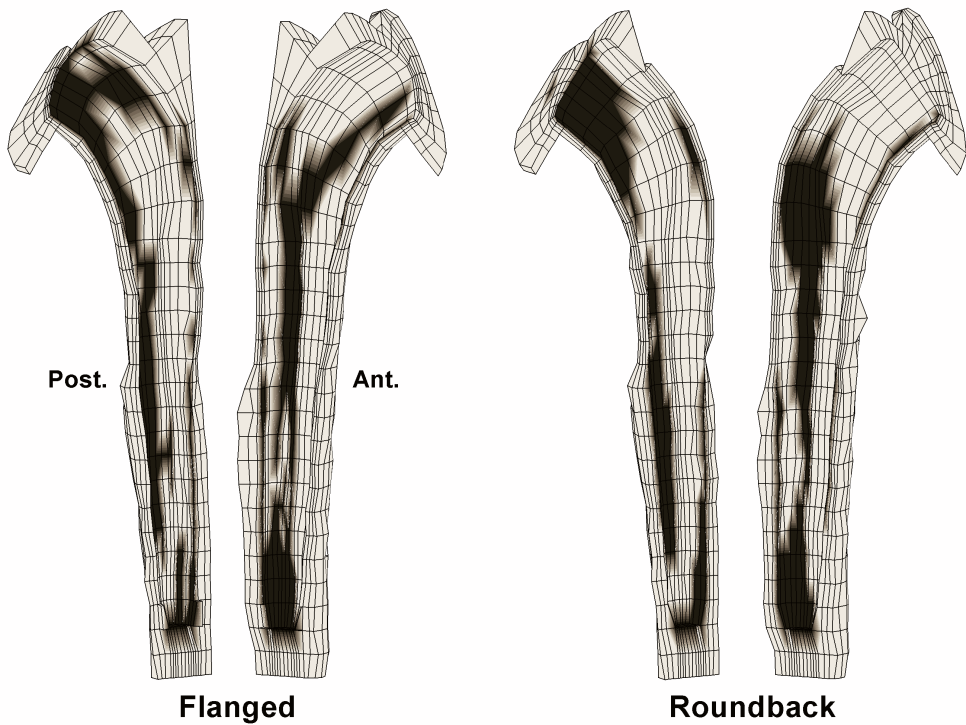


Figure 6: FEA models showing the areas of contact between the Capital Hip stem and the cement mantle for the flanged and roundback designs. The flanged stem had properties of stainless-steel, the roundback those of titanium alloy. The inside of the posterior part of the cement mantle is shown on the left and the inside of the anterior part on the right in each model. The dark zones indicate the regions where the stem contacted the cement mantle. Although these figures are taken at arbitrarily-chosen moments in the loading history, they are representative of the contact status during the entire simulation.

titanium-alloy stems and also between the roundback and flanged designs. However, in our simulation the effect of the design of stem on the crack formation was larger than that of the material of the stem. We attribute this to the differences in surface roughness between the titanium-alloy and stainless-steel stems, which our simulation was unable to detect. Further development of our simulation is necessary to incorporate these effects. Hence, our study has identified areas in which the simulation could be improved, but has further validated its potential to evaluate aspects of the design of stems such as material and geometry at a pre-clinical stage.

References

- Heller MO, Bergmann G, Deuretzbacher G, Durselen L, Pohl M, Claes L, Haas NP, Duda GN (2001). Musculo-skeletal loading conditions at the hip during walking and stair climbing. *J Biomech* 34(7):883-893.
- Huiskes R (1993). Failed innovation in total hip replacement. Diagnosis and proposals for a cure. *Acta Orthop Scand* 64(6):699-716.
- Kawate K, Maloney WJ, Bragdon CR, Biggs SA, Jasty M, Harris WH (1998). Importance of a thin cement mantle. Autopsy studies of eight hips. *Clin Orthop Relat Res* 355:70-76.
- Massoud SN, Hunter JB, Holdsworth BJ, Wallace WA, Juliusson R (1997). Early femoral loosening in one design of cemented hip replacement. *J Bone Joint Surg [Br]* 79(4):603-608.
- McGrath LR, Shardlow DL, Ingham E, Andrews M, Ivory J, Stone MH, Fisher J (2001). A retrieval study of capital hip prostheses with titanium alloy femoral stems. *J Bone Joint Surg [Br]* 83(8):1195-1201.
- Morlock M, Schneider E, Bluhm A, Vollmer M, Bergmann G, Muller V, Honl M (2001). Duration and frequency of every day activities in total hip patients. *J Biomech* 34(7):873-881.
- Murphy BP, Prendergast PJ (1999). Measurement of non-linear microcrack accumulation rates in polymethylmetacrylate bone cement under cyclic loading. *J Mater Sci Mater Med* 10(12):779-781.
- Murphy BP, Prendergast PJ (2002). The relationship between stress, porosity, and nonlinear damage accumulation in acrylic bone cement. *J Biomed Mater Res* 59(4):646-654.
- Poss R, Walker P, Spector M, Reilly DT, Robertson DD, Sledge CB (1988). Strategies for improving fixation of femoral components in total hip arthroplasty. *Clin Orthop Relat Res* 235:181-194.
- Prendergast PJ, Monaghan J, Taylor D (1989). Materials selection in the artificial hip joint using finite element stress analysis. *Clin Mater* 4:361-376.
- Ramamohan N, Grigoris P, Schmolz W, Chapell AM, Hamblen DL (2000). Early failure of stainless steel 3M Capital femoral stem. *J Bone Joint Surg [Br]* 82 (Suppl. 1):71.
- Ramaniraka NA, Rakotomanana LR, Leyvraz PF (2000). The fixation of the cemented femoral component. Effects of stem stiffness, cement thickness and roughness of the cement-bone surface. *J Bone Joint Surg [Br]* 82(2):297-303.
- Ritter MA, Zhou H, Keating CM, Keating EM, Faris PM, Meding JB, Berend ME (1999). Radiological factors influencing femoral and acetabular failure in cemented Charnley total hip arthroplasties. *J Bone Joint Surg [Br]* 81(6):982-986.
- Roy N, Hossain S, Ayeko C, McGee HM, Elsworth CF, Jacobs LG (2002). 3M Capital hip arthroplasty: 3-8-year follow-up of 208 primary hip replacements. *Acta Orthop Scand* 73(4):400-402.
- Sarmiento A, Gruen TA (1985). Radiographic analysis of a low-modulus titanium-alloy femoral total hip component. Two to six-year follow-up. *J Bone Joint Surg [Am]* 67(1):48-56.
- Stolk J, Maher SA, Verdonschot N, Prendergast PJ, Huiskes R (2003). Can finite element models detect clinically inferior cemented hip implants? *Clin Orthop Relat Res* 409:138-150.
- Stolk J, Verdonschot N, Cristofolini L, Toni A, Huiskes R (2002). Finite element and experimental models of cemented hip joint reconstructions can produce similar bone and cement strains in pre-clinical tests. *J Biomech* 35(4):499-510.
- Stolk J, Verdonschot N, Murphy BP, Prendergast

- PJ, Huiskes R (2004). Finite element simulation of anisotropic damage accumulation and creep in acrylic bone cement. *Eng Fract Mech* 71:513-528.
19. The Royal College of Surgeons of England (2001). 3M Capital Hip system. The lessons learned from an investigation. The Royal College of Surgeons of England, London.
20. UK Medical Devices Agency (1998). Hazard Notice 9801.
21. Verdonchot N, Huiskes R (1995). Dynamic creep behavior of acrylic bone cement. *J Biomed Mater Res* 29(5):575-581.
22. Yettram AL, Wright KW (1980). Dependence of stem stress in total hip replacement on prosthesis and cement stiffness. *J Biomed Eng* 2(1):54-59.

CO- and

anics of

I

.

Chapter 3

Finite element analysis of the effect of cementing concepts on implant stability and cement fatigue failure

Introduction

A thin cement mantle¹² and cement mantle defects have been associated with the formation of cement mantle cracks,⁴ leading to early failure of total hip arthroplasty.¹⁹ This evidence has resulted in the generally accepted rule to use a stem that is undersized compared with the broach used to prepare the intramedullary canal, to produce a cement mantle of at least 2-mm thickness. Using this technique, excellent survival rates have been obtained.¹⁰

In France, in the early 1970s, a surgical technique was developed contradicting this concept.^{6,7} The technique involves the removal of as much trabecular bone as feasible and the implantation of a canal-filling stem in a line-to-line fashion, meaning the size of the implant is equal to the size of the broach used to prepare the intramedullary canal. The goal is to transfer loads directly from the stem to the cortical bone and as such to “protect” the cement mantle.⁷ The technique results in a very thin cement mantle with multiple cement mantle defects.¹⁸ Surprisingly, this technique also resulted in excellent survival rates.^{6,17} This phenomenon

of two seemingly contradictory cementing concepts leading to good outcome has been referred to as the “French paradox”.⁷

Although both techniques apparently lead to good clinical results, variations in implant size, cement mantle thickness, and bone type surrounding the cement mantle will cause differences in the response to fatigue loading in terms of implant stability and cement crack formation. Previous studies suggested that large implants may provide superior rotational stability,²³ and that cement mantles supported by trabecular bone produce inferior results.¹ The aim of our study was to further evaluate the mechanical consequences of variations in cementing technique, using finite element analysis (FEA).

We hypothesized (1) undersized stems surrounded by a thick intact cement mantle would produce fewer cement fatigue cracks than canal-filling stems, (2) large canal-filling stems would rotate less than undersized stems, and (3) a cement mantle supported by trabecular bone would produce more cement cracks and more implant rotation than a cement mantle supported by cortical bone.

Materials and methods

We created a generic two-dimensional (2D) plane strain FEA model of a transverse slice of a Charnley-Kerboull stem replica (CMK; Stratec Medical, Oberdorf, Switzerland) cemented in a cadaver femur. This generic model was subsequently adapted to simulate arthroplasties resulting from various cementing techniques. The FEA models were subjected to a fatigue loading history, during which crack formation and implant rotation were simulated.

The model was created from computed tomography (CT) data used previously for geometric analyses

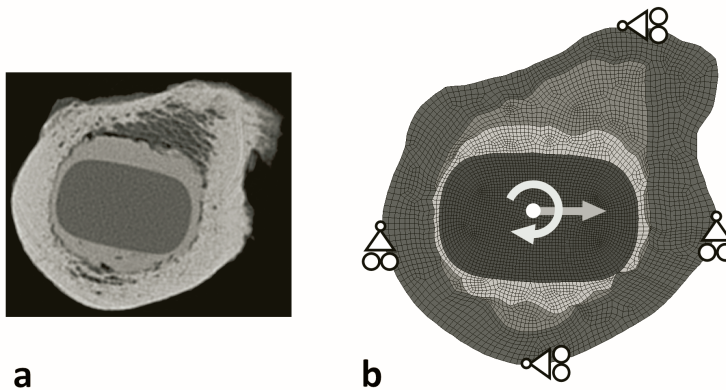


Figure 1: (a) The original CT image of a Charnley-Kerboull stem replica cemented line-to-line into a donor femur is shown, which served as the basis for all FEA models. (b) An example of an FEA model with a maximal canal-filling stem. From the center of the image to the outer edge, the implant, cement mantle, trabecular bone, and cortical bone are shown, consecutively. Indicated in this image are the loading conditions (arrows) and boundary conditions applied during the simulations.

of the cement mantle around line-to-line and undersized femoral implants.¹⁸ The model was based on a representative example of a Charnley-Kerboull stem implanted in a line-to-line fashion. For the FEA model, an image of the CT data set was taken at the level of the lesser trochanter. In the CT image, the contours of the cortical and trabecular bone, the cement mantle, and the stem were identified previously.¹⁸ The model was created based on these contours using an automatic mesher (MSC.MARC; MSC Software Corp, Santa Ana, CA). The models had a thickness of 5 mm and consisted of approximately 6,000 8-node brick elements and 12,500 nodal points (Figure 1).

We varied the size of the femoral implant to simulate both canal-filling and undersized implants. The undersized implants were based on the original Charnley-Kerboull implant geometry to exclude variability in the implant design, allowing us to study only the effect of cementing concepts. Considering the cross-sectional geometry of the Charnley-Kerboull stem did not differ much from that of the original Charnley roundback stem, we chose to use scaled down versions of the original Charnley-Kerboull implant for the models of the undersized stems. Consequently, the cement mantle thickness was varied inversely with femoral component size. Four cases were created: a model with an incomplete cement mantle (minimum thickness of 0 mm; maximal canal-filling stem), a thin mantle (minimum thickness of 1 mm; canal-filling stem), an average mantle (minimum thickness of 2 mm; undersized stem), and a thick cement mantle (minimum thickness of 3 mm; severely undersized stem) (Figure 2). Due to the typical shape of the implant, the cement mantle thickness was minimal in the medial and lateral parts of the reconstruction, while the thickness was larger in the anterior and posterior regions.

The type of bone supporting the cement mantle was varied by changing the material properties of the elements surrounding the cement mantle. Three variations were analyzed: a cement mantle supported by trabecular bone only (trabecular bone support, representing an implantation technique with poor cement pressurization), a mantle supported by trabecular and cortical bone (mixed bone support, representing an implantation technique with adequate cement pressurization), and a mantle maximally supported by cortical bone (cortical bone support, representing a surgical technique in which most of the trabecular bone is broached away or filled with cement) (Figure 2). To avoid mesh dependency of the results in the simulations, all models were derived from a single generic FEA model. In this model the mesh architecture was adapted such that all geometric variations in implant size, cement mantle thickness, and type of bone support could be modified by merely changing the material properties assigned to the elements. The material properties of the cortical bone,⁹ trabecular bone,⁵ bone cement⁸ and implant were assumed to be isotropic and linear elastic (Table 1). The implant was modeled with stainless steel material properties.

Contact between the implant and the cement was modeled using a node-to-surface contact algorithm (MSC.MARC). The implant-cement interface was assumed debonded from the start of the simulation, implying no tensile loads could be transferred over the interface, assuming a worst-case scenario. Friction was modeled using a Coulomb stick-slip model with a friction coefficient of 0.25, simulating a satin stem surface finish, consistent with the surface finish of the Charnley-Kerboull stems. The cement mantle was

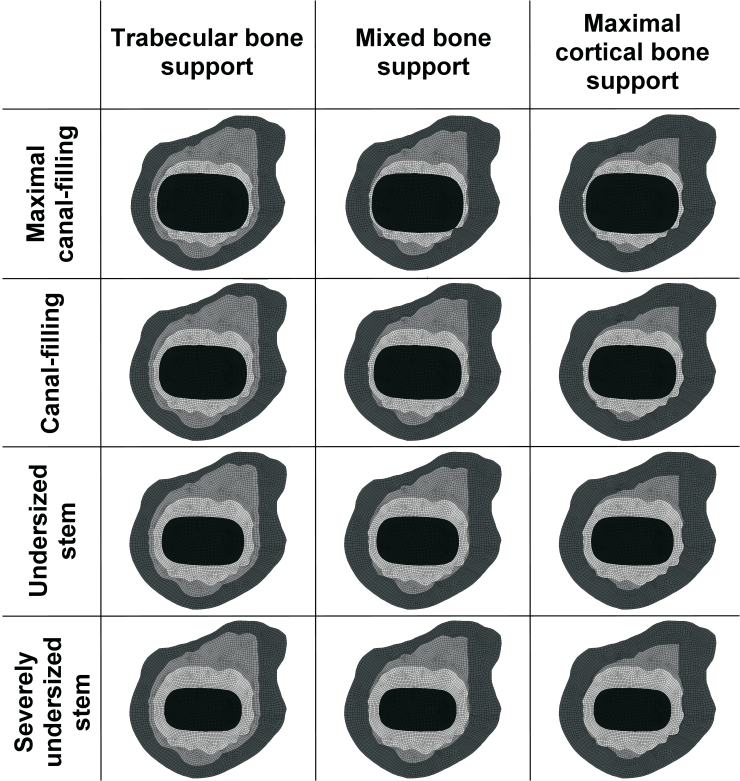


Figure 2: Twelve FEA models were created in total. Four different stem sizes (resulting in four different cement mantles, shown in the rows) were studied in combination with three different bone types supporting the cement mantle (shown in the columns).

assumed to be fixed to the surrounding cortical and trabecular bone.

For $2 \cdot 10^6$ cycles, the models were alternately loaded with a cyclic torque load and a transversal load. The loading configurations were applied in a ratio of 9:1, meaning that during 90% of the loading history a torque load was applied, while during 10% the transversal load was applied. The torque load represented a stair-climbing load, which is critical for implant stability.² Since our models were limited to only a slice of an entire reconstruction, the external loads had to be scaled down to the model size. We therefore assumed a torque load of 6.4 Nm acting on the models.² The transversal load represented a bending moment in the frontal plane, which can be as high as 80 Nm.² As a consequence, the implant will exert a medial force on the cement mantle in the proximal region, while more distally lateral forces are transferred to the cement. A transversal load of 400 N acting in the medial direction, represented bending in the frontal plane in our 2D models. Displacement in the antero-posterior direction was restricted in the medial and lateral part of the outer cortex, while displacement in the medio-lateral direction was restricted in the anterior and

Table 1: Material characteristics of the different structures of the FEA model

Model part	Young's modulus [GPa]	Poisson's ratio [-]
Stem	210	0.3
Bone cement	2.2 ¹⁹	0.3
Trabecular bone	1.0 ²¹	0.3
Cortical bone	7.0 ²⁰	0.4

posterior part of the outer cortex (Figure 1b). In this manner deformation and expansion of the cortical bone was allowed, enabling movement and deformation of the stem, cement and bone, while rigid body displacement of the models was restricted.

Because only a slice of an entire reconstruction was analyzed, a plane strain state was assumed in the model. Although usually 2D elements are used in such a case, we used three-dimensional (3D) brick elements to make the FEA models compatible with our fatigue crack formation algorithm. To compensate for this, all nodes on the top and bottom planes of the model were fixed in the axial direction.

Fatigue crack formation and creep were simulated using a custom-written algorithm based on FEA.²¹ Based on the local cement stress situation and the number of loading cycles, a small crack could occur at a certain location in the mantle. This crack was then accounted for mechanically by locally reducing the stiffness to virtually zero in the direction perpendicular to the crack. At the same location, an additional second and third crack could be formed, perpendicular to the first crack. Furthermore, during the simulation small cracks could propagate, thereby forming macrocracks that could eventually span the full cement mantle thickness. Similarly, creep deformation was simulated to occur locally in the cement mantle, also based on the local cement stress situation and the number of loading cycles. The formation of bone cement cracks was determined using so-called S-N curves,^{14,15} whereas the amount of local creep strain in the cement mantle was calculated using a creep law.²² This creep-damage algorithm has previously been used to differentiate between the survival of various implant designs.^{3,20}

During the simulations we monitored the number of cracks formed in the cement mantle. In order to allow for comparison between the various models, the number of cracks was normalized by division through the number of cracks that was ultimately possible to occur in the cement. The total number of cement cracks ultimately possible in the cement mantle was dependent on the size of the implant, and ranged from 17,500 to 38,000 for the models with the largest and smallest implant, respectively.

Additionally, the rotation of the femoral component with respect to the cortical bone was calculated and considered a measure for the level of implant stability. To calculate implant rotation, initial elastic deformations of the models were ignored to display only the long-term effect of creep and crack formation on implant rotation. To demonstrate the effect of type of bone supporting the cement mantle, cement damage formation and implant rotation as predicted by models with trabecular and cortical bone support

were calculated and presented relative to the results of models with mixed bone support, which was considered to be the standard situation.

Results

In contrast with our first hypothesis, the canal-filling stems produced fewer cracks in the cement mantle than the undersized stems (Figure 3). In general, the number of cracks formed in the cement mantle increased with decreasing implant size. Cyclic torque loading of the models caused cracks to appear in the cement mantle at the posteromedial and anterolateral corners of the stem (Figure 4). Cracks that crossed the full cement mantle thickness appeared first in the anterolateral corner of the cement mantle, in some cases followed by a secondary crack in the posteromedial corner. We observed full-thickness cracks in all models with undersized implants, whereas in the models with the maximal canal-filling implant, full-thickness cracks occurred only when the cement mantle was supported by trabecular bone. In two models with a severely undersized stem (cement mantle supported by mixed bone and cortical bone), full-thickness cracks caused the model not to converge after $1.25 \cdot 10^6$ cycles. Deformations in these models, in combination with the alternating loading profile, caused instabilities in the contact algorithm at the implant-cement interface. Differences in crack formation and implant rotation between models were therefore investigated at $1.25 \cdot 10^6$ cycles instead of at $2 \cdot 10^6$ cycles.

Consistent with our second hypothesis, after $1.25 \cdot 10^6$ loading cycles, canal-filling stems had rotated less than undersized stems (Figure 5). Creep and crack formation caused progressive rotation of the stem, particularly during the first $1 \cdot 10^6$ cycles. In some models, implant rotation suddenly increased when changing from the torque load to the transversal load. When the transversal load was subsequently reapplied, the stem settled again in a new and more stable position and implant rotation decreased again.

In general, models with a cement mantle supported by trabecular bone produced more cement mantle cracks and caused more implant rotation compared to the models in which the cement mantle was

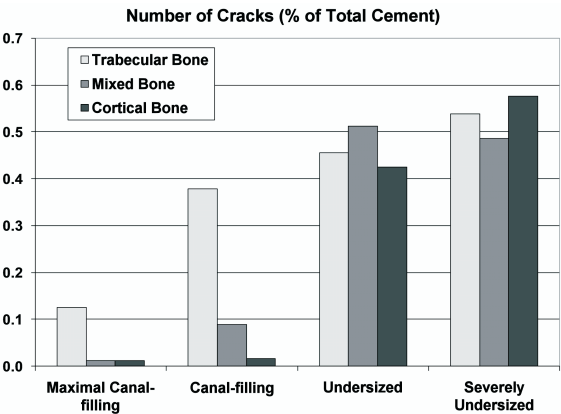


Figure 3: After 1.25 million loading cycles the models with undersized stems produced more cement cracks than models in which a canal-filling stem was simulated. The number of cracks was normalized through division by the maximal number of cracks that could possibly be simulated in the cement mantle.

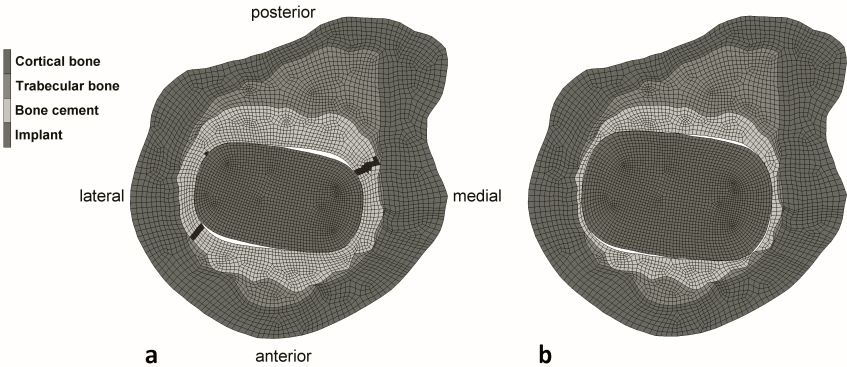


Figure 4: In (a), an FEA model with an undersized stem and mixed bone support is shown with two full-thickness cement mantle cracks, whereas in (b), which depicts an FEA model with a maximal canal-filling stem and mixed bone support, almost no cracks were formed during the simulation. The deformations are magnified by a factor of 10 for illustrative purposes.

supported by a mix of trabecular and cortical bone. In addition, increasing cortical bone reduced implant rotation and the number of cement cracks (Table 2).

Discussion

Although the FEA model we used was based on accurate and clinically relevant data of the Charnley-Kerboull stem, it obviously had certain limitations. In our study, we used a 2D rather than a 3D model to limit the computational costs while providing sufficient detail for analyzing the effects of changes in the cement mantle geometry. This limited the loads we could apply to in-plane loads, such as a torque load. The effect of axial loads, leading to implant subsidence and tangential stresses in the cement mantle, was

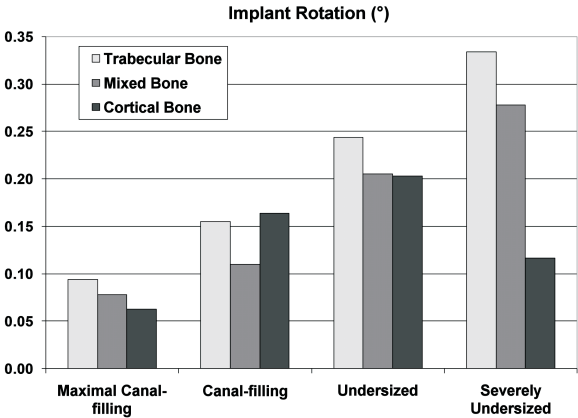


Figure 5: After 1.25 million loading cycles the maximal canal-filling stem rotated less than the undersized stem. The rotation values represent the rotation resulting from creep and crack formation in the cement mantles, since elastic deformations were omitted.

Table 2: Relative effect of type of bone support for the cement mantle on cement damage and implant rotation, compared to a situation in which the cement mantle is supported by mixed bone.

	Trabecular bone support	Cortical bone support
Cement damage	+ 331 %	- 20 %
Implant rotation	+ 25 %	- 6 %

not simulated in our models. However, it has been demonstrated that torque resulting from stair-climbing activities is the most detrimental load for cement mantle failure.² Moreover, implant subsidence may have been limited for the implant design we analyzed, considering it has a collar.

Our model was based on a single cross-section at the level of the lesser trochanter, not taking into account differences in the cross-sectional shape of other parts of the implants. However, our findings are similar to those of an FEA investigation of Massin et al.¹³ who used 3D FEA models of entire cemented reconstructions to analyze the effects of implant-cement bond and implant size. In that study, the proximal canal fill of implants were varied (100 - 90 - 80 - 70 % of the optimal fill). The results of that study showed that an optimal fill (large implant) increased the rotational stability. In addition, their results demonstrated that loads are mainly transferred in the proximal region of the reconstruction, which provides a further justification for our choice to perform analyses at the level of the lesser trochanter. Unfortunately, to our knowledge, no data are available on experimental mechanical testing or implant retrieval analysis to verify our findings against.

Regardless of the fact that only one level of the cemented reconstruction was analyzed, our results may to some extent have been dependent on the specific geometry that we used. We model a specific cross section of the CT data-set rather than creating an average shape, because we expected a specific geometry would enable our models to better differentiate between the various cases. We selected a “representative” cross-sectional from a previous study.¹⁸ This cross-section comprised typical features of line-to-line reconstructions, such as a thin cement mantle in the antero-medial region.¹⁸

An additional limitation to our study is the fact that we only analyzed the Charnley-Kerboull implant, although it is used most widely when performing line-to-line reconstructions.¹⁷ Consequently, our results and subsequent conclusions apply only for this implant. This choice limited the scope of our work, since we did not analyze design variations, such as implant shape and surface roughness. Such variations may have consequences for the implant-cement bond, implant subsidence and cement mantle abrasion. However, in our study, we assumed the stem was not bonded to the cement mantle from the start of the simulation, as several studies have shown that implant-cement debonding occurs relatively early in the life-span of a cemented reconstruction.⁴ In addition, implant surface roughness variations may affect cement mantle abrasion. For instance, polished, collarless implants may be more susceptible to subsidence and micromotions than collared implant with a high surface roughness, although they may produce less

abrasive wear debris.²³ These phenomena were not included in the current calculations.

In the models with an undersized stem and maximal cortical cement mantle support, we assumed all trabecular bone was filled with bone cement. This interdigitated region was represented in the FEA model by material properties of bone cement as a result of the lack of fatigue data on interdigitated cement, although its strength may be lower than that of pure bone cement.¹⁶ Therefore, our FEA model possibly over-predicted the mechanical properties of the cement surrounding the undersized stems in the case of maximal cortical bone support.

Based on the excellent survival rates,³⁰ one would expect a thick, intact cement mantle would be more advantageous than a cement mantle with defects. In contrast, our data indicate a canal-filling stem performs better than an undersized implant. This may be explained by the fact that, when using a larger implant, the loads applied to the implant are transferred over a larger stem-cement interface, reducing cement stresses and fatigue crack formation. In addition, direct load transfer from implant to femoral bone may further reduce the cement stresses. This suggests that decreasing the stem size to achieve a thicker cement mantle may not always be paying, at least not from a mechanical point of view. As such, our results give a possible explanation for the good results obtained by surgeons adhering to the line-to-line implantation technique.

Biologic factors such as postoperative bone remodeling and particle-induced osteolysis were not taken into account in our simulations. For instance, periprosthetic bone resorption may be more pronounced in reconstructions with canal-filling implants, thereby affecting the mechanical behavior. Furthermore, the larger number of cement mantle defects around canal-filling stems³⁸ may be detrimental *in vivo*, because they allow easier access of cement and polyethylene debris particles to the bone-cement interface, inducing osteolysis.¹¹ Hence, from this perspective, undersized stems would be beneficial. On the other hand, undersized stems caused full-thickness cement mantle cracks to occur earlier in the cement, thereby also creating early pathways for particles to reach the surrounding bone. Nonetheless, biological processes that play a role *in vivo* may provide an additional explanation why undersized stems are so successful, while in this study they were inferior to canal-filling stems.

Our data indicate trabecular bone support results in a mechanically inferior cement mantle. These data are consistent with those of Ayers and Mann,¹ who reported trabecular bone support elevated the stresses in cement mantle. This stresses the importance of the use of pressure lavage and adequate cement pressurization in order to achieve a maximal cement penetration into cancellous bone, if possible up to the stiff inner cortex.

In conclusion, our data suggest (1) undersized stems surrounded by a thick, intact cement mantle produce more cement fatigue cracks than canal-filling stems surrounded by a thin cement mantle, (2) large canal-filling stems rotate less than undersized stems, and (3) a cement mantle supported by trabecular bone produced more cement cracks and implant rotation than a cement mantle supported by cortical bone.

References

1. Ayers D, Mann K (2003). The importance of proximal cement filling of the calcar region: a biomechanical justification. *J Arthroplasty* 18(7 Suppl 1):103-109.
2. Bergmann G, Graichen F, Rohlmann A (1995). Is staircase walking a risk for the fixation of hip implants? *J Biomech* 28(5):535-553.
3. Janssen D, Aquarius R, Stolk J, Verdonshot N (2005). Finite-element analysis of failure of the Capital Hip designs. *J Bone Joint Surg [Br]* 87(11):1561-1567.
4. Jasty M, Maloney WJ, Bragdon CR, O'Connor DO, Haire T, Harris WH (1991). The initiation of failure in cemented femoral components of hip arthroplasties. *J Bone Joint Surg [Br]* 73(4):551-558.
5. Kaneko TS, Bell JS, Pejic MR, Tehranzadeh J, Keyak JH (2004). Mechanical properties, density and quantitative CT scan data of trabecular bone with and without metastases. *J Biomech* 37(4):523-530.
6. Kerboull L, Hamadouche M, Courpied JP, Kerboull M (2004). Long-term results of Charnley-Kerboull hip arthroplasty in patients younger than 50 years. *Clin Orthop Relat Res* 418:112-118.
7. Langlais F, Kerboull M, Sedel L, Ling RS (2003). The 'French paradox.' *J Bone Joint Surg [Br]* 85(1):17-20.
8. Lewis G (1997). Properties of acrylic bone cement: state of the art review. *J Biomed Mater Res* 38(2):155-182.
9. Lotz JC, Gerhart TN, Hayes WC (1991). Mechanical properties of metaphyseal bone in the proximal femur. *J Biomech* 24(5):317-329.
10. Malchau H, Herberts P, Eisler T, Garellick G, Soderman P (2002). The Swedish Total Hip Replacement Register. *J Bone Joint Surg [Am]* 84 Suppl 2:2-20.
11. Maloney WJ, Jasty M, Rosenberg A, Harris WH (1990). Bone lysis in well-fixed cemented femoral components. *J Bone Joint Surg [Br]* 72(6):966-970.
12. Mann KA, Gupta S, Race A, Miller MA, Cleary RJ, Ayers DC (2004). Cement microcracks in thin-mantle regions after in vitro fatigue loading. *J Arthroplasty* 19(5):605-612.
13. Massin P, Astoin E, Lavaste F (2003). [Influence of proximal stem geometry and stem-cement interface characteristics on bone and cement stresses in femoral hip arthroplasty: finite element analysis]. *Rev Chir Orthop Reparatrice Appar Mot* 89(2):134-143.
14. Murphy BP, Prendergast PJ (1999). Measurement of non-linear microcrack accumulation rates in polymethylmetacrylate bone cement under cyclic loading. *J Mater Sci Mater Med* 10(12):779-781.
15. Murphy BP, Prendergast PJ (2002). The relationship between stress, porosity, and nonlinear damage accumulation in acrylic bone cement. *J Biomed Mater Res* 59(4):646-654.
16. Race A, Miller MA, Ayers DC, Mann KA (2003). Early cement damage around a femoral stem is concentrated at the cement/bone interface. *J Biomech* 36(4):489-496.
17. Scheerlinck T, Casteleyn PP (2006). The design features of cemented femoral hip implants. *J Bone Joint Surg [Br]* 88(11):1409-1418.
18. Scheerlinck T, de Mey J, Deklerck R, Noble PC (2006). CT analysis of defects of the cement mantle and alignment of the stem: in vitro comparison of Charnley-Kerboul femoral hip implants inserted line-to-line and undersized in paired femora. *J Bone Joint Surg [Br]* 88(1):19-25.
19. Star MJ, Colwell CW, Jr., Kelman GJ, Ballock RT, Walker RH (1994). Suboptimal (thin) distal cement mantle thickness as a contributory factor in total hip arthroplasty femoral component failure. A retrospective radiographic analysis favoring distal stem

- centralization. J Arthroplasty 9(2):143-149.
20. Stolk J, Janssen D, Huiskes R, Verdonschot N (2007). Finite element-based preclinical testing of cemented total hip implants. Clin Orthop Relat Res 456:138-147.
 21. Stolk J, Verdonschot N, Murphy BP, Prendergast PJ, Huiskes R (2004). Finite element simulation of anisotropic damage accumulation and creep in acrylic bone cement. Eng Fract Mech 71:513-528.
 22. Verdonschot N, Huiskes R (1995). Dynamic creep behavior of acrylic bone cement. J Biomed Mater Res 29(5):575-581.
 23. Verdonschot N, Huiskes R (1998). Surface roughness of debonded straight-tapered stems in cemented THA reduces subsidence but not cement damage. Biomaterials 19(19):1773-1779.

cemented

hip arthro

Chapter 4

Why would cement porosity reduction be clinically irrelevant, while experimental data show the contrary?

Introduction

The longevity of cemented total hip arthroplasty (THA) is dependent on the quality of the cement mantle surrounding the implant. Cyclic loading may eventually lead to fatigue failure of bone cement and subsequent implant loosening, after which surgical intervention is required.^{12,15,16} To postpone revision surgery as long as possible, cementing techniques have been developed aimed at improving the quality of the cement mantle. Vacuum mixing of bone cement, for example, removes air inclusions from the cement during mixing, so that cement porosity is minimized and the strength of the cement mantle is increased. The benefit of porosity reduction for bone cement survival is mostly based on experimental findings. Results from laboratory bench tests have shown that the reduction of porosity increases the fatigue life of bone cement specimens.^{5,6,13,18,22} Lewis,¹⁸ for instance, found that porosity was more than ten times reduced by vacuum mixing, while the fatigue life increased more than two times compared to hand mixed cement.

In clinical practice, however, the effect of porosity reduction on the longevity of THA is subject to debate.

Ling and Lee³⁹ studied the long-term results of Exeter hip replacements and discovered a number of stems implanted with extremely porous cement, as a result of an alternative mixing technique. When the survivorship of this group was compared to that of the other replacements, they found no difference in clinical outcome and concluded that “porosity reduction is clinically irrelevant”. Moreover, the Swedish Hip Registry²⁰ has shown an increased risk for revision for the first 3.3 years postoperatively when applying the vacuum mixing technique instead of hand mixing. Technical mishandling was suggested as a potential explanation for the increased risk. Hence, no clear relation between porosity reduction and longevity was found.

The question arises as to why the effect of porosity reduction on the fatigue life of bone cement emerges so clearly from experimental testing, while clinical outcome studies fail to demonstrate a distinct difference. Experimental test specimens are very different in geometry from the *in vivo* cement mantle. *In vitro* specimens are mostly dog-bone shaped and are tested under uniaxial or bending loads, with rather homogeneous stress distributions in the cement. Irregularities, such as pores, will likely have a significant effect on the local stress distribution as these cause local stress concentrations. By reducing porosity, stress concentrations are minimized, which is beneficial for the fatigue life of the specimen. However, the cement mantle surrounding a hip implant has a much more complex shape. Stress singularities usually

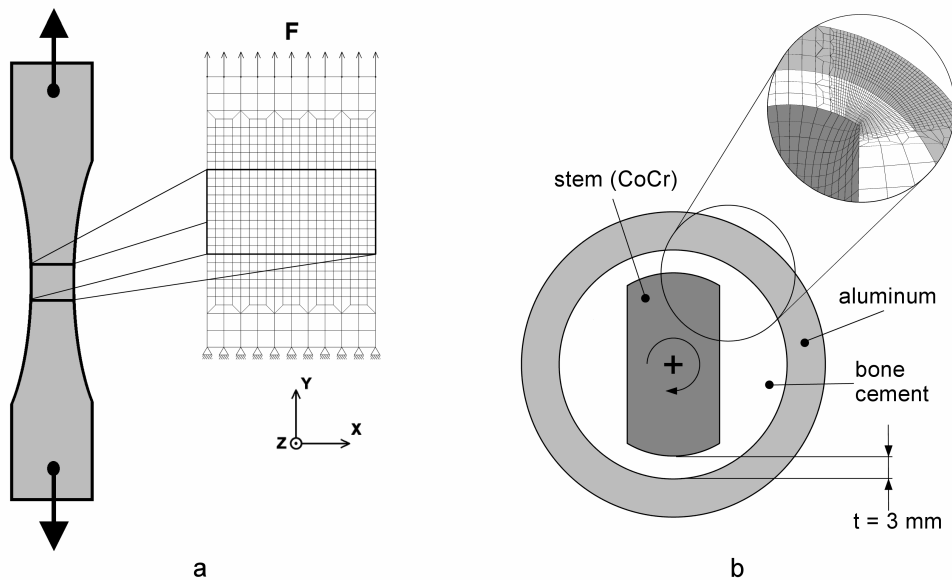


Figure 1: (a) Fatigue testing specimen with the FEA model that was analyzed. Creep and damage were modeled only in the mid-portion of the mesh. (b) Representation of the transverse slice model with a detail of the FEA mesh.

occur at locations around sharp corners of the implant, resulting in a widely varying stress distribution. The local stress-amplifying effect of a pore may be overshadowed by these stress singularities. Hence, porosity reduction may have a relatively small effect on the fatigue life of the *in vivo* cement mantle.

We hypothesized that the discrepancy in the effect of porosity reduction on the fatigue life of bone cement in test specimens and *in vivo* reconstructions is dependent on differences in the homogeneity of the stress distribution. Using finite element analysis (FEA), we analyzed the effect of porosity on fatigue life in models of a test specimen and a transverse slice of a reconstruction. For both models, we simulated fatigue failure for three different levels of porosity, as well as for a pore-free case, and compared the results.

Methods

Fatigue failure of bone cement was simulated using an FEA-based algorithm that incorporated creep and damage accumulation during cyclic fatigue loading. The algorithm was originally developed to study damage accumulation¹² within the cement mantle around femoral implants and was described in detail by Stolk et al.^{26,29} The algorithm incorporated a creep-law that was determined for Simplex P bone cement.³¹ The amount of creep was dependent on the local Von-Mises stress and the number of loading cycles.

The damage accumulation was based on Continuum Damage Mechanics.^{3,4,29} Micro-cracks, referred to as damage, were assumed to accumulate in the cyclically loaded material. The amount of damage that was formed was dependent on the S-N curve of the bone cement, in which the number of cycles to failure was expressed as a function of the local stress. An anisotropic damage approach was adopted, indicating that different amounts of damage could accumulate in different directions.

A macro-crack was assumed to occur once the amount of damage had locally reached a critical level in a certain direction. In that case, the stiffness of the cement, and thereby its load carrying properties, were reduced to virtually zero in the critical direction. A second and third crack could be formed perpendicular to the first. When three perpendicular cracks were formed, the stiffness was lost in all three directions, and the material locally lost its load bearing capability in all directions. The damage accumulation and subsequent macro-crack formation was monitored for each integration point in the cement individually. By failure of multiple adjoining integration points, cracks could propagate through the cement. The ratio of the actual number of loading cycles during a timestep and the number of cycles to failure determined the amount of damage that was formed during each time increment.

First, we applied the algorithm to a 3D FEA model of a specimen that is often used in tensile fatigue testing of bone cement (Figure 1a). We modeled only the mid-portion of the specimen (height = 3.2mm, 8 elements; width = 8 mm, 20 elements; and thickness = 3.5 mm, 8 elements), which is the region where failure occurs in experiments. The model was built of 8-node isoparametric brick elements and consisted of 4000 elements and 4789 nodal points. The cement was assumed to be isotropically linear elastic (Table 1). The model was constrained in the y-direction at the lower end, while at the upper end, a distributed load was applied in the y-direction. The displacement in the x and z-direction was constrained both at the top

Table 1: Material properties used in the FEA models.

Part of the model	Material	Elastic Modulus [GPa]	Poisson's ratio
Stem	CoCr	200	0.3
Cement	Polymethylmethacrylate	2.2	0.3
Ring	Aluminum	70	0.3

and at the bottom of the model to mimic the Poisson behavior of an actual fatigue testing specimen. Cyclic loading was simulated with a peak tensile stress level of 15 MPa. Creep and damage were only modeled in the mid-portion of the model. The simulation proceeded until structural failure occurred. The moment of structural failure was defined as the moment at which cracks had propagated over the full cross-sectional area and the specimen had lost its entire load bearing capabilities.

The second model represented a transverse slice of a cemented THA with a sharp-cornered stem (Figure 1b) and was previously used to study crack growth around a sharp-cornered stem.^{11,28} The model comprised a stem that was cemented in an 8 mm thick aluminum ring, with a minimal cement mantle thickness of 3 mm. The thickness of the transverse slice was 1 mm. The model was built of 8-node isoparametric brick elements with a 1 mm depth and consisted of 3496 elements and 7802 nodal points. The nodes on the front and back planes were fixed in the axial direction to obtain plane strain loading. The nodes on the outer rim of the ring were fixed in all directions. All materials were assumed to be isotropically linear elastic (Table 1). The cement–aluminum interface was assumed to be completely bonded, while the stem–cement interface was assumed to be debonded from the start of the simulation. Contact between the stem and the cement was modeled with a node-to-surface contact algorithm (MSC.Software Corporation, Santa Ana, CA). Friction was modeled with a coefficient of 0.25. The stem was loaded with a cyclic torque of 2.58 nm peak load. Two million loading cycles were simulated in the model. This caused identical cracks to propagate into the cement from the upper right and lower left corners of the stem. The length of the cracks after two million loading cycles was taken as a measure of structural failure.

In both models, the local stresses used in the fatigue failure simulation were spatially averaged using a stress concentration limiter.²⁸ By averaging the stresses, a stress distribution was obtained that was independent of the level of mesh refinement of the FEA-model. The effect of the averaging algorithm is governed by the critical distance, which determines the area over which the stress is averaged. This parameter was previously optimized²⁸ such that the crack propagation rates corresponded to those found experimentally.¹¹ The same critical distance was used for the current simulations.

Porosity was introduced into the models by assigning a near-zero stiffness to a number of elements. Levels of two, four, and nine volume percent porosity were applied. For both models and for each level of porosity, three different random pore distributions were created. A pore-free case was also analyzed for both models.

As we included physical pores in the models, we required an S–N curve of pore-free bone cement for the

simulations. Therefore, we used an adapted version of an S–N curve of hand mixed cement.²² The virgin S–N curve was obtained by mimicking fatigue experiments with hand mixed bone cement (personal communication²²), through FEA simulations with the fatigue testing specimen model. For this purpose, three different random pore distributions were introduced into the FEA model of the fatigue testing specimen. The porosity level was 9%, corresponding with the level of porosity in hand mixed cement. Fatigue simulations were performed at stress levels of 10 and 20MPa. Subsequently, the fatigue life returned by the simulations, defined as the number of cycles to structural failure, was compared with the actual fatigue life from experiments for hand mixed cement.²² Based on the differences between actual fatigue life and the fatigue life resulting from the simulations, the S–N curve that was used as input was adjusted. With this new S–N curve, these simulations were subsequently rerun. This process was repeated until a satisfactory correspondence between the simulated and experimentally established fatigue life was obtained. The resulting S–N curve was then used for all simulations.

For both the test specimen and THA transverse slice models, the stress distribution in the cement was monitored, as well as the amount of damage and the crack distribution. Furthermore, for the test specimen, the number of cycles to structural failure defined the lifetime of the specimen. For the transverse slice model, the crack length after two million cycles was taken as a measure of failure. The direction of the crack in the cement mantle was also determined. Differences between the porosity groups in the lifetime of the test specimen and in the final crack length in the transverse slice model were tested with a one way analysis of variance (with $p < 0.05$ for significance).

Results

Porosity caused elevated stress levels in the test specimen models of beyond 25 MPa, while in the pore-free model, the stress level was equal to the applied global stress level of 15 MPa. In all porous specimens, the high stress level was maintained until structural failure occurred. The highest stress level was found in the

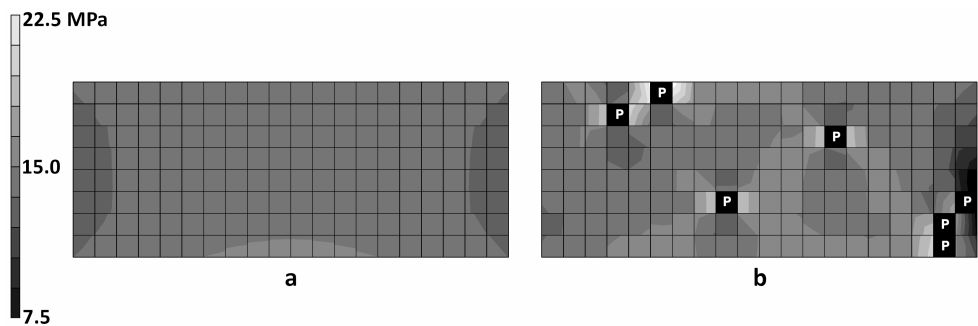


Figure 2: Initial maximum principal stress present in the model of the fatigue testing specimen (a) without porosity and (b) with a porosity level of 4%. Only the mid-portion of the model is displayed. Porotic elements are indicated with "P".

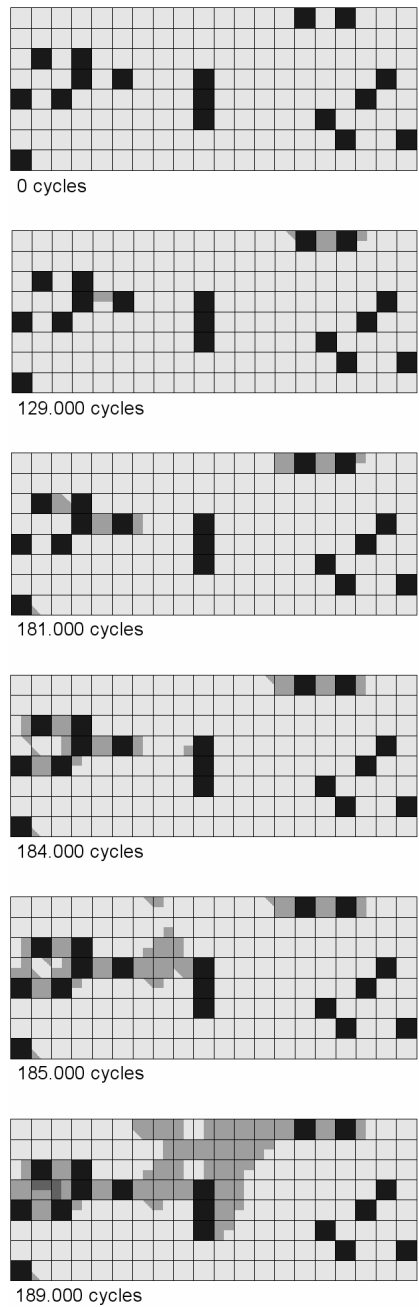


Figure 3: Crack development in the fatigue test specimen model with a porosity level of 9%. Only the mid-portion of the model is displayed. The black elements indicate pores; the dark gray areas represent cracks that are formed in the cement. Notice the cracks growing from pore to pore.

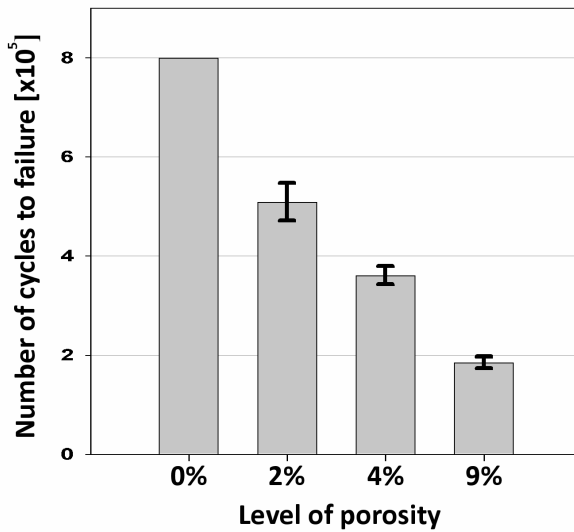


Figure 4: Number of cycles to structural failure of the fatigue test specimen model.

9% porosity specimens, with stresses up to 33 MPa. High stress concentrations were found around pores in the models (Figure 2a and b). Cracks were initiated at these locations and then grew to one another, creating larger cracks (Figure 3). This process continued until complete structural failure occurred. The number of cycles to failure was significantly dependent on the porosity level; by reducing porosity from 9% to 0%, the fatigue life of the specimen increased more than four times (Figure 4).

In the transverse slice model, little differences were found between the stress distributions for the different porosity cases. Local stresses were unaffected by the presence of pores (Figure 5a and b). At the start of the simulations in all models, the highest stress level occurred at the corner of the stem. A crack formed there that then propagated into the cement mantle, with the peak cement stress level in front of the crack tip during the entire simulation. With increasing crack length, the stress level at the crack tip was reduced, which slowed the crack propagation rate. Porosity had little effect on the crack direction (Figure 6a and b). The final crack length after 2 million cycles was approximately 1.2 mm for all models (Figure 7).

Discussion

In the current study, we investigated the effect of porosity reduction on fatigue failure of acrylic bone cement in two different FEA models. The aim was to determine whether the effect of porosity reduction on the fatigue life of bone cement would vary between different local stress distributions, as present in test specimens and THA reconstructions. Under homogeneous stress conditions, as present in test specimens, porosity had a large effect on the longevity, whereas in a stress field with singularities, as present around a hip implant, the life-time was independent of the level of porosity.

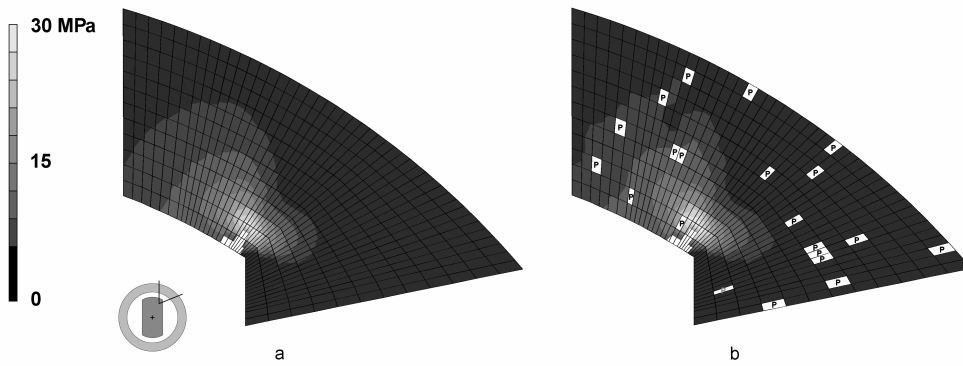


Figure 5: Peak stress distribution in the cement mantle of the transverse slice model after 8000 loading cycles, with (a) 0% porosity and (b) 4% porosity. Porotic elements are indicated with “P”. Only the upper right part of the cement mantle is shown. In both models, the white area at the corner indicates the crack that is formed in the cement.

Porosity was introduced into the models by assigning a near-zero stiffness to elements, which entailed that the shape of the pores in the models was hexahedral instead of spherical. Hence, the stress distribution around the pores in the models was most likely different from the stress distribution around pores in real bone cement. If the models were locally refined, each corner of such a pore would represent a singularity. However, since single elements cannot capture this singularity, from a numerical perspective, these corners did not exist in our models. This was beneficial for our modeling approach, but the question still remains whether the stress distribution around pores was well reflected by our models.

Timoshenko and Goodier³⁰ derived an analytical elasticity solution to calculate the effect of a small spherical cavity and found that the stresses are 2.045 times higher compared to a structure without the cavity. This theory was previously used by Harrigan and Harris to predict the stress level around an implant in case of the presence of a pore.⁹ In our models of porotic fatigue test specimens, the maximum principal stress around a pore was a factor of 1.5 increased with respect to the model without pores (Figure 2). The discrepancy between this factor and the factor derived by Timoshenko and Goodier is a consequence of the stress averaging procedure that was used in our study. In areas of high stress concentrations, stress averaging caused the local stress levels to decrease. Therefore, the stresses around the pores in Figure 2b are in the 20 MPa range rather than the 30 MPa range. However, Stolk et al. previously showed that to simulate a crack propagation that is mesh independent and that corresponds with experimental findings,¹¹ the stress averaging procedure should be used.²⁸

Another consequence of the manner of modeling porosity was that the S–N curve used in the damage simulation had to be adapted, as no suitable fatigue data of poreless PMMA was available. The adapted

S–N curve described the fatigue strength of theoretically pore-free bone cement. With the combination of this S–N curve and the pores in the models, the fatigue behavior at different porosity levels was mimicked. Experimentally determined S–N curves for hand mixed and vacuum mixed bone cement showed that the life-times were approximately 170,000 and one million cycles, respectively, at a stress level of 15 MPa.²² Previous porosity studies show that our 9% and 0% porosity cases roughly matched the level of porosity found in hand mixed and vacuum mixed cement, respectively.^{14,18,32} At these porosity levels, our test specimen model failed after 180,000 and 800,000 cycles, respectively. Thus, there was a high level of agreement between the experimentally determined life-times²² and those found in the current study.

Limitations existed in the simulations with the transverse slice model that should be noted. First, the geometry of the model was simplified compared with a real THA. Instead of the entire reconstruction, only a transverse slice at mid-stem level was modeled. Furthermore, the model was loaded with torque only. However, several studies suggest that a torque load causes the highest cement mantle stresses and the largest amount of damage *in vivo*.^{2,20,27} The limitations of our study affect the degree of correspondence of the model with a real reconstruction, but we were primarily interested in the effect of porosity reduction on the longevity of bone cement under different stress distributions. This model, although it was not entirely representative of a real THA, did allow us to analyze the effect of porosity reduction on the longevity of the cement mantle with a relevant stress distribution. We therefore believe that the model was suitable for the current investigation.

In the model of a transverse slice of a THA, a relatively sharp cornered stem was used. These sharp corners are unfavorable for the loading of the cement, since high stress concentrations are induced. Therefore,

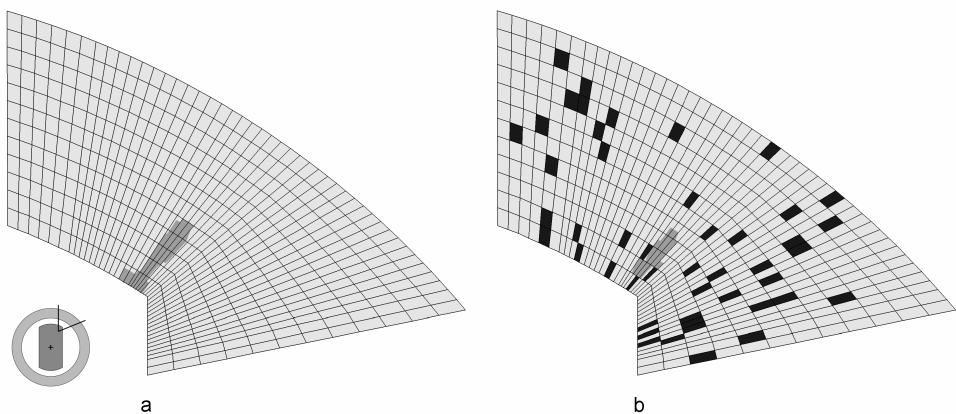


Figure 6: Crack in the cement mantle after two million cycles of loading in (a) the pore-free model and in (b) the transverse slice model with a porosity level of 9%. Only the upper right part of the cement mantle is shown. The dark gray area represents the crack in the cement; the porotic elements are colored black.

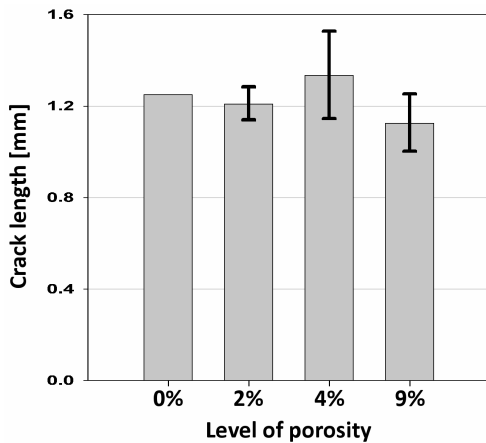


Figure 7: Length of the crack in the cement mantle of the transverse slice model after two million loading cycles.

sharp corners are avoided in most of the stems that are currently available, in order to reduce the stress singularities and to provide a more homogeneous stress distribution in the cement mantle. Our simulations with the test specimen models showed that under a homogeneous stress distribution, the effect of porosity reduction on the longevity of the cement specimens was substantial. Therefore, in stem designs that promote an equal load distribution, the reduction of porosity in the cement might be more relevant than in designs that cause high stress concentrations in the cement. The difference between the test specimens and the THA model found in this study might be smaller in such a case.

In this study we compared the effect of porosity on the fatigue life of bone cement in plain test specimens and in a transverse slice of a reconstruction by comparing the number of cycles to failure of the test specimen with the length of the crack that was formed in the cement mantle of the reconstruction. Preferably, we would have used the number of cycles to failure of the cement mantle in the transverse slice model as a measure. However, during the applied loading history, cracks reaching the full cement mantle thickness did not occur in any model. We therefore assumed that the level of failure could be indicated by the length of the crack that was formed in the cement mantle.

Besides fracture of the mantle, a real THA is subject to other failure mechanisms that were not simulated in our transverse slice model. One such mechanism is osteolysis, elicited by polyethylene or cement wear particles that migrate to the bone–cement interface where they activate macrophages.¹²

An effect of bone cement that has not been included in the current simulations is shrinkage. Shrinkage is proposed to result from polymerization of the cement,⁷ but may also be caused by the variations in the cement temperature during and after curing.^{1,24} In THA, shrinkage of the cement mantle around the stem causes residual circumferential hoop stresses, which can even cause pre-load cracks.^{17,23,24} Vacuum mixed cement shrinks more during curing than hand mixed cement.^{8,21} Therefore, in a real THA, the effect of

shrinkage may be more detrimental for reconstructions with a vacuum mixed cement mantle. If this is true, the beneficial effect of porosity reduction *in vivo* might be cancelled out by the increased residual stresses caused by the higher level of shrinkage. This could be another explanation for the fact that the effect of porosity reduction on the longevity of hip reconstructions is hard to demonstrate in clinical follow-up studies. In contrast, shrinkage does not cause high residual stresses in specimens for experimental testing since the deformation of the specimens is not restricted by an adjacent implant and a cancellation of the beneficial effect of porosity reduction does not occur.

Rimnac et al.²⁵ studied the effect of centrifugation on the fracture properties of acrylic bone cements. They performed experiments with notched and pre-cracked specimens and found that the fatigue crack propagation rate was not affected by centrifugation. This was attributed to the fact that the preliminary crack in the specimens produced a stress concentration that was more severe than that of any pore. Our FEA study supports this observation and quantifies the critical role of stress singularities in the *in vivo* cement mantle.

It can be concluded from our study that the effect of porosity reduction on the fatigue life of bone cement is dependent on the stress state present in the cement. The simulations with the fatigue testing specimen model indicate that under homogeneous stress conditions, porosity reduction increased the longevity of cement, which corresponds with findings from standard laboratory bench tests.^{6,13,18,22} In clinical practice, however, a homogeneous stress state does not occur. Failure of the cement mantle is governed by local stress singularities. In these situations the process of fatigue failure was not affected by the level of porosity. Our results show that the discrepancy found between cement survival in clinical and experimental studies can be explained by differences in the cement stress distribution.

References

1. Ahmed AM, Nair R, Burke DL, Miller J (1982). Transient and residual stresses and displacements in self-curing bone cement - Part II: thermoelastic analysis of the stem fixation system. *J Biomech Eng* 104(1):28-37.
2. Bergmann G, Deuretzbacher G, Heller M, Graichen F, Rohlmann A, Strauss J, Duda GN (2001). Hip contact forces and gait patterns from routine activities. *J Biomech* 34(7):859-871.
3. Chaboche JL (1988). Continuum damage mechanics: Part 1 - General concepts. *J Appl Mech* 55:59-64.
4. Chaboche JL (1988). Continuum damage mechanics: Part 2 - Damage growth, crack initiation and crack growth. *J Appl Mech* 55:65-72.
5. Davies JP, Burke DW, O'Connor DO, Harris WH (1987). Comparison of the fatigue characteristics of centrifuged and uncentrifuged Simplex P bone cement. *J Orthop Res* 5(3):366-371.
6. Dunne NJ, Orr JF, Mushipe MT, Eveleigh RJ (2003). The relationship between porosity and fatigue characteristics of bone cements. *Biomaterials* 24(2):239-245.
7. Gilbert JL, Hasenwinkel JM, Wixson RL, Lautenschlager EP (2000). A theoretical and experimental analysis of polymerization shrinkage of bone cement: A potential major source of porosity. *J Biomed Mater Res* 52(1):210-218.
8. Hamilton HW, Cooper DF, Fels M (1988). Shrinkage of centrifuged cement. *Orthop Rev* 17(1):48-54.
9. Harrigan TP, Harris WH (1991). A three-dimensional non-linear finite element study of the effect of cement-prosthesis debonding in cemented femoral total hip components. *J Biomech* 24(11):1047-1058.
10. Herberts P, Malchau H (1997). How outcome studies have changed total hip arthroplasty practices in Sweden. *Clin Orthop Relat Res* 344:44-60.
11. Hertzler J, Miller MA, Mann KA (2002). Fatigue crack growth rate does not depend on mantle thickness: an idealized cemented stem construct under torsional loading. *J Orthop Res* 20(4):676-682.
12. Huiskes R (1993). Failed innovation in total hip replacement. Diagnosis and proposals for a cure. *Acta Orthop Scand* 64(6):699-716.
13. James SP, Jasty M, Davies J, Piehler H, Harris WH (1992). A fractographic investigation of PMMA bone cement focusing on the relationship between porosity reduction and increased fatigue life. *J Biomed Mater Res* 26(5):651-662.
14. Jasty M, Davies JP, O'Connor DO, Burke DW, Harrigan TP, Harris WH (1990). Porosity of various preparations of acrylic bone cements. *Clin Orthop Relat Res* 259:122-129.
15. Jasty M, Maloney WJ, Bragdon CR, O'Connor DO, Haire T, Harris WH (1991). The initiation of failure in cemented femoral components of hip arthroplasties. *J Bone Joint Surg [Br]* 73(4):551-558.
16. Kawate K, Maloney WJ, Bragdon CR, Biggs SA, Jasty M, Harris WH (1998). Importance of a thin cement mantle. Autopsy studies of eight hips. *Clin Orthop Relat Res* 355:70-76.
17. Lennon AB, Prendergast PJ (2002). Residual stress due to curing can initiate damage in porous bone cement: experimental and theoretical evidence. *J Biomech* 35(3):311-321.
18. Lewis G (1999). Effect of mixing method and storage temperature of cement constituents on the fatigue and porosity of acrylic bone cement. *J Biomed Mater Res* 48(2):143-149.
19. Ling RS, Lee AJ (1998). Porosity reduction in acrylic cement is clinically irrelevant. *Clin Orthop Relat Res* 355:249-253.

20. Mann KA, Bartel DL, Wright TM, Burstein AH (1995). Coulomb frictional interfaces in modeling cemented total hip replacements: a more realistic model. *J Biomech* 28(9):1067-1078.
21. Muller SD, Green SM, McCaskie AW (2002). The dynamic volume changes of polymerising polymethyl methacrylate bone cement. *Acta Orthop Scand* 73(6):684-687.
22. Murphy BP, Prendergast PJ (2002). The relationship between stress, porosity, and nonlinear damage accumulation in acrylic bone cement. *J Biomed Mater Res* 59(4):646-654.
23. Nuno N, Avanzolini G (2002). Residual stresses at the stem-cement interface of an idealized cemented hip stem. *J Biomech* 35(6):849-852.
24. Orr JF, Dunne NJ, Quinn JC (2003). Shrinkage stresses in bone cement. *Biomaterials* 24(17):2933-2940.
25. Rimnac CM, Wright TM, McGill DL (1986). The effect of centrifugation on the fracture properties of acrylic bone cements. *J Bone Joint Surg [Am]* 68(2):281-287.
26. Stolk J, Verdonschot N, Huiskes R (2002). Can finite element based pre-clinical tests differentiate between cemented hip replacement stems according to clinical survival rates? Transactions of the 49th annual meeting of the Orthopaedic Research Society, New Orleans, LA, USA .
27. Stolk J, Verdonschot N, Huiskes R (2002). Stair Climbing is More Detrimental to the Cement in Hip Replacement than Walking. *Clin Orthop Relat Res* 405:294-305.
28. Stolk J, Verdonschot N, Mann KA, Huiskes R (2003). Prevention of mesh-dependent damage growth in finite element simulations of crack formation in acrylic bone cement. *J Biomech* 36(6):861-871.
29. Stolk J, Verdonschot N, Murphy BP, Prendergast PJ, Huiskes R (2004). Finite element simulation of anisotropic damage accumulation and creep in acrylic bone cement. *Eng Fract Mech* 71:513-528.
30. Timoshenko, S. P. and Goodier, J. N. (1970). Theory of elasticity. McGraw-Hill, New York.
31. Verdonschot N, Huiskes R (1995). Dynamic creep behavior of acrylic bone cement. *J Biomed Mater Res* 29(5):575-581.
32. Wang JS, Toksvig-Larsen S, Muller-Wille P, Franzen H (1996). Is there any difference between vacuum mixing systems in reducing bone cement porosity? *J Biomed Mater Res* 33(2):115-119.

ented tot
throplas

Chapter 5

The contradictory effects of pores on fatigue cracking of bone cement

Introduction

Porosity is generally considered to have an adverse effect on the survival of cemented total hip arthroplasties (THA). Therefore, new mixing techniques such as centrifuging and vacuum mixing have been introduced in the past with the objective to reduce air inclusions in the polymethylmethacrylate (PMMA) during mixing, thus improving the fatigue strength. The beneficial effect of porosity reduction on the fatigue life of bone cement has been shown in numerous fatigue experiments.^{4,5,12,14} Based on these experimental findings one would expect that a clear difference can also be found between the survival of implants cemented with hand-mixed versus vacuum-mixed cement. There is, however, only a small number of clinical studies on the effect of vacuum mixing. The Swedish Register has shown a beneficial effect of vacuum mixing on the long term,⁶ although a study by Ling and Lee disagrees with these findings.¹³ There seems to be a lack of convincing evidence for the beneficial clinical effect of porosity reduction, suggesting that the effect of a pore on the fatigue life of bone cement is different in an *in vivo* situation.

Topoleski et al.¹⁹ studied *in vivo* microcrack patterns in retrieved cement mantles with the objective to determine critical *in vivo* failure mechanisms. They found that pores in the cement clearly affected the fatigue crack propagation. In search of a more basic understanding of the material characteristics controlling fracture resistance, Topoleski et al. inspected *in vitro* fatigue fracture surfaces on a microscopic scale.²⁰ In this study, they found that pores acted as nucleation sites for microcracks. These microcracks accelerated the macrocrack propagation in the cement mantle. Remarkably, however, they also described

a beneficial effect of pores on the fracture properties of bone cement. They hypothesized that pores increase the damage zone in front of a macrocrack, thereby dispersing the crack energy and effectively “blunting” the crack, which slows down the macrocrack propagation in the cement mantle.

This hypothesis goes against the general belief that under all circumstances pores have a detrimental effect on the survival of bone cement. However, it may explain why the beneficial effect of porosity reduction methods in bone cement is less pronounced than anticipated from experimental findings. In this study we tried to simulate the effects of pores on fatigue failure of bone cement. For this purpose, we modeled a transverse slice of a THA in which we introduced pores. Using finite element analysis (FEA), we investigated whether we could identify the contradictory effects of pores on fatigue cracking of bone cement, as described by Topoleski et al.^{19,20} We furthermore tried to elucidate the underlying mechanical processes governing the type of effect of a pore on fatigue cracking and tried to assess under which circumstances pores would either have a beneficial or a detrimental effect on the mechanical survival of the cement mantle. These findings should explain why there is a discrepancy between clinical and experimental findings.

Materials and methods

The FEA model we used for this study was adapted from a model that was previously used to simulate cement crack growth.^{7,27} The current model represented a transverse slice of a cemented THA, comprising a metal stem with a fillet radius of 2 mm at the corners, surrounded by a layer of cement and a femur with a trabecular and cortical layer (Figure 1). The minimal cement mantle thickness was 3 mm, the trabecular and cortical layer had a thickness of 4 mm, and the thickness of the transverse slice was 1 mm. The stem was cyclically loaded with a torque load of 2.58 Nm for two million loading cycles. The cortical layer was fixed at its four quadrants such that rigid body displacement of the model was restrained, while allowing

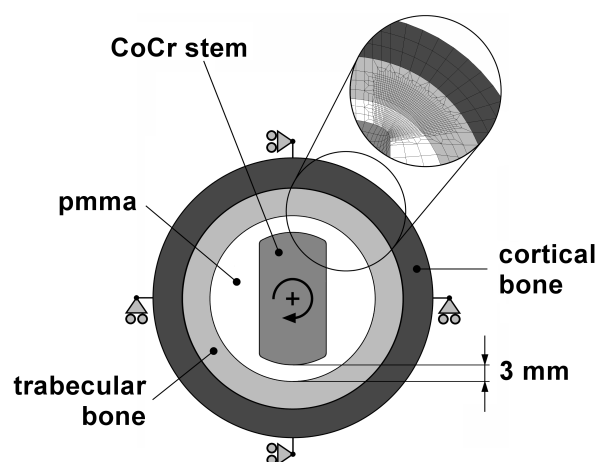


Figure 1: Schematic representation of the FEA model of a transverse slice of a THA, showing the constraints of the model and a detail of the upper right corner of the FEA model.

Table 1: Material properties used in the FEA models.

Part of the model	Material	Elastic Modulus [GPa]	Poisson's ratio
Stem	CoCr	200	0.3
Cement	Polymethylmethacrylate	2.2	0.3
Bone	Trabecular bone	1.0	0.3
	Cortical bone	17	0.3

deformation and expansion of the model (Figure 1). Because the model represented only a slice of a whole reconstruction, a plane strain state was assumed to be present. For this purpose, the nodes on the top and the bottom plane were fixed in the axial direction. We used eight-node brick elements to create our models to make them compatible with our damage algorithm.

Fatigue loading would cause identical cracks to propagate into the cement from the upper right and lower left corners of the stem. Crack propagation was simulated using an FEA algorithm that incorporated creep and damage accumulation. The algorithm was originally developed for testing according to the damage accumulation scenario,⁹ and has previously been described in detail by Stolk et al.^{16,18} The damage accumulation was based on a Continuum Damage Mechanics approach.^{2,3,18} In so-called S–N curves the number of cycles to failure was expressed as a function of the local stresses. As we included porosity in the models, we required an S–N curve of pore-free bone cement. We therefore used an adapted version of an S–N curve of hand-mixed cement derived by Murphy and Prendergast.¹⁴ The algorithm furthermore incorporated a creep-law that was determined for Simplex P bone cement by Verdonchot and Huiskes.²¹ The amount of creep was dependent on the local Von-Mises stress and the number of loading cycles.

All materials were assumed to be isotropically linear elastic (Table 1). Note that for the viscoelastic cement, this only holds for the elastic part of the material behavior. The cement–trabecular bone interface was assumed to be completely bonded, while the stem–cement interface was assumed to be debonded from the start of the simulation. Contact between the stem and the cement was modeled with a node-to-surface contact algorithm (MSC.Software Corporation, Santa Ana, CA). Friction was modeled with a friction coefficient of 0.25. The local stresses that were used in the simulation of fatigue failure were spatially averaged using a stress concentration limiter.¹⁷ In this way, a stress distribution was obtained that was independent of the level of mesh refinement of the FEA model.

We used the FEA model for two series of simulations. In a first series of analyses we introduced a large single pore in the FEA model. This pore had a circular shape, with a diameter of 1 mm. We varied the location of the pore in the cement mantle. With an initial fatigue simulation, we established the crack that would be formed in a pore-free the cement mantle. This crack was virtually straight, with a width of approximately one element, and almost entirely propagated through the cement mantle (Figure 2). We then reran the FEA simulation from the start (with no cracks present in the cement), with a pore at a

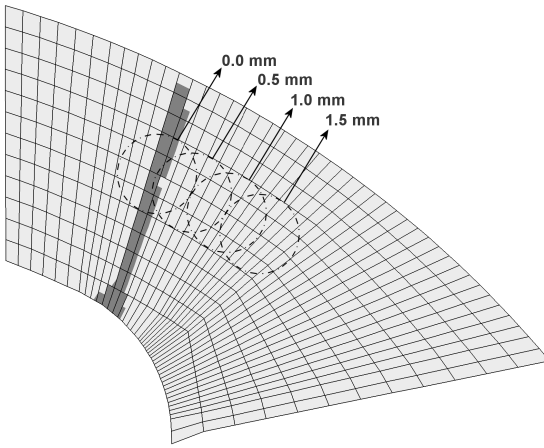


Figure 2: The upper right corner of the cement mantle of the pore-free model, showing the crack that was formed after two million loading cycles. The locations where a single large pore will be modeled in the cement mantle are indicated, together with the distance between the original crack and the pore.

distance of 0, 0.5, 1.0 and 1.5 mm from the crack path we found with the pore-free model (Figure 2). Using the results of the simulation with the pore-free model as a reference, we determined the effect of a pore in the cement mantle on the damage process.

In a second series of simulations, we analyzed the effect of multiple, smaller pores in the cement mantle. For this purpose, we generated random pore distributions in the cement at a porosity level of 2, 4, and 9%. In this series, pores were introduced by locally reducing the stiffness of randomly chosen elements to near zero. Therefore, the size of the pores was dependent on the size of the elements, which had varying dimensions, but they were not larger than approximately 0.40 mm in length or 0.20 mm in width. The size of a pore was furthermore dependent on the number of adjoining porotic elements. For each porosity level, we generated three different pore distributions and compared the crack formation in these models with that in the pore-free model.

Results

A single large pore present in the cement mantle clearly affected the crack propagation process, although the type of effect varied between the different models. In all models, the pore acted as a crack initiator. In the model with a pore located on the original crack path, the crack propagation was accelerated. This was caused by the elevated stress level in this model, due to the presence of the pore (Figure 3). After only 783,000 cycles, a full thickness crack was formed in the cement (Figure 4a). In the model in which the pore was located 0.5 mm from the original path, after 55,000 cycles, a secondary crack was initiated at the pore. The two cracks grew to one another, thereby deviating the primary crack from its original crack path (Figure 4b). The crack propagated further from the pore, but a full thickness crack was not reached. When the distance between the pore and the original crack path was increased to 1.0 mm, two secondary cracks

were initiated at the pore. However, in this model the primary and secondary cracks did not grow to one another. The secondary cracks in combination with the pore reduced the stress level in the cement (Figure 3), thereby slowing down crack propagation. After two million cycles the primary crack did not even reach halfway the cement mantle (Figure 4c). When the pore was placed at 1.5 mm from the initial crack path, also secondary cracks were formed at the pore, but the crack decelerating effect was less (Figure 4d).

In the models with multiple smaller pores, the effect of the pores on the crack formation was similar to that found in the models with a single pore. As in the models with a single large pore, in the second series of simulations cracks were initiated at pores in all models. Surprisingly, the level of porosity seemed to have no effect on failure of the cement mantle. The process was, however, affected by the distribution of the pores in the region of the stress intensity caused by the propagating primary crack. This resulted in a rather chaotic failure behavior in the different models. Therefore, we were unable to find a relation between the crack length or amount of damage and the level of porosity in the models. However, to clarify the phenomena that occurred, we will discuss three models displaying the typical effects of pores.

A model with 2% porosity displayed a crack accelerating effect. In this model a full thickness crack was formed after 1.7 million loading cycles, in contrast with the pore-free model mentioned before, in which the crack had not yet reached the full cement thickness after two million loading cycles. The primary crack went through two pores in the cement, accelerating the crack propagation (Figure 4e). A crack-deviating effect was found in a model with 4% porosity. In this model, a large pore was present due to the clustering of three porotic elements. The primary crack had deviated from its path and proceeded through this pore (Figure 4f). A full cement mantle thickness crack was not reached in this model. In a model with 9% porosity, a crack-decelerating effect was noticed. In this model, a primary crack was formed at a pore at the stem–cement interface. The propagation of this crack was slowed down by the formation of a secondary crack, which was also initiated at a pore at the stem–cement interface. These cracks grew to one another

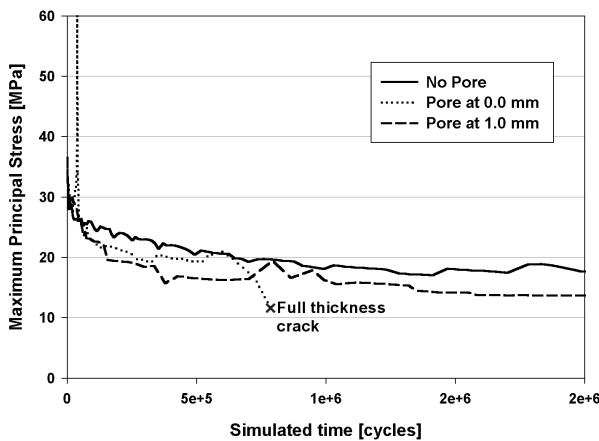


Figure 3: Maximum principal stress in the cement mantle in the pore-free model and in the models with a single large pore at a distance of 0.0 and 1.0 mm from the original crack.

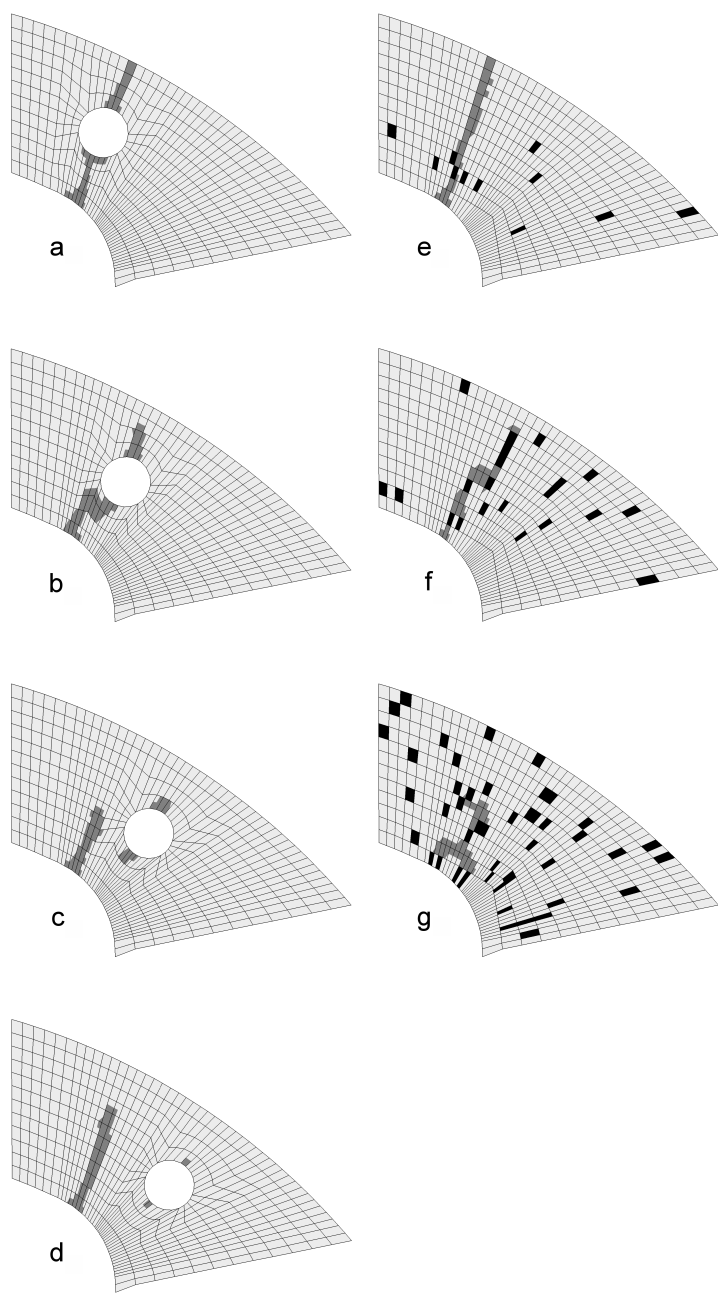


Figure 4: Crack formation patterns in the upper right corner of the cement mantle of the models with a single large pore at a distance of 0.0, 0.5, 1.0, and 1.5 mm from the original crack (a– d) and in models with a porosity level of 2, 4, and 9% (e– g).

and subsequently propagated towards a group of pores. The final crack after two million loading cycles reached approximately halfway the cement mantle thickness (Figure 4g).

Discussion

In this study we tried to simulate the effects of pores on fatigue failure of bone cement. Topoleski et al.^{19,20} found in their study that pores promote fatigue crack propagation and act as crack nucleation sites for microcracks. We were able to simulate the same effects in our models. Due to the stress elevating effect of the pores, in some cases, the crack propagation was accelerated and microcracks were initiated at pores in the cement.

In one of their articles,²⁰ Topoleski et al. furthermore stated the controversial hypothesis that pores may also act as crack decelerators, but they did not provide any evidence to support this hypothesis. The results of the current study, however, do support their hypothesis. In some of our models, the crack propagation was slowed down with respect to the crack propagation in the pore-free model, due to the presence of pores in the model. These results suggest that pores may both have a detrimental and a beneficial effect on the mechanical survival of bone cement.

We tried to elucidate which features govern the type of effect of a pore on the fatigue failure process. The results show that the effect was not dependent on the size of the pore, because similar effects were noticed both in the models with a large pore and in the models with smaller pores. We furthermore found that the level of porosity in the models with multiple pores was not associated with a particular type of effect on the crack propagation. However, we did find that the type of effect was dependent on the location of the pores within the stress field. When a pore was located directly on a crack path, the stress at the tip of a crack was elevated, which accelerated the crack propagation. When a pore was located in the neighborhood of the crack path, the distance of the pore to the crack path determined the effect of the pore. When a pore was sufficiently close to the crack, the elevated stress level deviated the crack from its path. If it was located a little further away from the crack, the pore was not able to deviate the crack, but slowed down the crack propagation. Due to the presence of the pore, the crack energy was dispersed, which in most cases caused secondary cracks to be formed at the pore. When a pore was located even further away, the effect of the pore on the crack propagation was diminished.

The mechanisms that determine the effect of a pore on the crack formation process in bone cement may give an explanation for the differences between experimental and clinical findings. In test specimens, typically, a homogeneous stress distribution is present. Discontinuities in the cement, such as pores, therefore evoke stress intensities and have a significant effect on the mechanical survival of a test specimen. This is the reason of the detrimental effects of pores emerging so evidently from fatigue experiments. However, the difference between the survival of implants inserted with hand mixed cement or vacuum mixed cement is less evident.^{6,13} In an *in vivo* cement mantle the stress distribution is inhomogeneous due to the nature of the external loads and the geometry of the cement mantle. In such a varying stress distribution the crack

formation process is ruled by local stress intensities, and therefore, the detrimental effect of pores may be less pronounced, while the beneficial effect of the pores may emerge. Therefore, some reconstructions may benefit from cement porosity, while others may not. In smaller clinical studies these two opposite effects may cancel out each other, and therefore a beneficial effect of porosity may only be demonstrated in a very large clinical study.

Besides the mechanisms described by Topoleski et al.,^{19,20} other factors may also influence the effect of porosity reduction in a clinical situation. James et al.,¹⁰ for instance, found higher concentrations of pores at the stem–cement interface than in the bulk cement. These higher concentrations were found in hand-mixed cement, but also in cement that was centrifuged. In another study, Race et al.¹⁵ found that fatigue cracks mainly originated at the bone–cement interface, which was attributed to trabeculae penetrating the cement mantle. These factors influence the crack patterns that are formed in *in vivo* cement mantles, and therefore, may affect the efficacy of porosity reduction. Such variations are beyond the scope of this article, but it should be possible to incorporate these in our FEA model and analyze their effects on the fatigue failure of the cement mantle.

Although we were able to simulate the effects of pores in a clinically relevant stress situation, there were some limitations to our models. The loading of the models was rather simplified with respect to *in vivo* loads. Furthermore, we only considered a transverse slice of a THA, rather than a model of an entire reconstruction. Thus, we tried to simulate a three-dimensional situation with a two-dimensional model. These simplifications made it possible to identify the different effects of pores on the crack propagation in the cement mantle, albeit that in our model the crack cannot pass the pore proximally or distally. We expect that in a three-dimensional model the same effects will be found, because in such a case the crack formation would still be ruled by stress intensities in the cement mantle. Therefore, the location of a pore with respect to local stress intensities would still determine its effect on the macrocrack propagation process.

Another difference between our model and the clinical situation was that *in vivo* preload cracks may exist, caused by a combination of shrinkage during curing and stress risers such as pores.¹¹ Furthermore, the process of crack formation may be dependent on the level of porosity at the stem–cement interface. Cooling of the stem prior to insertion generates extensive interface porosity, while by preheating, the level of interface porosity can be reduced.¹ Preload cracks and interface porosity affect the survival of cemented reconstructions to a certain extent. These phenomena were not explicitly included in our study. We do, however, believe that the effect of pores on cement cracking reflected by our study is similar to that *in vivo*, except for cases of excessive preload cracking or extreme levels of interface porosity. Due to the random pore distributions, in some cases pores were located at the stem–cement interface (Figure 4g). These cases, however, did not affect the overall conclusion of our study. Furthermore, because pores were introduced in a similar manner as cracks were simulated, we believe that preload cracks also would have a limited effect on the findings of our study.

A drawback in our simulation is that the tip of the simulated crack is not sharp, in contrast with models of others who have simulated crack propagation in bone cement.⁸ Therefore, the stress intensity at the crack tip in our models may be smaller than that at an actual crack tip. However, our damage algorithm was validated against experiments with bone cement,^{7,27} which gives an indication of the accuracy of the crack propagation in our models.

In the models with multiple pores, the pores had a square shape, because they were simulated by reducing the stiffness of entire elements, while actual pores are spherically shaped. Because the difference in the shape could possibly affect the mechanical behavior of the pores, we compared the stress distribution around square pores with the distribution around pores that were modeled such that they were spherical. The results showed that the stress distributions in both models were virtually identical.

Compared to the fractographic study by Topoleski et al.,²⁰ the material properties of the cement were simplified. They found that besides pores, other discontinuities in the material, such as BaSO₄ particles, also affected the crack propagation. They found that fatigue cracks tended to propagate through the interbead matrix, rather than through prepolymerized PMMA beads. In our study, we considered the bone cement to be isotropical and linear elastic. However, on a macroscopic scale, corresponding with the coarseness of our meshes, this is a justified assumption.

In this study, we tried to elucidate what governs the type of effect of pores on fatigue cracking of bone cement. We were able to simulate the effects of pores on fatigue cracking of bone cement reported by Topoleski et al.^{19,20} Moreover, we were able to provide evidence for the hypothesis that in some cases pores may also have a beneficial effect on the crack propagation.²⁰ We found that the location of a pore with respect to the crack path determines its effect on the crack propagation. The location of a pore in the local stress field therefore determines whether it has a beneficial or a detrimental effect on the mechanical survival of cement mantles. This phenomenon explains why the beneficial effects of porosity reduction in bone cement around THA components is less pronounced than anticipated from experimental findings.

References

1. Bishop NE, Ferguson S, Tepic S (1996). Porosity reduction in bone cement at the cement-stem interface. *J Bone Joint Surg [Br]* 78(3):349-356.
2. Chaboche JL (1988). Continuum damage mechanics: Part 1 - General concepts. *J Appl Mech* 55:59-64.
3. Chaboche JL (1988). Continuum damage mechanics: Part 2 - Damage growth, crack initiation and crack growth. *J Appl Mech* 55:65-72.
4. Davies JP, Burke DW, O'Connor DO, Harris WH (1987). Comparison of the fatigue characteristics of centrifuged and uncentrifuged Simplex P bone cement. *J Orthop Res* 5(3):366-371.
5. Dunne NJ, Orr JF, Mushipe MT, Eveleigh RJ (2003). The relationship between porosity and fatigue characteristics of bone cements. *Biomaterials* 24(2):239-245.
6. Herberts P, Malchau H (1997). How outcome studies have changed total hip arthroplasty practices in Sweden. *Clin Orthop Relat Res* 344:44-60.
7. Hertzler J, Miller MA, Mann KA (2002). Fatigue crack growth rate does not depend on mantle thickness: an idealized cemented stem construct under torsional loading. *J Orthop Res* 20(4):676-682.
8. Heuer DA, Mann KA (2000). Fatigue fracture of the stem-cement interface with a clamped cantilever beam test. *J Biomech Eng* 122(6):647-651.
9. Huiskes R (1993). Failed innovation in total hip replacement. Diagnosis and proposals for a cure. *Acta Orthop Scand* 64(6):699-716.
10. James SP, Schmalzried TP, McGarry FJ, Harris WH (1993). Extensive porosity at the cement-femoral prosthesis interface: a preliminary study. *J Biomed Mater Res* 27(1):71-78.
11. Lennon AB, Prendergast PJ (2002). Residual stress due to curing can initiate damage in porous bone cement: experimental and theoretical evidence. *J Biomech* 35(3):311-321.
12. Lewis G (1999). Effect of mixing method and storage temperature of cement constituents on the fatigue and porosity of acrylic bone cement. *J Biomed Mater Res* 48(2):143-149.
13. Ling RS, Lee AJ (1998). Porosity reduction in acrylic cement is clinically irrelevant. *Clin Orthop Relat Res* 355:249-253.
14. Murphy BP, Prendergast PJ (2002). The relationship between stress, porosity, and nonlinear damage accumulation in acrylic bone cement. *J Biomed Mater Res* 59(4):646-654.
15. Race A, Miller MA, Ayers DC, Mann KA (2003). Early cement damage around a femoral stem is concentrated at the cement/bone interface. *J Biomech* 36(4):489-496.
16. Stolk J, Maher SA, Verdonchot N, Prendergast PJ, Huiskes R (2003). Can finite element models detect clinically inferior cemented hip implants? *Clin Orthop Relat Res* 409:138-150.
17. Stolk J, Verdonchot N, Mann KA, Huiskes R (2003). Prevention of mesh-dependent damage growth in finite element simulations of crack formation in acrylic bone cement. *J Biomech* 36(6):861-871.
18. Stolk J, Verdonchot N, Murphy BP, Prendergast PJ, Huiskes R (2004). Finite element simulation of anisotropic damage accumulation and creep in acrylic bone cement. *Eng Fract Mech* 71:513-528.
19. Topoleski LD, Ducheyne P, Cuckler JM (1990). A fractographic analysis of in vivo poly(methyl methacrylate) bone cement failure mechanisms. *J Biomed Mater Res* 24(2):135-154.
20. Topoleski LD, Ducheyne P, Cuckler JM (1993). Microstructural pathway of fracture in poly(methyl

- methacrylate) bone cement. *Biomaterials* 14(15):1165-1172.
21. Verdonshot N, Huiskes R (1995). Dynamic creep behavior of acrylic bone cement. *J Biomed Mater Res* 29(5):575-581.

d total

plasty

Chapter 6

Experimental micro-mechanics of the cement-bone interface

Introduction

A mechanically stable cement–bone interface is essential for long-term viability of joint replacements that utilize cement fixation. Postoperatively the bone–cement interface may be immediately compromised due to cement polymerizing heat necrosis,²¹ the reaming process,⁷ or local monomer toxicity.¹⁶ Hence, a small layer of inferior tissue could develop between cement and bone that may make the interface more compliant, reduce its strength, and lead to early implant migration. However, relationships between these factors have not been established. In well-vascularized areas, necrotic bone may remodel into healthy bone,²⁴ resulting in direct bone–cement contact, though this bone may not be fully mineralized.^{9,13,22}

Under ideal conditions, the cement–bone interface may remain intact for years without an adverse biological response.¹¹ However, conditions are often compromised, leading to progressive interface failure accompanied by clinical radiolucencies, component migration, and pain. The exact mechanism for loosening is likely multifactorial with contributions from osteolysis and micromotion at the interface, bony changes due to stress adaptation and aging, and locally high fluid pressure.³⁰

A great deal is known about the strength of the cement–bone interface,^{3,4,6,17,29} but surprisingly little is known about its micro-mechanical behavior (local deformations, stress levels, and motions due to loading). The term micromotion is often used to describe the small motions that can occur between implant, cement, and bone, but these descriptions are often indicative of global motion between different components of the reconstruction.^{13,27} Which of the two materials (bone or cement) fails first and how failure is affected

by the quality and architecture of the (trabecular) bone and the cement interdigitation remain unknown. Further, substantial micromotion (via sliding and opening) at the intact interface might occur, thereby promoting particle migration. An understanding of deformations and motion that occur at the interface is important to understand the role of mechanical loading in the loosening process as this may influence, or be influenced by each of the mechanisms described above.

We utilized digital image correlation techniques to quantify the micro-mechanics of the cement–bone interface of laboratory-prepared cemented total hip replacements when subjected to quasistatic tensile and compressive loading. We addressed four research questions: (1) does the majority of deformation localize to the contact interface between cement and bone?; (2) is the interface more compliant in tension than in compression?; (3) does a relationship exist between interface compliance, interface contact area, and interface strength?; and (4) when loaded to failure, does the majority of damage occur at the cement or bone adjacent to the interface?

Materials and methods

Cement–bone specimens were created with interfaces that would represent those generated at the time of surgery for cemented total hip replacement. Six fresh-frozen proximal femurs were obtained from the SUNY Upstate Anatomical Donors Program (mean age, 74; range, 50–92, 4 male). Specimens were stripped of soft tissue, potted in an alignment fixture, and prepared for cementation of a femoral component. The femoral neck was cut about 1 cm above the lesser trochanter, the canal was broached for an Exeter implant, bottle-brush lavage with aggressive irrigation was used, and a distal plug was placed beyond the stem tip. To simulate endosteal bleeding conditions, the femur was immersed in a blood analog solution to just below the level of the cut. The blood analog was warmed to 37°C. Surgical bone cement (Simplex

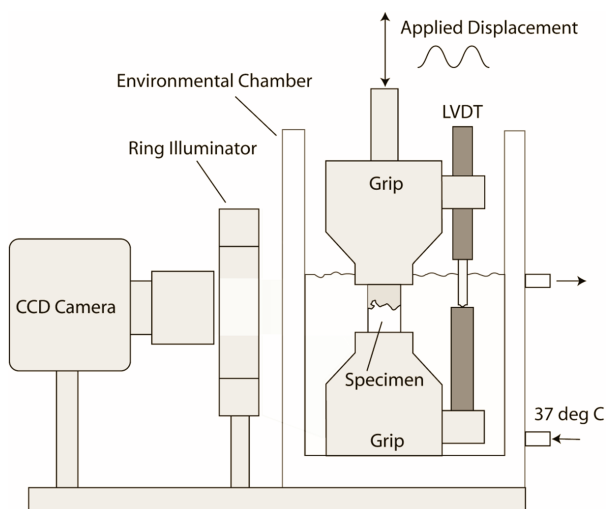


Figure 1: Schematic representation of the experimental setup used to capture deformation of cement/bone composites during mechanical loading.

P, Stryker Corp., Mawah, NJ) was mixed in an ACM mixer (Stryker Instruments, Kalamazoo, MI) for 2 min with vacuum (-580 mm Hg) applied for the final 90 s. Cement was introduced to the canal in a retrograde fashion when the cement reached a viscosity of 1000 Pa-s, the mantle was then pressurized, and a PMMA replica Exeter stem was inserted when the cement reached a viscosity of 2000 Pa-s. A replica Exeter stem was used to allow for adequate cement for gripping following sectioning.

Following cement cure for 4 days in the blood analog, parallel-piped specimens were prepared by transverse sectioning of the femurs using a water-irrigated diamond-bladed saw with further sectioning to produce cement/bone composite specimens that were nominally 5×10 mm in cross-section. These specimens were further machined with an end mill to insure that the faces were orthogonal. A total of 21 specimens were prepared using this protocol.

The mechanical testing apparatus consisted of a set of parallel grips housed in an environmental chamber into which the specimen was placed (Figure 1). An LVDT was used to measure grip displacements. Loading was provided by a screw-driven machine in displacement control at 0.5 mm/min; force was measured by an in-line load cell. Prior to testing, a black enamel paint was used to provide contrast and texture for one specimen face containing cement and bone. A digital camera (Spot RT) with 8.9 micron/pixel resolution and telecentric lens was used to capture surface images during loading at a frequency of 4 Hz. The image resolution of the tests was lower than that used for crack damage imaging (described later) because the field of view was larger, encompassing the entire specimen and edge of grips. The loading and camera images were synched via a TTL signal from the camera. Specimens were placed in the environmental chamber at 37°C, which was filled with circulating calcium buffered saline, and was allowed to equilibrate for 10 min before testing.

The initial testing consisted of fully reversible tension-compression loading for 10 cycles to ± 0.01 mm based on grip-to-grip displacement. This magnitude was chosen based on pilot work to insure that permanent damage did not occur. On the 10th full loading cycle, images were obtained of the specimen face, resulting in about 90 frames of data. Following this test, specimens were loaded in uniaxial tension to failure, defined as a 50% drop in peak load. The goal was to impart substantial damage to the specimen, while still allowing it to remain intact for postprocessing.

Commercial digital image correlation (DIC) software (RapidCorrelator, Xstream Software, Ottawa, Ontario, Canada) was used to determine displacements of discrete zones of the cement/bone composite specimens during loading. Displacement fields at discrete locations (40 by 40 pixels (0.12 mm²) in Figure 2) along the center line were determined. Relative displacements between adjacent markers were then calculated to indicate motion of the bone, contact interface, visible interdigitated region, and cement. At the contact interface, measurement squares were placed immediately above and below the interface. The RMS error for the DIC system using the LVDT as the standardized measurement device was 0.000395 mm. Visible interdigitated regions were not always evident on the image face. As such, displacements on the surface were measured at either four (11 specimens) or five (10 specimens) locations, depending on

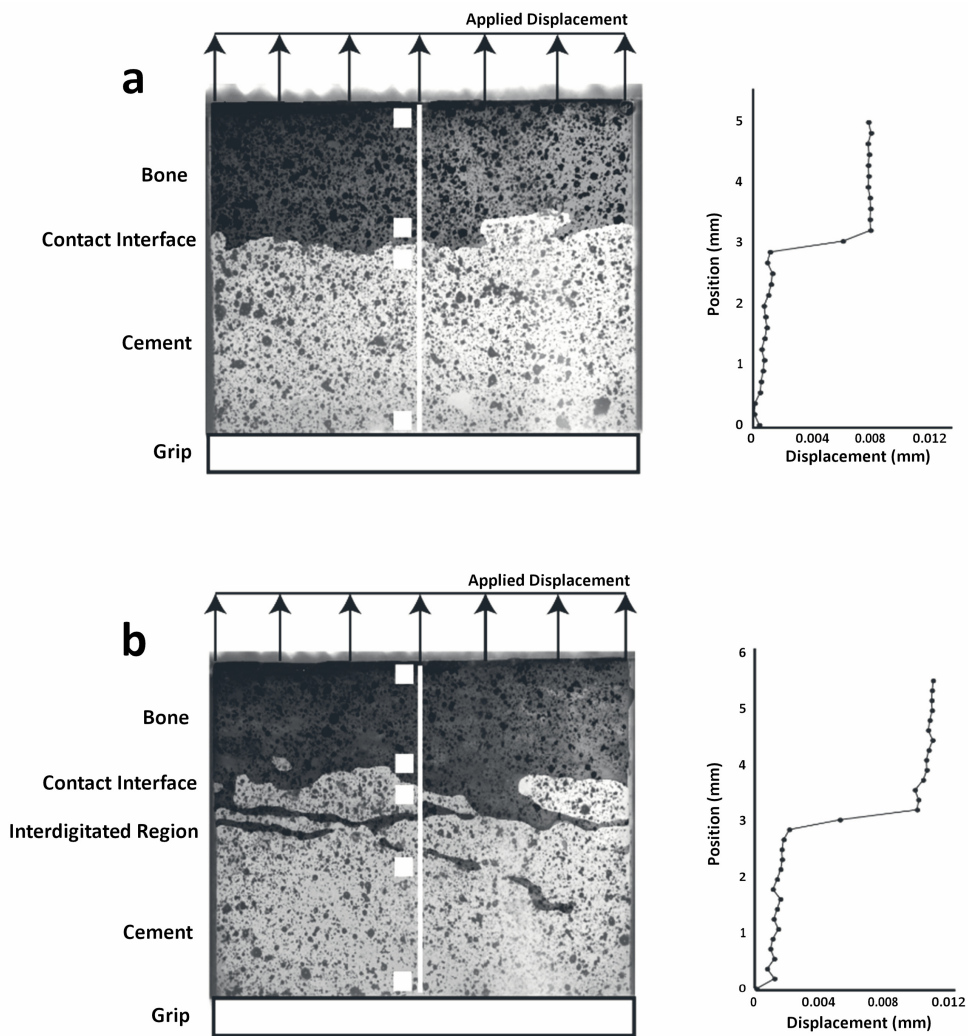


Figure 2: Digital images of specimens with contact interface (a) and interdigitated/contact interface regions (b) along the midline of the cement–bone interface. Graphs to the right represent vertical displacement fields along the white center line of the respective specimens with specimens loaded in tension (vertical direction). Sampling areas for digital image correlation measurements are shown as white squares indicating regions that span displacement measurements for bone, contact interface, interdigitated region, and cement.

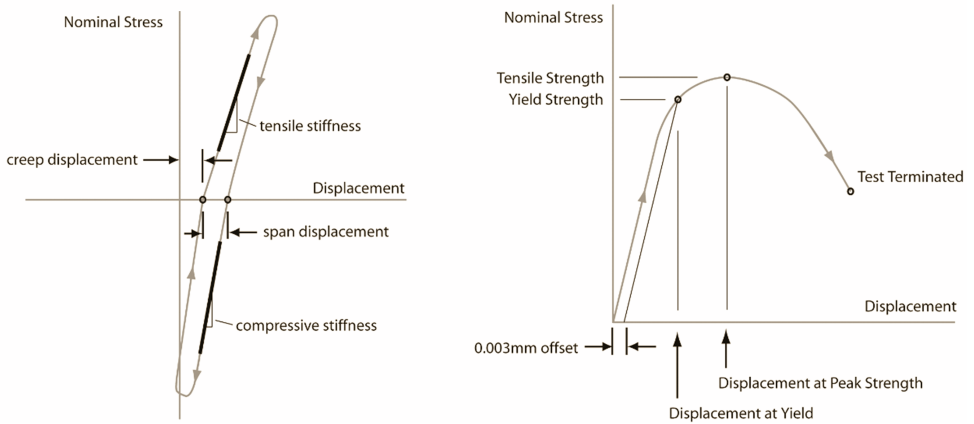


Figure 3: Descriptive measures for cyclic (left) tension-compression loading and single cycle tensile load-to-failure (right) experiments.

whether an interdigitated region was visible.

Using the DIC data, the local motion of the contact interface/visible interdigitated region was quantified for the cyclic nondestructive testing in terms of tensile compliance, compressive compliance, creep displacement at 10th loading cycle, and span displacement at 10th loading cycle (Figure 3). Apparent stress was calculated as force divided by cross-sectional area of the specimen. Strain was not determined because of material/interface discontinuities. For tensile tests to failure, yield strength was determined using a linear offset of 0.003mm (Figure 3). The displacement at yield, tensile strength, and displacement at tensile yield were also calculated.

To document microstructure, specimens were scanned at 12 μm isotropic resolution using a microCT (55 kV/ 145 mA, Scanco μCT 40, SCANCO Medical AG, Basserdorf, Switzerland) prior to loading. Interface contact area was estimated using MIMICS solid modeling software (Figure 4). First, cement and bone three-dimensional (3D) objects were created from the CT scan data by separately thresholding cement and bone regions based on CT gray scale intensity. The 3D cement object was then dilated by two voxels (24 μm), and the Boolean intersection between the cement and bone objects was determined. This volume was divided by the amount of the cement dilation operation (24 μm), resulting in an estimated contact area between cement and bone. This is only an estimate of contact area and is limited by the microCT resolution.

Prior to loading, to document initial bone damage, specimens were immersed in 0.1% calcein for 12 h followed by 10-min rinse in deionized water. Specimen surfaces were sanded to remove surface stain to reveal any microcracks. A fluorescent dye penetrant (Aquacheck, Sherwin Inc, South Gate, CA) was applied for 10 min followed by 10-min rinse. Epifluorescence imaging of all four specimen faces were collected at

5.8 μm resolution using a stereomicroscope with digital camera (Spot RT, Diagnostic Instruments, Sterling Hts., MI). Following loading, the staining and imaging process was repeated to document crack growth. Cracks in cement and bone were manually traced and measured (Image Pro, Media Cybernetics, Bethesda, MD) to document number, average length, and length sum of cracks for the four image surfaces. Crack measurements were divided into preexisting cracks (before loading), growth from preexisting cracks, new cracks, and total crack growth. Growth from preexisting cracks was defined as cracks extending from existing cracks or immediately adjacent to existing cracks. Crack numbers and average length were not calculated for the growth measures because cracks sometimes bifurcated from existing cracks and also grew diffusely adjacent to an existing crack. Images from the posttest specimens were superimposed over those from pretest specimens to differentiate between new and existing cracks.

Paired t-tests were used to determine if compliance was different in tension and compression. Linear regression analysis was used to determine relationships between interface compliance and strength, estimated interface contact area and strength, displacement at yield and yield strength, and compliance and contact area. Because compliance and contact area were not coupled, a stepwise regression was

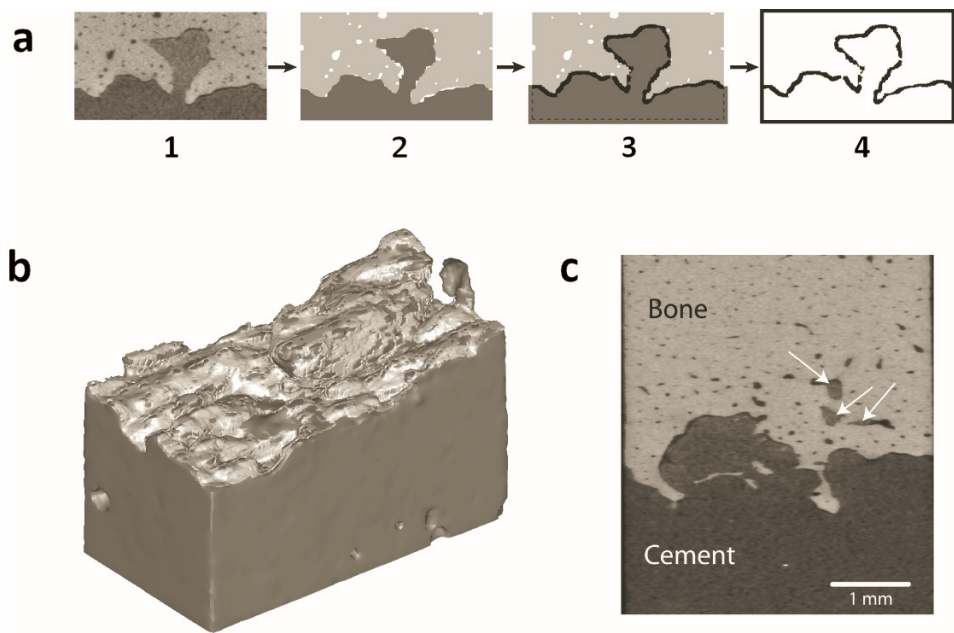


Figure 4: Approach used to estimate contact area between cement and bone (a): the initial microCT scan set (1) was segmented into cement and bone (2), followed by a region growing operation of the cement (3), and calculation of the Boolean intersection between cement and bone (4). A 3D reconstruction (b) of the cement (dark gray) and region of intersection with bone (light gray). Also illustrated (c) are regions of cement flow into lacunar scale spaces in the cortical bone (arrows).

Table 1: Fraction of total displacement attributed to various components of the cement-bone composite structure.

Component	Tension	Compression
Contact interface / interdigitated region	0.83 (0.19)	0.64 (0.28)
Cement	0.07 (0.08)	0.21 (0.20)
Bone	0.11 (0.16)	0.15 (0.17)

Measurements taken at maximum tension/compression stress levels during cyclic loading. Mean values for 21 specimens (standard deviation in parentheses).

performed to determine if both compliance and contact area contributed to specimen strength. Finally, paired t-tests with Bonferroni corrections for multiple sampling were used to determine if crack damage quantified (the length sum measurements) was greater in the cement or bone.

Results

The majority of the displacement during both tensile (83%) and compressive (64%) elastic loading occurred at the cement-bone interface (Table 1). A clear displacement jump or discontinuity between the cement and bone was indicated by the graphs of displacements along the center line of the specimens (Figure 2). In regions where there was visible interdigitation (the central region of Figure 2b), the displacement distribution became more complex with areas of displacement compatibility, indicating limited relative displacement between cement and bone.

The tension/compression load-displacement response (Figure 5) revealed hysteresis during the loading cycle. Displacements of bone and cement were small in comparison with the contact interface/interdigitation region and had relative displacements on the order of the RMS error of the DIC system. The total DIC excursions (from top of bone to base of cement) were lower in magnitude than the LVDT measurements, due to motion between the grips and the specimen and the outboard location of the LVDT that would exaggerate any off axis motion.

Specimens with surface evidence of a contact interface alone were delineated from those with a contact interface and an apparent interdigitated region (Table 2). All specimens had lower interface compliance in compression than in tension ($p = 0.0001$), and those with a visible interdigitated region were more compliant than those with only a contact interface ($p = 0.049$). For a 1 MPa applied stress, the mean opening and closing displacements across the interface were 0.0048 and 0.0036 mm, respectively. Limited creep deformation occurred between the 1st and 10th loading cycle (0.0008 mm), and hysteresis quantified using the span was about 0.003 mm.

The tensile strength of the specimens (Table 3) was negatively correlated with tensile interface compliance ($r^2 = 0.47$, $p = 0.0006$), indicating that specimens with less motion at the interface were stronger. In addition, tensile strength and the contact area between cement and bone were positively correlated ($r^2 = 0.48$, $p =$

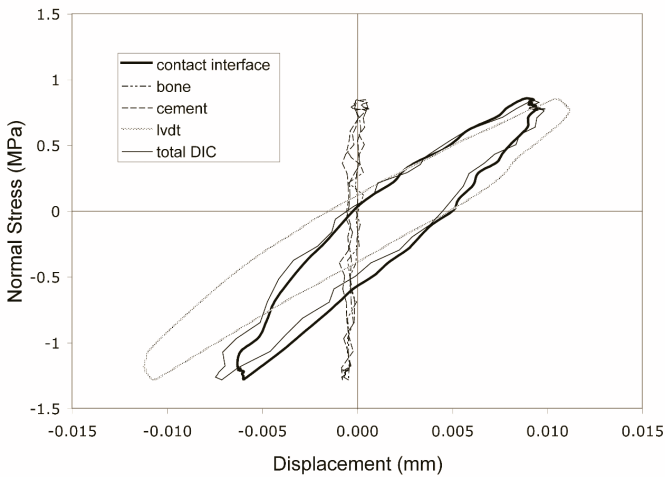


Figure 5: Example of cyclic nominal stress versus displacement response for the cement/bone composite structure. Total DIC displacement was measured from the top of the bone to the bottom of the cement and does not include the grips. The LVDT measurement indicates outboard displacements measured between the grips.

0.0005). Interestingly, compliance and contact area measures were very weakly correlated ($r^2 = 0.096$, $p = 0.174$). In a stepwise regression model, both interface compliance and contact area contributed to interface strength ($r^2 = 0.72$, $p < 0.0001$).

Interface displacement at yield ($0.014 \text{ mm} \pm 0.004 \text{ mm}$) was not a function of yield strength ($r^2 = 0.006$, $p = 0.737$, Figure 6), and this parameter exhibited a moderate coefficient of variation (0.3). The postyield response as measured by interface displacement at peak tensile strength ($0.041 \text{ mm} \pm 0.017 \text{ mm}$) had a variance four times greater than was found for the displacement at yield. These findings suggest that interface displacement at yield could be used as a failure criterion, given that it was independent of specimen strength and exhibited low variability.

Significantly more preexisting damage was found in the cement than bone and more total crack growth occurred in the cement as measured by crack length sum (Table 4). While virtually none of the bone crack

Table 2: Mechanical response of the contact interface/interdigitated region for nondestructive tension/compression loading.

Test parameter	Specimens exhibiting	Specimens exhibiting	All specimens
	contact interface (n = 11)	interdigitated region (n=10)	
Tensile compliance [mm/MPa]	0.0049 (0.0027)	0.0088 (0.0042)	0.0067 (0.0039)
Compressive compliance [mm/MPa]	0.0036 (0.0021)	0.0067 (0.0034)	0.0051 (0.0031)
10 th cycle creep [mm]	0.0011 (0.0024)	0.0006 (0.0025)	0.0008 (0.0024)
10 th cycle span [mm]	0.0026 (0.0013)	0.0036 (0.0019)	0.0031 (0.0017)

Mean (standard deviation) values are shown.

Table 3: Mechanical response of the contact interface/interdigitated region for tensile strength tests.

Test parameter	Specimens exhibiting contact interface (n = 11)	Specimens exhibiting interdigitated region (n=10)	All specimens
Yield strength (MPa)	2.54 (1.14)	1.92 (1.32)	2.24 (1.24)
Tensile strength (MPa)	3.38 (1.30)	2.64 (1.45)	3.03 (1.39)
Displacement at yield (mm)	0.013 (0.003)	0.016 (0.005)	0.014 (0.004)
Displacement at tensile strength (mm)	0.037 (0.014)	0.046 (0.019)	0.041 (0.017)

Mean (standard deviation) values are shown.

growth occurred from existing damage regions, 42% of the cement crack growth was from preexisting damage regions. Cracks were generally short (about 0.20 mm), but were more numerous in the cement compared to the bone.

Discussion

Our results show that the actual contact interface is responsible for the majority of motion of cement–bone structures when subjected to tensile or compressive loading. This interface is more compliant in tension than in compression, but even in compression, considerable closing motion occurs at the interface. To date, the compliance of the contact interface has not been considered in terms of modeling the load transfer in cemented implant applications.^{10,12} However, a simple exercise with a one-dimensional system can illustrate the potential relevance. Consider a 3-mm-thick cement mantle between stem and bone subjected to 1 MPa tensile load; a displacement of 1 mm would be attributable to the cement and nearly 5 mm attributable to the contact interface, based on our compliance measurements. Hence, inclusion of a realistic compliant interface is equivalent to reducing the cement modulus to 17% of a nominal level. Of course, load transfer is more complex than what is described here, but this clearly shows that micromotion

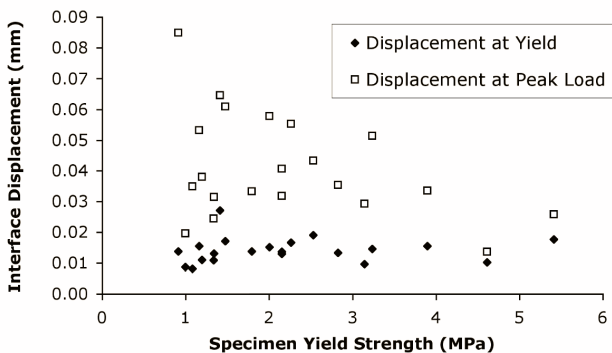


Figure 6: Displacement at yield and peak load as a function of specimen yield strength. The displacement at yield was not a function of yield strength ($r^2 = 0.006$; $p = 0.74$) and had much less variability than displacement at peak load.

Table 4: Crack number, average length, and length sum measurements for bone and cement micro-cracks

Type	Cement			Bone			p Value
	Crack number	Average length [mm]	Length sum [mm]	Crack number	Average length [mm]	Length sum [mm]	
Preexisting cracks	33 (21)	0.19 (0.05)	6.22 (4.20)	7 (6)	0.17 (0.10)	1.13 (1.02)	0.003
Growth from preexisting cracks			2.30 (2.33)			0.20 (0.43)	0.003
New cracks	25 (17)	0.13 (0.04)	3.30 (2.32)	10 (5)	0.26 (0.10)	2.48 (1.36)	0.129
Total crack growth			5.61 (3.49)			2.68 (1.40)	0.003

Measurements were made for preexisting cracks (prior to loading), load-induced growth from preexisting cracks, and load-induced new cracks.

Total crack growth is the sum of growth from preexisting cracks and new cracks.

Data presented are means (standard deviations) for 21 specimens.

p Values represent Bonferroni corrected paired t-tests between cement and bone with correction for multiple sampling to test for differences in length sum.

at the contact interface can markedly affect the load transfer mechanism.

Our study has limitations including the lack of biological reaction due to polymerization heat, trauma, and monomer toxicity. Moreover, neither incorporation of a long-term response of the bone due to the presence of the cement material, nor adaptation to a new loading environment was considered. The contact interface could become either more or less compliant with time *in vivo*, depending on multiple factors. To assess this possibility, test samples from retrieved hip reconstructions should be tested and compared with our *in vitro* results. We believe that our samples were nevertheless representative of the immediate postoperative environment; care was taken to simulate initial conditions through realistic bony preparation, cementing technique, and simulated surgical environment.

An additional limitation was that the fatigue damage response of the interface was not considered. Creep damage was previously documented under fatigue loading, but how this is manifested at the cement–bone interface is unclear. The microcrack generation in cement and bone as well as sliding and opening between cement and bone surfaces seen here under single-cycle failure loading may also occur under fatigue loading conditions. Additional experimental work is needed to delineate the role of micro-mechanical behavior and gross structural response under fatigue loading. In general, the cyclic loading response determined here, including hysteresis, should also occur in high-cycle fatigue tests.

That the strength of the cement–bone interface was correlated with the contact area between cement and bone was not surprising. Previous studies showed that interface strength can depend on appositional contact²⁰ or amount of bone interdigitated with cement.^{8,18} The morphology and orientation of the trabecular bone adjacent to the interface likely play a role in the strength and compliance of the visible interdigitated regions. Further work is needed to quantify trabecular structure, particularly in high stress

regions where failure would be expected. Interestingly, the apparent elastic modulus and strength of interdigitated cement/bone composites from vertebroplasty procedures was not a function of bone volume fraction, though a reduction in both strength and elastic modulus was noted when compared to bulk cement.²⁵

Dividing specimens into two groups, those that exhibit a visible interdigitated region and those that did not, provides only an approximation of the complete structure of the interface. All specimens had interdigitation to some degree. Because only surface displacements could be determined, the 3D deformation through the specimen is unknown. However, specimens with documented interdigitation had greater compliance compared to specimens exhibiting only a contact interface. This is reasonable because specimens with interdigitated regions had more surface discontinuities between cement and bone compared to the contact interface cases. Tensile stiffness of a cement–bone construct is related to tensile strength.²⁴ However, we showed that the opening motion at the interface was correlated with strength. The mechanism behind this relationship is unclear, but may be influenced by load transfer paths and relative interlock between cement and bone. This interlock was not quantified, other than contact area, but may relate to cement flow along the endosteal wall of the bone (Figure 4). Further work to identify factors contributing to interface compliance will likely rely on computational modeling to understand load transfer mechanisms and the role of bone/cement morphology, in combination with improved quantification of the interlock. Micro-interlock may also occur on another level where bone grows in apposition with the cured cement. Skripitz and Aspenberg showed that the cement–bone tensile strength can reach 0.9 MPa for naturally cured cement against cortical bone compared to limited strength (0.07 MPa) of polished cement placed against cortical bone.²⁸

Our ability to quantify apposition between cement and bone was limited by the resolution of the microCT scanner. Small interface gaps, about 1 to 2 voxels (12–24 μm) would likely not be detected due to partial volume effects in the thresholding operation. Because the dilation operation of the cement was 2 voxels, the estimated contact area will likely be high, thereby neglecting smaller gaps. Synchrotron source microCT may be capable of resolving submicron gaps, but was not available for our study. Even so, the potential for apposition between cement and bone was quantified and represents a reasonable representation of interdigitation.

Implementation of compliance to interface elements between cement and bone in finite element models using these new measures would not be difficult and could account for differences in tensile and compressive compliance.^{23,31} Two components of additional compliance might be needed: one for the contact interface and one for the interdigitated region. A displacement-based damage model could be implemented, which is appealing because displacement at yield was independent of interface strength. However, further work is needed with fatigue loading to develop a comprehensive damage model.

For our loading regime, damage occurred to both bone and cement. Interestingly, there was an appreciable amount of pretest damage to the cement possibly due to high residual stresses from shrinkage upon

curing.¹⁵ Pretest damage was recorded previously in laboratory-prepared cemented components.²⁶ Additional damage might have been induced from specimen preparation. However, bulk cement subjected to cutting does not exhibit such damage.²⁶ The load-induced damage occurred about 40% of the time from regions that had previously been damaged. The high prevalence of new damage from regions with existing damage suggests that residual stress-induced damage may be an important contributor to interface failure.

Interface motions on the order of 5 μm for a nominal 1 MPa load across the interface⁵ suggests that the interface can serve as a conduit for submicron size particles and as a mechanism to generate fluid pressures. Massin and colleagues¹⁹ showed that polyethylene particles can migrate around non-loosened cemented femoral components to the distal end of the mantle and suggested that they progress through porosity in cancellous bone. Particles might also move along the interface, aided by fluid motion upon loading. Local pressure generation is also possible at the interface given the conformity between cement and bone. Pressure related bone loss is well documented.^{3,2} The combination of fluid pressure, interface motion, and potential for the interface to act as a conduit for particles may lead to an osteolytic response.

In summary, (1) the vast majority (up to 83%) of the total motion is localized at the contact interface between cement and bone, (2) the interface compliance is higher in tension than in compression, (3) under tensile loading, the interface compliance is inversely proportional to the strength but only weakly correlated with contact area and, in addition, the strength is higher with increasing contact area, and (4) when loaded to failure most crack growth is in the cement rather than in the bone.

Acknowledgements

This work was funded by the NIH grant AR42017-11. Cement was donated by Stryker Orthopaedics.

References

1. Aspenberg P, Van d, V (1998). Migration, particles, and fluid pressure. A discussion of causes of prosthetic loosening. *Clin Orthop Relat Res* 352:75-80.
2. Astrand J, Skripitz R, Skoglund B, Aspenberg P (2003). A rat model for testing pharmacologic treatments of pressure-related bone loss. *Clin Orthop Relat Res* 409:296-305.
3. Balu GR, Noble PC, Alexander JW, Vela VL (1994). The effect of intramedullary reaming on the strength of the cement/bone interface. Transactions of the 40th annual meeting of the Orthopaedic Research Society, New Orleans, LA, USA.
4. Bugbee WD, Barrera DL, Lee AC, Convery FR (1992). Variations in shear strength of the bone-cement interface in the proximal femur. Transactions of the 38th annual meeting of the Orthopaedic Research Society, Washington, DC, USA.
5. Chang PB, Mann KA, Bartel DL (1998). Cemented femoral stem performance. Effects of proximal bonding, geometry, and neck length. *Clin Orthop Relat Res* 355:57-69.
6. Dohmae Y, Bechtold JE, Sherman RE, Puno RM, Gustilo RB (1988). Reduction in cement-bone interface shear strength between primary and revision arthroplasty. *Clin Orthop Relat Res* 236:214-220.
7. Garcia OG, Mombiola FL, De La Fuente CJ, Aranguiz MG, Escribano DV, Martin JV (2004). The influence of the size and condition of the reamers on bone temperature during intramedullary reaming. *J Bone Joint Surg [Am]* 86(5):994-999.
8. Graham J, Ries M, Pruitt L (2003). Effect of bone porosity on the mechanical integrity of the bone-cement interface. *J Bone Joint Surg [Am]* 85(10):1901-1908.
9. Gruen TA, McNeice GM, Amstutz HC (1979). "Modes of failure" of cemented stem-type femoral components: a radiographic analysis of loosening. *Clin Orthop Relat Res*(141):17-27.
10. Janssen D, Aquarius R, Stolk J, Verdonschot N (2005). Finite-element analysis of failure of the Capital Hip designs. *J Bone Joint Surg [Br]* 87(11):1561-1567.
11. Jasty M, Maloney WJ, Bragdon CR, Haire T, Harris WH (1990). Histomorphological studies of the long-term skeletal responses to well fixed cemented femoral components. *J Bone Joint Surg [Am]* 72(8):1220-1229.
12. Jeffers JR, Browne M, Lennon AB, Prendergast PJ, Taylor M (2007). Cement mantle fatigue failure in total hip replacement: experimental and computational testing. *J Biomech* 40(7):1525-1533.
13. Karrholm J, Borssen B, Lowenhielm G, Snorrason F (1994). Does early micromotion of femoral stem prostheses matter? 4-7-year stereoradiographic follow-up of 84 cemented prostheses. *J Bone Joint Surg [Br]* 76(6):912-917.
14. Kim DG, Miller MA, Mann KA (2004). Creep dominates tensile fatigue damage of the cement-bone interface. *J Orthop Res* 22(3):633-640.
15. Lennon AB, Prendergast PJ (2002). Residual stress due to curing can initiate damage in porous bone cement: experimental and theoretical evidence. *J Biomech* 35(3):311-321.
16. Lu JX, Huang ZW, Tropiano P, Clouet DB, Remusat M, Dejou J, Proust JP, Poitout D (2002). Human biological reactions at the interface between bone tissue and polymethylmethacrylate cement. *J Mater Sci Mater Med* 13(8):803-809.
17. MacDonald W, Swarts E, Beaver R (1993). Penetration and shear strength of cement-bone interfaces in vivo. *Clin Orthop Relat Res* 286:283-288.
18. Mann KA, Ayers DC, Werner FW, Nicoletta RJ, Fortino

- MD (1997). Tensile strength of the cement-bone interface depends on the amount of bone interdigitated with PMMA cement. *J Biomech* 30(4):339-346.
19. Massin P, Viguier E, Flautre B, Hardouin P, Astoin E, Duponchel B (2004). Migration of polyethylene debris along well-fixed cemented implants. *J Biomed Mater Res B Appl Biomater* 68(2):140-148.
 20. Miller MA, Race A, Gupta S, Higham P, Clarke MT, Mann KA (2007). The role of cement viscosity on cement-bone apposition and strength: an in vitro model with medullary bleeding. *J Arthroplasty* 22(1):109-116.
 21. Mjoberg B (1986). Loosening of the cemented hip prosthesis. The importance of heat injury. *Acta Orthop Scand Suppl* 221:1-40.
 22. Morberg PH, Johansson CB, Reigstad A, Rokkum M (2001). Vital staining of bone in stable, retrieved femoral surface replacement prostheses: a microscopic study of undecalcified ground sections. *J Arthroplasty* 16(8):1004-1009.
 23. Moreo P, Perez MA, Garcia-Amar JM, Doblare M (2006). Modelling the mixed-mode failure of cement-bone interfaces. *Eng Fract Mech* 73(10):1379-1395.
 24. Paul HA, Bargar WL (1986). Histologic changes in the dog acetabulum following total hip replacement with current cementing techniques. *J Arthroplasty* 2(1):71-76.
 25. Race A, Mann KA, Edidin AA (2007). Mechanics of bone/PMMA composite structures: an in vitro study of human vertebrae. *J Biomech* 40(5):1002-1010.
 26. Race A, Miller MA, Ayers DC, Mann KA (2003). Early cement damage around a femoral stem is concentrated at the cement/bone interface. *J Biomech* 36(4):489-496.
 27. Race A, Miller MA, Clarke MT, Mann KA, Higham PA (2006). The effect of low-viscosity cement on mantle morphology and femoral stem micromotion: a cadaver model with simulated blood flow. *Acta Orthop* 77(4):607-616.
 28. Skripitz R, Aspenberg P (1999). Attachment of PMMA cement to bone: force measurements in rats. *Biomaterials* 20(4):351-356.
 29. Stone JJ, Rand JA, Chiu EK, Grabowski JJ, An KN (1996). Cement viscosity affects the bone-cement interface in total hip arthroplasty. *J Orthop Res* 14(5):834-837.
 30. Sundfeldt M, Carlsson LV, Johansson CB, Thomsen P, Gretzer C (2006). Aseptic loosening, not only a question of wear: a review of different theories. *Acta Orthop* 77(2):177-197.
 31. Waide V, Cristofolini L, Stolk J, Verdonschot N, Boogaard GJ, Toni A (2004). Modelling the fibrous tissue layer in cemented hip replacements: experimental and finite element methods. *J Biomech* 37(1):13-26.

l6tot b

yt26lq

Chapter 7

Finite element simulation of cement-bone interface micro-mechanics; a comparison to experimental results

Introduction

Finite element analysis (FEA) is a valuable tool for investigation of the mechanical behavior of total hip arthroplasty. One of its main advantages is the ability to isolate clinical variables and study their effect on the mechanical behavior of reconstructions in a highly controlled manner. In the past, FEA has been used to analyze various aspects of total hip arthroplasty, such as implant migration,^{9,35} the effect of implant design and material on long-term mechanical survival,^{10,17,33} debonding of the implant-cement interface^{27,37} and micromotions at the implant-bone interface.^{29,32}

The fidelity of FEA studies depends on the accuracy and completeness of the experimental and clinical data that is used as input for the models. Much data is already available on the mechanical properties and behavior of implants, bone cement,^{18,25} the implant-cement interface^{5,22} and bone.^{12,13,34} Research on the cement-bone interface, however, has mainly been focused on the strength of the interface at an apparent level,^{1,2,6,7,25,26,21} while relatively little is known about the micro-mechanical behavior of the interface.

The cement-bone interface consists of complex structures of cement penetrating into the cortical bone structure and filling up inter-trabecular marrow spaces, thereby creating a highly variable interlock between bulk cement and bone. The cement-bone interface provides the fixation of the cement mantle in the femur. Hence, the stability of the cement mantle and the implant is directly dependent on the mechanical behavior of the cement-bone interface.

Recently, experiments have been performed to determine the micro-mechanical behavior of the cement-bone interface.²³ Small laboratory cement-bone specimens containing that interdigitated cement-bone interface were loaded in fully reversible tension-compression, while monitoring the local micromotion of the cement, bone and the cement-bone interface. The results showed that the majority of the displacement response localized at the cement-bone interface region. The cement-bone interface had a relatively low stiffness compared to that of the adjacent bone and cement, and the interface was more compliant in tension than in compression. Substantial hysteresis occurred during one tension-compression cycle. Upon failure loading, more cracks were found in the cement than in the bone, indicating that the cement is the weaker material at the cement-bone interface.

The goal of the present study was to assess whether realistic FEA simulations of cement-bone interface experiments could be performed in an effort to understand the micro-mechanics of this interface more thoroughly. For this purpose, FEA models were created based on micro-computed tomography (μ CT) data of the actual experimental specimens. These models included the complex interdigitated bone-cement morphology, with simulated frictional contact at the interface. We investigated the following hypotheses using μ FEA models of the cement-bone structures containing the interdigitated cement-bone interface: (1) μ FEA models can produce a cement-bone interface stiffness that is similar to experimental observations in both tension and compression loading; (2) Deformations of μ FEA models will localize to the cement-bone interface while the cement and bone will have a limited contribution to global deformation; (3) Including friction at the cement-bone interface will result in a hysteresis behavior similar to the experimental findings; (4) The quantity of cement at risk of fatigue failure is greater than that of bone.

Methods

The experimental protocol will be briefly reviewed since it served as a basis for the FEA simulations performed here. Ten cement-bone interface specimens were prepared from *in vitro* cemented total hip arthroplasties in fresh-frozen proximal femurs (six femurs, mean age 74, 4 male).²³ The reconstructions were prepared using third generation cementing techniques. Following cement cure, specimens containing the cement-bone interface were sectioned from the reconstructions (10x10x5 mm) and were scanned at an isotropic resolution of 12 μ m (Scanco μ CT 40, Scanco Medical AG, Basserdorf, Switzerland). The specimens were cut from various parts of the reconstruction (2 medial, 2 lateral, 3 anterior, 3 posterior), at different levels of the reconstruction (ranging from 40 to 110 mm below resection level).

The specimens were loaded for 10 cycles of fully reversible tension and compression, with a displacement

amplitude of 10 μm based on grip-to-grip displacement. The applied stress and local deformations were measured during the tenth cycle. The local deformations were measured using digital image correlation (DIC) techniques.²³ For each specimen twelve sampling points were taken: three columns of four sampling points located in the bone (two points) and the cement (two points) (Figure 1a). The experimental sampling points were chosen immediately adjacent to the interface and in the bulk of the cement and bone. Due to the large intra- and inter-sample variability, it was not possible to use equidistant sampling points, particularly in case of the contact interface. By tracking the displacements of these points, the deformation of the bone, cement and the cement-bone interface could be calculated separately. The results of the three columns were averaged to establish the 'global' deformations of the bone, cement and interface. Stress-displacement curves were generated from which the stiffness of the cement, bone and cement-bone interface in tension and compression were calculated, as well as the relative motion of the bone, cement and cement-bone interface. Finally, the hysteresis during one tension-compression cycle was determined, expressed as the horizontal span of the stress-displacement curve as it crossed the x-axis.

FEA models of the cement and bone were created based upon μCT data of the ten experimental specimens (Figure 1b) using image processing and solid modeling software (Mimics 11.1, Materialise, Leuven, Belgium). Segmentation of the μCT data was performed based on the local grayscale, which ranged from -1,000 to 3,071 (cement -100 to 999, bone 1,000 to 3,071). Gaps in the segmented data (due to high grayscale BaSO_4 in the cement or cavities in the bone) were filled manually. Region growing operations were performed on the cement and bone to exclude small particles that were not connected to the bulk cement or bone. After a Boolean subtraction operation between cement and bone to prevent initial mesh penetration, a

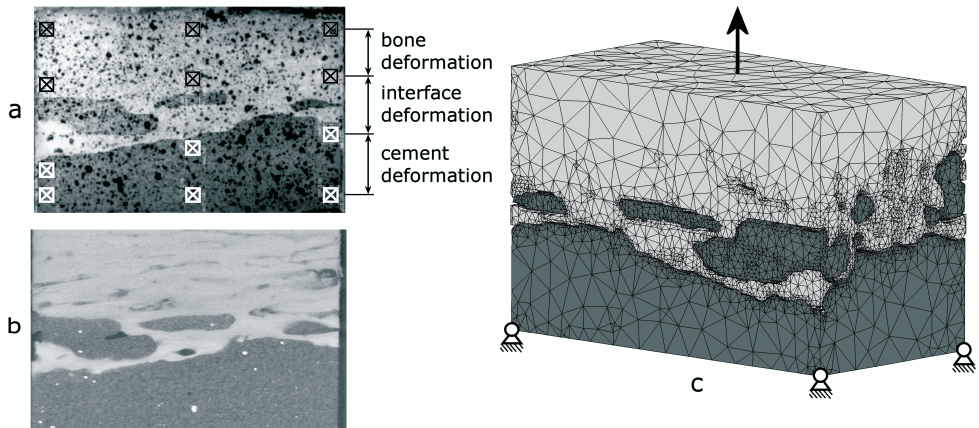


Figure 1: (a) Image of an experimental specimen in which 12 DIC sampling points are indicated, (b) μCT slice and (c) the FEA model of the cement-bone interface specimen.

one-voxel (12 μm) erosion operation was performed on the cement to prevent mesh penetration during the subsequent remeshing procedure. Triangular surface meshes were created for the bone and cement objects using a $6 \times 6 \times 6$ voxel interpolation (based on the original μCT data set) to limit the number of elements to a reasonable level for analysis. This entailed that the triangular surfaces were based on outer contours that were interpolated over six voxels in the transversal and longitudinal direction. During surface meshing, one iteration of smoothing was applied with a smooth factor of 0.5. The surface meshes were further remeshed to adjust elements with poor aspect ratios and further reduce the number of triangular elements (split-based remeshing, 2 iterations, min. edge length 7.5 μm , max. edge length 1.0 mm, max. geometrical error 15 μm). The meshes were then exported to an FEA pre-processor for solid modeling (Patran 2005r2, MSC Software Corporation, Santa Ana, CA, USA). The resulting models (cement and bone) consisted on average of approximately 300,000 tetrahedral elements and 71,000 nodal points (Figure 1c). All models were aligned with the experimental orientation based on digital images that were taken for the DIC-measurements during the experiments.

The bone and cement were considered to be linear elastic materials. The bone material properties were assigned based upon the μCT grayscale values. The elements were mapped back to the original μCT -data set, after which the weighted average of the grayscale was calculated for each element (Mimics11.1, Materialise, Leuven, Belgium). The element grayscale values were converted to equivalent HA-densities by means of a calibration phantom. Subsequently, a linear relationship between the HA-density and the Young's modulus was assumed,¹⁹ resulting in bone stiffness values ranging from 0.1 to 20,000 MPa ($\nu = 0.3$). The cement was assumed to have constant material properties ($E = 3,000$ MPa; $\nu = 0.3$).

Contact between the cement and bone was modeled using a double-sided node-to-surface contact algorithm (MSC.Marc2007, MSC Software Corporation, Santa Ana, CA, USA). Contact between the cement and bone was assumed to be debonded from the start of the simulation, meaning that tensile loads could only be transferred over the interface by means of an interlock of the cement and bone, rather than by a gluing capacity of the cement. Friction at the interface was modeled using a bilinear Coulomb friction model, assuming a friction coefficient of 0.3.

The gap at the interface between the cement and bone was quantified for the original segmented μCT data and the tetrahedral FEA models. A stereology approach was used in which the gap between the cement and bone was measured at 32 equidistant (1.0 mm spacing) locations over the surface of the interface for each specimen. The gap was measured using image processing software (Mimics 11.1, Materialise, Leuven, Belgium) with a resolution of 10 microns. A scatter plot was created for the μCT and FEA data to allow comparison between the nature of the gap distributions measured and simulated at the interface. The difference between the μCT and FEA gap measurements on a point-by-point basis was used to determine the error in the mesh generation procedure.

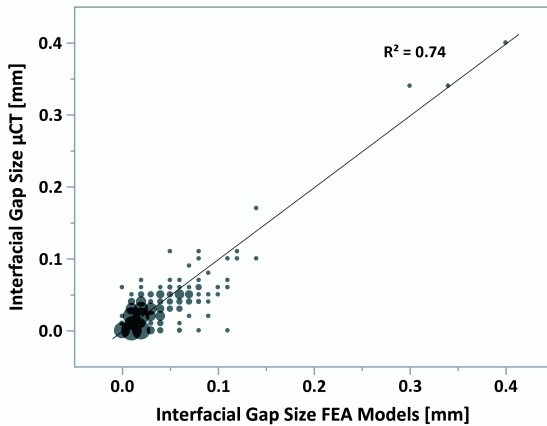


Figure 2: Bubble plot for measurement of gaps at the cement-bone interface from μ CT scan data and the FEA mesh, with bubble size proportional to the number of measurements. Data are based on 32 sampling points per specimen using a stereology approach.

The models were loaded for a cycle of fully reversible tension and compression, mimicking the experimental protocol. During the simulation, the distal end of the cement was fixed in all directions, while the proximal end of the bone was displaced in the longitudinal direction (Figure 1c). The displacements were applied to a node rigidly linked to all nodes of the proximal bone surface. This restricted tilting of the bone, while allowing for displacement in the transversal directions. The experimental results indicated that during tension-compression loading of the specimens slip had occurred at the grips. We therefore decided to load the specimens based on the applied apparent stress levels, rather than to apply a displacement amplitude of 10 μ m. Thus, the proximal end of the bone was displaced with incremental steps of 1.0 μ m until the maximal levels of tension and compression measured during the experiment were reached.

Stress-displacement curves were calculated by mimicking the experimental DIC-measurements. The twelve sampling points (Figure 1a) were reproduced in the FEA models to calculate the deformations of the bone, cement and the cement-bone interface. To allow for settling of the contact algorithm, the first part of the loading curve (from zero to full tension) was ignored. The subsequent full tension-compression cycle was used for analysis of the results.

From the calculated stress-displacement curves, the stiffness of the cement-bone interface in tension and compression were calculated, as well as the relative motion of the bone, cement and cement-bone interface and the horizontal span of the curve. We furthermore investigated whether there was a correlation between the contact area and the stiffness in tension and compression. The contact area was calculated previously from μ CT data of the specimens.²³ The stress distributions in the bone and cement were calculated at maximum tension and compression loading state. The stress distributions were normalized and expressed in terms of the applied apparent stress level. Additionally, the volumes of bone and cement at risk for fatigue failure were calculated. As a fatigue limit for bone and cement, the stress level was taken at which failure would occur after 1.0 million loading cycles (10 and 60 MPa for cement and bone, respectively).^{3,25}

Results

The correlation plot showed a similar pattern for the μ CT and FEA mesh stereology measurements of gap distribution at the cement-bone interface (Figure 2). The FEA mesh tended to underestimate the amount of the interface in direct contact (0 micron gap) when compared to the μ CT (7.1% vs. 27.8% of all measurements). However, both had similar distributions (33.7% FEA mesh vs. 36.8% μ CT) with gaps less than or equal to the scanner resolution (12 microns). The difference between the FEA and μ CT interfacial gap was not normally distributed (Kolmogorov-Smirnov normality test). Results are therefore presented by the median and first and third quartile values. The median error was zero microns with first and third quartile errors of -10 microns and 20 microns, respectively. The range of errors was from -60 to 110 microns, but these were outliers in the data. In point-by-point comparison, 61% of all measurements differed by less than 10 microns for the μ CT when compared to the FEA mesh.

The stress-displacement curves predicted by the FEA simulations were similar to those found experimentally (Figure 3). In most cases there was a horizontal shift of the experimental and computational curves with respect to the zero point, caused by settling of the contact algorithm in the FEA models and by running-in phenomena during the first nine cycles of the experimental specimens.

Consistent with the experimental findings, the predicted FEA stiffness of the interface was higher in compression than in tension, although the FEA tension/compression ratio was somewhat higher than found experimentally (Table 1). There was a weak positive correlation between the stiffness in tension and compression predicted by the FEA simulations and the experimental stiffness ($r^2 = 0.37$, Table 2). The average error between the computational and experimental stiffness was 8.3% and 29.8% in tension and compression, respectively. FEA models in which the stiffness in compression did not correlate well with the experimental stiffness did not automatically also have a weak correlation in tension, and vice versa. There was a weak correlation between the FEA predicted stiffness in tension and compression and the contact area of the specimens ($r^2 = 0.29$ and $r^2 = 0.16$, respectively; Table 2), which was similar to the experimental

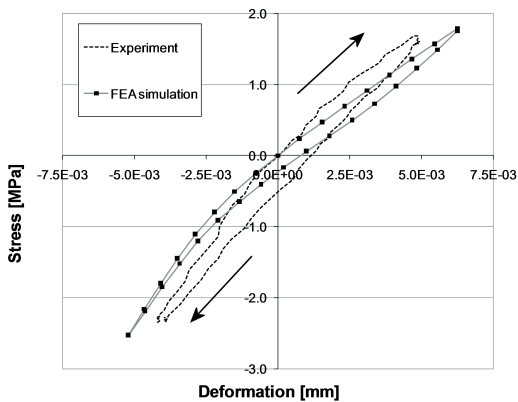


Figure 3: Experimental and computational force-displacement at the contact interface of a single specimen. The arrows indicate the loading direction. For illustrative purposes, the experimental and computational curves have been shifted to make them pass the point of zero stress and displacement.

Table 1: Comparison of experimental and FEA compression/tension stiffness ratio, span, and relative deformation of cement-bone contact as percentage of the total deformation. Mean and standard deviation values are shown for the 10 specimens (standard deviation in parentheses).

Test Parameter	Experiments	FEA
Compression/tension stiffness ratio [-]	1.35 (0.12)	1.66 (0.39)
Span [μm]	2.52 (1.36)	1.66 (1.44)
Relative deformation in Tension [% of total]	88.8 (8.7)	88.2 (12.2)
Relative deformation in Compression [% of total]	87.3 (10.3)	81.9 (14.9)

findings ($r^2 = 0.21$ and $r^2 = 0.21$ for experimentally measured tension and compression, respectively).

The experimental results showed that both in tension and compression the majority of the deformation (more than 80%) took place at the cement-bone interface (Table 2). Similar interface deformations were predicted by the FEA simulations (Table 2). In the experiments the bone deformed more than the cement, both in compression and tension, while in the FEA models the cement deformed more than the bone (Figure 4).

Similar to the experiment, the FEA models predicted a horizontal span in the stress-displacement curve (Figure 3). The frictional phenomena simulated at the cement-bone interface of the FEA models tended, however, to underestimate the horizontal span that was found experimentally (Table 1).

Table 2: Stiffness of the cement-bone interface in tension and compression, as measured experimentally and predicted by the FEA simulations. The contact area is given as a measure for the level of cement-bone interdigitation.

	Tensile stiffness [MPa/mm]		Compressive stiffness [MPa/mm]		Contact area [mm^2]
	Experimental	FEA	Experimental	FEA	
1	60	81	86	97	103
2	113	133	165	171	68
3	127	45	170	112	35
4	136	191	195	390	43
5	213	323	249	585	94
6	214	319	316	467	91
7	217	267	208	496	68
8	270	296	314	408	100
9	283	110	354	165	37
10	346	282	458	438	169

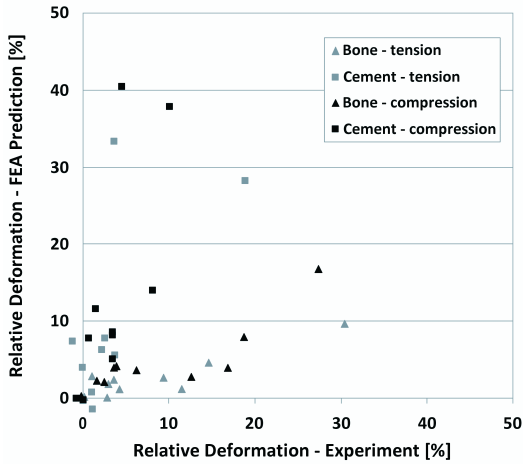


Figure 4: Experimental versus FEA predicted deformation of the bulk cement and bone. The deformations are expressed relative to the total deformation of the cement-bone interface specimens.

Highly stressed areas of the cement and bone indicated regions at the interface where loads were transferred between the cement and bone (Figure 5). At the maximum tension loading state, the maximum principal stress was higher than the applied stress level in 70% of the bone volume and in 63% of the cement volume (Figure 6). At maximum compression state, the minimal principal stress was greater than the applied stress level in 71% of the bone and in 66% of the cement. On average, only 0.01% of the total bone was at risk of fatigue failure, against 0.85% of the cement. Some parts of the models were loaded up to more than 10 times the apparent stress level.

Discussion

FEA models of the cement-bone interface using μ CT-based morphology with a frictional interface between cement and bone led to a structural response that was similar to those found experimentally. Consistent with the experimental findings, the simulated interface stiffness was higher in compression than in tension. There remains, however, room for improvement relative to the correlation between the simulated and experimental stiffness values.

Since we assumed in our models that the cement-bone interface was unbonded, one could argue that the weak correlation between the computational and experimental stiffness values is caused by the fact that cement-bone adhesion was not included in the simulations. Results of a preliminary study with multiple bone-cement interface models showed, however, that when glued contact was assumed at the interface, the stiffness both in tension and compression are overestimated by more than a factor of two.¹¹ Furthermore, other authors previously reported that PMMA has limited adhesive properties to bone.^{20,31} Considering the presence of fluids in the bone (blood, fat, marrow) at the time of cement insertion, the assumption that cement does not adhere to the bone is very plausible.

Friction at the interface was modeled with a coefficient of 0.3. In a separate parametric study we varied the friction coefficient and investigated its effect on the stiffness and span predicted by the models.¹¹ The results of that study indicated that a lower coefficient led to a stiffness reduction and an increased span. Increasing the friction coefficient had the opposite effect. The friction coefficient chosen for the current study matched the experimental values the closest.

The results of the FEA simulations showed that the majority (more than 80%) of the deformation took place at the interface between the cement and bone, both in tension and compression, which was similar to the experimental findings. This implies that current macroscopic FEA models of cemented total hip reconstructions with a fully bonded cement-bone interface may substantially underestimate the actual local deformations and, subsequently, the stability of the reconstruction. This could be corrected for by interpositioning relatively flexible elements (more flexible in tension than under compression) at the cement-bone interface.

In the current study we focused on the micro-mechanical behavior of the cement-bone interface under tension-compression loads. The actual *in vivo* loading conditions are generally more complicated than those studied here, consisting of combinations of tension/compression and shear loads. Currently, experiments are being performed in which the shear behavior of the interface is investigated, as well as the fatigue behavior of the interface. Data from such experiments provide information that can be used to

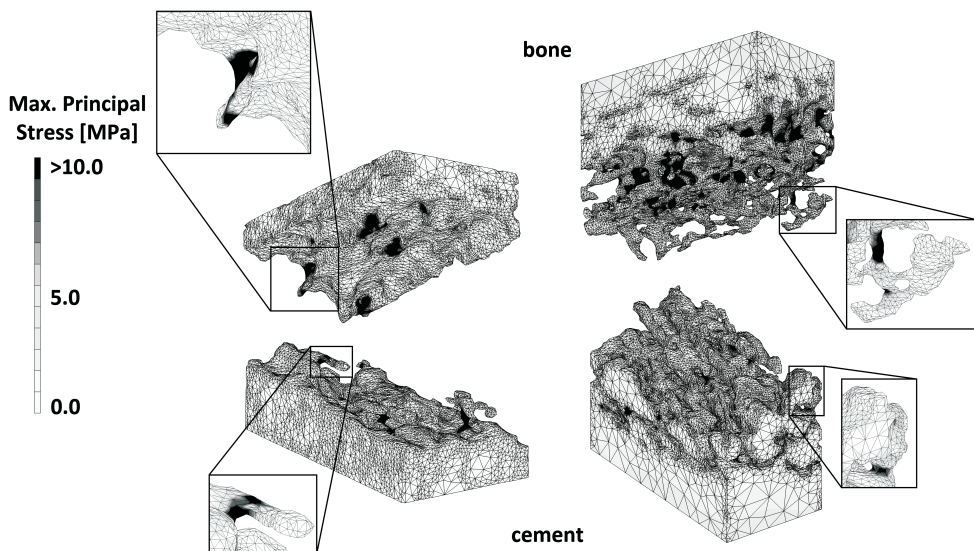


Figure 5: Maximal principal stress distribution in an FEA model with little (left) and a lot of interdigitation (right), under maximal tension load. The enlargements show bone and cement structures that experienced high stress levels, indicating that these structures contributed to load transfer over the cement-bone interface.

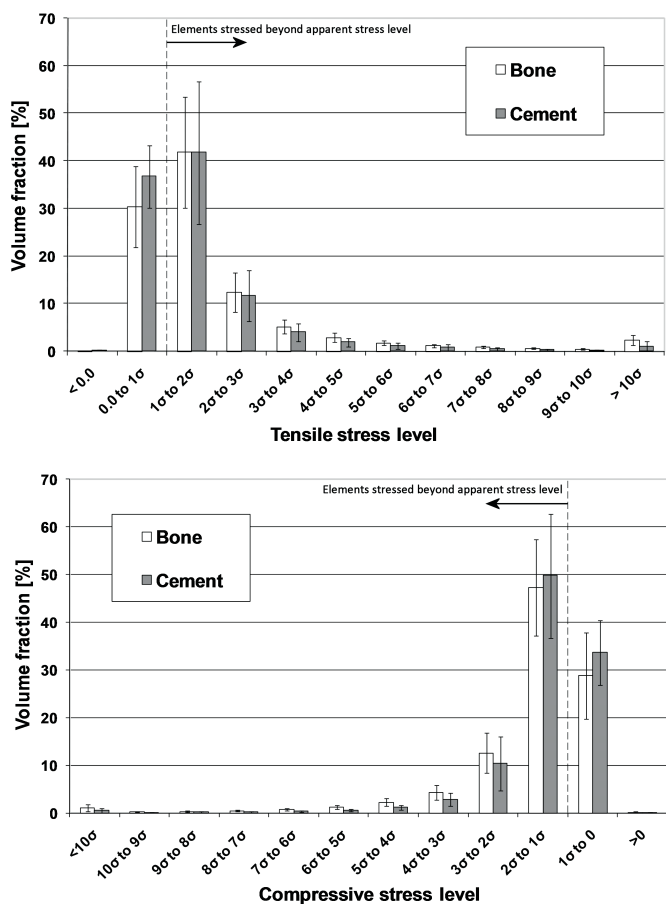


Figure 6: Stress distribution in the bone and cement during maximum tension (top) and compression (bottom). The error bars indicate the standard deviation of the data for each stress level.

further develop micro-mechanical FEA models such as presented in the current study.

The simulations predicted more deformation of the cement than bone, while opposite results were found in the experiments. However, the experimental deformations of the cement and bone were relatively small (majority smaller than 1.0 μm), compared to the accuracy of the DIC system used for the measurements (0.395 μm).²³ In addition, the cement was assumed to be homogeneous in the FEA models, while in the experiments local artifacts such as the presence of high-stiffness barium sulfate particles may have affected the DIC surface measurements.

The μFEA models underestimated the hysteresis that was noticed in the experimental tension-compression curves. Besides frictional phenomena at the sliding cement-bone interface, other phenomena such as

viscoelastic behavior or fluid flow at the interface may have been responsible for this behavior in the experiments. Since in the current study linear elastic isotropic material properties were assigned to the cement and bone, the FEA models were unable to capture viscoelastic material behavior that may have occurred in the experiments, which may explain the underestimation of the hysteresis in the current models.

The additional value of FEA with respect to experimental testing is the ability to evaluate internal stresses in the bone and cement. The current results showed that the stress levels in the majority of the bone and cement adjacent to the interface were higher than the applied stress level, both in tension and compression. This difference between the apparent and local stress levels has previously been demonstrated in microstructural FEA models of trabecular bone.^{26,40} Our results furthermore showed that more cement than bone was at risk of fatigue failure. This is consistent with the experiments, in which after destructive testing of the interface specimens more cracks were found in the cement than in the bone.²⁴ This can be explained by the fact that the differences between the bone and cement stresses was relatively small, while bone has a higher fatigue strength and ultimate tensile and compressive strength than bone cement.^{3,18,19,25}

The FEA models were relatively successful in recreating the geometry of the interface between cement and bone, but were ultimately limited by the resolution of the CT scanner and geometrical errors generated by the remeshing process. The geometrical errors were generally within one voxel error between the FEA meshes and the segmented μ CT data. To assess the relative contributions of interface contact, interlock morphology, and gap width at the cement-bone interface to interface stiffness, a regression model of the original set of experimental data²³ was performed. Both contact fraction ($p < 0.0001$) and interlock morphology ($p = 0.0003$) contributed to prediction of the interface tensile stiffness ($r^2 = 0.67$, $p = 0.0003$). The width of the cement-bone gap did not contribute to the regression model ($p = 0.60$). Also in our FEA models the interfacial gaps correlated poorly with the calculated span ($r^2 = 0.0018$, $p = 0.0010$) and tensile stiffness ($r^2 = 0.022$, $p = 0.0008$). This suggests that the magnitude of the gaps has a negligible effect on the actual mechanical behavior of the interface. Thus, it appears the interface micro-mechanics are dominated by the local morphology such as the interface contact and interlock morphology. This is reasonable because the micro-mechanical behavior may be more dependent on locations where no gaps (or only small gaps) are present, since at these points load transfer occurs earlier in the loading history than at points that have yet to come in contact.

In the current study we used a linear relationship between the bone density and the Young's modulus.¹⁹ Other authors previously used power laws relating the bone density to a certain Young's modulus in case of CT-data,^{4,14,39} or a constant tissue modulus in case of μ CT data,^{8,36} based upon the assumption that the μ CT resolution is high enough to capture the trabecular structures that would otherwise appear as lower grayscale on normal CT scans. We performed initial analyses with models in which we varied the way of assigning bone material properties, applying a constant bone modulus and various linear and power laws.

The results of that study showed that the applied material law had only a minor effect on the current outcome measures, most likely due to the relatively high resolution of our CT-data and due to the relatively large effect of the contact interface mechanics.

Previous FEA models of interfaces in total hip arthroplasty have been focused on debonding processes of the stem-cement interface^{27,37} and their effects on implant micromotions and cement failure.^{28,38} Furthermore, research has been conducted on the micromotions and osseointegration of the implant-bone interface in case of uncemented implants.^{24,30,32} The current study provides information that may help to better understand the load transfer mechanisms taking place at the cement-bone interface.

In summary, the general micro-mechanical response of the cement-bone interface was reproduced, using only a frictional contact at the interface. This suggests that the cement-bone interface should be regarded as mechanically unbonded. It therefore seems that the initial, post-surgery bond between cement and bone, is purely generated by the interlock rather than by a gluing capacity of bone cement to bone. This emphasizes the importance of obtaining a good mechanical cement-bone interlock during total joint surgery, for instance by using pulse lavage of the intramedullary canal prior to implantation, pressurization of the cement after stem insertion, and possibly adding anchoring holes.

Returning to our original hypotheses, it was determined that (1) μ FEA models of the cement-bone interface were able to reproduce stiffness values similar to experimental observations, although there is room for improvement, (2) the majority of the deformation took place at the cement-bone interface while the cement and bone had a limited contribution to the global deformation; (3) by including friction at the cement-bone interface, hysteresis behavior as seen experimentally could partly be simulated; (4) more cement than bone was at risk of fatigue failure.

Acknowledgements

This work was funded by the NIH grant AR42017.

References

1. Arola D, Stoffel KA, Yang DT (2006). Fatigue of the cement/bone interface: the surface texture of bone and loosening. *J Biomed Mater Res B Appl Biomater* 76(2):287-297.
2. Bean DJ, Convery FR, Woo SL, Lieber RL (1987). Regional variation in shear strength of the bone-polymethylmethacrylate interface. *J Arthroplasty* 2(4):293-298.
3. Carter DR, Hayes WC (1976). Fatigue life of compact bone--I. Effects of stress amplitude, temperature and density. *J Biomech* 9(1):27-34.
4. Carter DR, Hayes WC (1977). The compressive behavior of bone as a two-phase porous structure. *J Bone Joint Surg [Am]* 59(7):954-962.
5. Davies JP, Harris WH (1993). Strength of cement-metal interfaces in fatigue: comparison of smooth, porous and precoated specimens. *Clin Mater* 12(2):121-126.
6. Dohmae Y, Bechtold JE, Sherman RE, Puno RM, Gustilo RB (1988). Reduction in cement-bone interface shear strength between primary and revision arthroplasty. *Clin Orthop Relat Res* 236:214-220.
7. Funk MJ, Litsky AS (1998). Effect of cement modulus on the shear properties of the bone-cement interface. *Biomaterials* 19(17):1561-1567.
8. Hou FJ, Lang SM, Hoshaw SJ, Reimann DA, Fyhrie DP (1998). Human vertebral body apparent and hard tissue stiffness. *J Biomech* 31(11):1009-1015.
9. Huiskes R, Verdonschot N, Nivbrant B (1998). Migration, stem shape, and surface finish in cemented total hip arthroplasty. *Clin Orthop Relat Res* 355:103-112.
10. Janssen D, Aquarius R, Stolk J, Verdonschot N (2005). Finite-element analysis of failure of the Capital Hip designs. *J Bone Joint Surg [Br]* 87(11):1561-1567.
11. Janssen D, Mann KA, Verdonschot N (2008). Micro-mechanical modeling of the cement-bone interface: The effect of friction, morphology and material properties on the micromechanical response. *J Biomech* 41(15):3158-3163.
12. Kaneko TS, Bell JS, Pejic MR, Tehranzadeh J, Keyak JH (2004). Mechanical properties, density and quantitative CT scan data of trabecular bone with and without metastases. *J Biomech* 37(4):523-530.
13. Kaneko TS, Pejic MR, Tehranzadeh J, Keyak JH (2003). Relationships between material properties and CT scan data of cortical bone with and without metastatic lesions. *Med Eng Phys* 25(6):445-454.
14. Keller TS (1994). Predicting the compressive mechanical behavior of bone. *J Biomech* 27(9):1159-1168.
15. Kim DG, Miller MA, Mann KA (2004). Creep dominates tensile fatigue damage of the cement-bone interface. *J Orthop Res* 22(3):633-640.
16. Krause WR, Krug W, Miller J (1982). Strength of the cement-bone interface. *Clin Orthop Relat Res* 163:290-299.
17. Lennon AB, Britton JR, MacNiocaill RF, Byrne DP, Kenny PJ, Prendergast PJ (2007). Predicting revision risk for aseptic loosening of femoral components in total hip arthroplasty in individual patients--a finite element study. *J Orthop Res* 25(6):779-788.
18. Lewis G (1997). Properties of acrylic bone cement: state of the art review. *J Biomed Mater Res* 38(2):155-182.
19. Lotz JC, Gerhart TN, Hayes WC (1991). Mechanical properties of metaphyseal bone in the proximal femur. *J Biomech* 24(5):317-329.
20. Lucksanasombool P, Higgs WA, Ignat M, Higgs RJ, Swain MV (2003). Comparison of failure characteristics of a range of cancellous bone-bone cement composites. *J Biomed Mater Res A* 64(1):93-104.
21. Mann KA, Ayers DC, Werner FW, Nicoletta RJ, Fortino MD (1997). Tensile strength of the cement-bone

- interface depends on the amount of bone interdigitated with PMMA cement. *J Biomech* 30(4):339-346.
22. Mann KA, Bartel DL, Wright TM, Inghraffea AR (1991). Mechanical characteristics of the stem-cement interface. *J Orthop Res* 9(6):798-808.
 23. Mann KA, Miller MA, Cleary RJ, Janssen D, Verdonshot N (2008). Experimental micromechanics of the cement-bone interface. *J Orthop Res* 26(6):872-879.
 24. Moreo P, Perez MA, Garcia-Aznar JM, Doblare M (2007). Modelling the mechanical behaviour of living bony interfaces. *Comput Methods in Appl Mech Engrg* 196(35-36):3300-3314.
 25. Murphy BP, Prendergast PJ (2002). The relationship between stress, porosity, and nonlinear damage accumulation in acrylic bone cement. *J Biomed Mater Res* 59(4):646-654.
 26. Nagaraja S, Couse TL, Guldberg RE (2005). Trabecular bone microdamage and microstructural stresses under uniaxial compression. *J Biomech* 38(4):707-716.
 27. Perez MA, Garcia-Aznar JM, Doblare M, Seral B, Seral F (2006). A comparative FEA of the debonding process in different concepts of cemented hip implants. *Med Eng Phys* 28(6):525-533.
 28. Perez MA, Grasa J, Garcia-Aznar JM, Bea JA, Doblare M (2006). Probabilistic analysis of the influence of the bonding degree of the stem-cement interface in the performance of cemented hip prostheses. *J Biomech* 39(10):1859-1872.
 29. Reggiani B, Cristofolini L, Varini E, Viceconti M (2007). Predicting the subject-specific primary stability of cementless implants during pre-operative planning: preliminary validation of subject-specific finite-element models. *J Biomech* 40(11):2552-2558.
 30. Rubin PJ, Rakotomanana RL, Leyvraz PF, Zysset PK, Curnier A, Heegaard JH (1993). Frictional interface micromotions and anisotropic stress distribution in a femoral total hip component. *J Biomech* 26(6):725-739.
 31. Skripitz R, Aspenberg P (1999). Attachment of PMMA cement to bone: force measurements in rats. *Biomaterials* 20(4):351-356.
 32. Spears IR, Pfeleiderer M, Schneider E, Hille E, Morlock MM (2001). The effect of interfacial parameters on cup-bone relative micromotions. A finite element investigation. *J Biomech* 34(1):113-120.
 33. Stolk J, Janssen D, Huiskes R, Verdonshot N (2007). Finite element-based preclinical testing of cemented total hip implants. *Clin Orthop Relat Res* 456:138-147.
 34. Taddei F, Pancanti A, Viceconti M (2004). An improved method for the automatic mapping of computed tomography numbers onto finite element models. *Med Eng Phys* 26(1):61-69.
 35. Taylor M, Tanner KE, Freeman MA, Yettram AL (1995). Cancellous bone stresses surrounding the femoral component of a hip prosthesis: an elastic-plastic finite element analysis. *Med Eng Phys* 17(7):544-550.
 36. Van Rietbergen B, Weinans H, Huiskes R, Odgaard A (1995). A new method to determine trabecular bone elastic properties and loading using micromechanical finite-element models. *J Biomech* 28(1):69-81.
 37. Verdonshot N, Huiskes R (1997). Cement debonding process of total hip arthroplasty stems. *Clin Orthop Relat Res* 336:297-307.
 38. Verdonshot N, Huiskes R (1997). The effects of cement-stem debonding in THA on the long-term failure probability of cement. *J Biomech* 30(8):795-802.
 39. Wirtz DC, Schiffers N, Pandorf T, Radermacher K, Weichert D, Forst R (2000). Critical evaluation of known bone material properties to realize anisotropic FE-simulation of the proximal femur. *J Biomech* 33(10):1325-1330.

40. Yeni YN, Zelman EA, Divine GW, Kim DG, Fyhrie DP (2008). Trabecular shear stress amplification and variability in human vertebral cancellous bone: relationship with age, gender, spine level and trabecular architecture. *Bone* 42(3):591-596.

tot betne

zalqorht

Chapter 8

Micro-mechanical modeling of the cement-bone interface: the effect of friction, morphology and material properties

Introduction

In cemented total hip arthroplasty, fixation of the implants in the bone is achieved by bone cement inserted in a doughy form at the time of operation. The cement subsequently penetrates into bone lacunar and trabecular spaces, forming a complex interlock between the cement and bone, ensuring fixation of the cement mantle within the bone.

Much research has been conducted to determine the strength of the cement-bone interface.^{1,2,5,6,10,11,15} However, these studies simplify the cement-bone interface to an apparent level, whereas in reality this interface is a morphologically complex cement-bone composite.

Recently, experiments have been performed to determine the micro-mechanical behavior of the cement-bone interface.¹⁶ Interface specimens were subjected to nondestructive fully reversible tension–compression loads, while the local micromotions of the cement, bone and cement-bone interface were monitored. The results showed that the interface is more compliant than the cement and bone. Substantial

hysteresis occurred during one tension–compression cycle, attributed to sliding contact at the interface. It remains, however, unclear how loads are transferred across the interface, as this could not be assessed.

Cement–bone adhesion may play a role in the mechanical response observed experimentally, although it may be compromised by fat, blood and other fluids that are present in the bone during cement insertion. On the other hand, the micro-mechanical behavior of the cement–bone interface may also be attributed to the shape-closed interlock of cement penetrated into the bone trabecular and lacunar spaces, combined with frictional phenomena.

In addition to this, variations in the cement–bone interface morphology may affect the micromechanical response of the shape-closed interlock. For instance, more cement penetration may enhance the mechanical properties of the interface. On the other hand, cement is known to shrink during polymerization,^{4,7} which may cause gaps to occur at the cement–bone interface, causing inferior mechanical properties at the interface.

A third possible factor affecting the micro-mechanical behavior of the cement–bone interface is the variability of cement material properties. Lower modulus cement has been considered as an approach to reduce interface stresses.⁶ The stiffness of commercially available bone cements varies between roughly 2.0 and 3.0 GPa.¹² The effect of this variation on the actual micro-mechanical response of the cement–bone interface is unclear.

In order to gain insight in the micro-mechanical behavior of the cement–bone interface, we developed a micro-mechanical finite element analysis (FEA) model based on an experimental cement–bone interface specimen¹⁶ and analyzed the effect of parametric variations of frictional, morphological and material properties on the mechanical response. We asked the following questions: (1) are the mechanical properties of the cement–bone interface caused by frictional phenomena via shape-closed mechanical interlock or by adhesive properties of the cement?; (2) how do interface morphological variations affect the micro-mechanical response of the cement–bone interface? and (3) how do variations in cement stiffness affect the micromechanical response of the cement–bone interface?

Methods

The FEA models used for the parametric analyses were created from microcomputed tomography (μ CT) scans of a cement–bone interface specimen (Figure 1a) that was previously tested experimentally.¹⁶ The specimen ($5 \times 5 \times 10 \text{ mm}^3$) was sectioned from a cemented total hip arthroplasty in a fresh frozen proximal human cadaver femur. The specimen was μ CT-scanned at a $12 \text{ }\mu\text{m}$ isotropic resolution (Scanco μ CT 40, Scanco Medical AG, Basserdorf, Switzerland; Figure 1b).

FEA meshes were created using commercial software (Mimics 11.1, Materialise, Leuven, Belgium). The cement and bone were segmented based upon the image grayscale. In general, the segmented cement and bone consisted of one large part and some small parts. The smaller parts were removed by performing a region growing operation. Next, a one-voxel erosion operation was performed on the cement to prevent

interpenetration between cement and bone. Surface models were generated for cement and bone. To keep element number to a tractable level the triangular surface meshes were generated after a $6 \times 6 \times 6$ voxel reduction. The surface meshes were remeshed to reduce the number of elements and generate element shapes with appropriate aspect ratios. Four-node tetrahedral meshes were created from the surface meshes (Patran 2005r2, MSC Software Corporation, Santa Ana, CA, USA). The resulting model existed of approximately 3,35,000 elements and 80,000 nodes (Figure 1c), and was regarded as the “normal” interface morphology model.

The bone and cement were considered to be linear elastic. The bone properties were assigned based upon μ CT grayscale values, which were converted to equivalent HA-densities using a calibration phantom. A linear relationship between the HA-density and the Young’s modulus was assumed,²³ resulting in stiffness values ranging from 0.1 to 20.0 GPa ($\nu = 0.3$). The cement was assumed to have uniform material properties ($E = 3.0$ GPa; $\nu = 0.3$; Simplex P, Stryker Orthopaedics, Mahwah, NJ, USA).

Contact between the cement and bone was modeled using a double-sided node-to-surface contact algorithm (MSC.MARC 2005r3, MSC Software Corporation, Santa Ana, CA, USA). The contact algorithm simulated contact between nodes of one contact body and the element surface of the other body. The detection and implementation of contact and friction was achieved through a direct constraint model. In order to study the effect of cement adhesion in one model an ideally bonded contact interface was simulated. Adhesion was only simulated in areas where no gaps were present. In these areas, direct constraints placed on the nodes were adapted such that no relative tangential and normal motions could occur. To study the effect of friction, we varied the friction coefficient in five other models ($\mu = 0.0$; 0.3; 0.7;

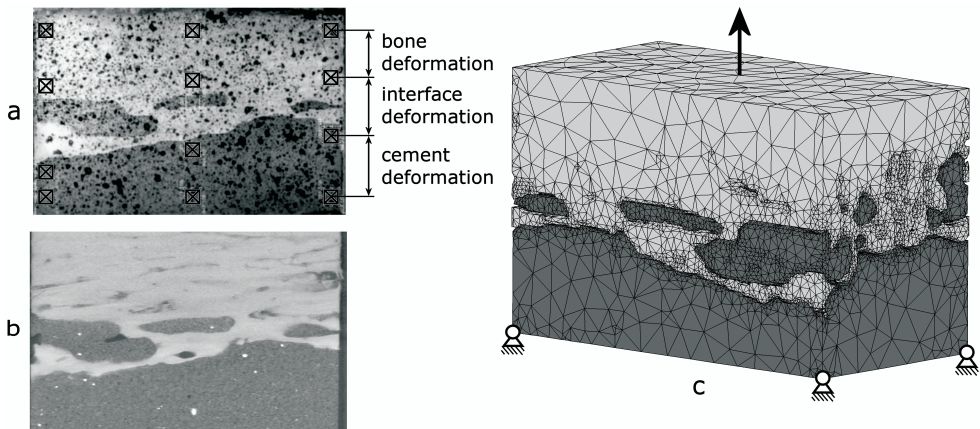


Figure 1: (a) Image of a specimen that was tested experimentally in which the twelve DIC sampling points are indicated; (b) a μ CT image of the same specimen and (c) the FEA model of the cement-bone interface specimen created from the μ CT-data, with the boundary conditions indicated.

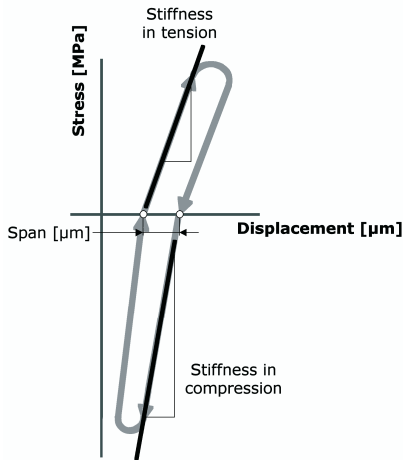


Figure 2: Schematic stress-displacement diagram with the outcome measures used in the current study.

1.0 and 3.0). Friction was modeled using a bilinear Coulomb friction model. This model is based on relative tangential displacements, and assumes that stick and slip conditions correspond to reversible (elastic) and permanent (plastic) relative displacements.

In two models the effect of morphological variations was studied. In the first model the effect of additional gaps at the contact interface was simulated, representing an interface achieved by an inferior cementing technique. Due to absence of morphological data we chose a numerical approach to simulate interface gaps. We applied an additional one-voxel erosion operation, causing an additional gap of roughly 12 μm at the cement bone interface. In a second model, optimal cement penetration was simulated by filling all bone lacunar cavities with cement, even at locations where no cement was present according to the μCT data.

Finally, two models were analyzed in which low and intermediate stiffness bone cement was simulated (Young's modulus of 2.0 and 2.5 GPa, respectively). In models with morphological and cement stiffness variations frictional contact was assumed with the default friction coefficient (0.3).

All models were loaded for one cycle of fully reversible tension–compression, mimicking the experimental protocol.¹⁶ During the simulation, the distal end of the cement was fixed in all directions, while the proximal end of the bone was displaced in the longitudinal direction (Figure 1c). The proximal end was fixed such that tilting was restricted, while displacement in the transversal directions was allowed. Incremental displacement steps of 1.0 μm were applied until the maximal experimental levels of tension (1.04 MPa) and compression (-2.03 MPa) were reached (Figure 2).

In the experiments, digital image correlation techniques were used to quantify bone, interface and cement deformations.¹⁶ Twelve sampling points were taken (Figure 1a): three columns of four sampling points located in the bone (two points) and the cement (two points). By tracking the relative displacements of

the bone points the local deformation of the bone was calculated. In the same manner the deformation of the cement and interface were calculated. This was done for the three columns, after which the calculated deformations of the cement, bone and contact interface were averaged to establish the 'global' deformations. To enable direct comparison of the mechanical behavior of the models relative to the experiments, the same locations were used in the models to calculate deformation.

We determined stress-displacement curves and calculated the interface stiffness in tension and compression by fitting linear lines through the curves. Consistent with the experimental study¹⁶ the stiffness was expressed as the ratio of the applied stress and the deformation (MPa/mm) instead of the strain at the interface, since discontinuities in the interface materials and morphology prevented the use of an unambiguous strain measure. Finally, we calculated the horizontal span of the stress-displacement curves, which served as a measure for hysteresis occurring in the models (Figure 2).

Results

In cases where the cement-bone interface was assumed to be unbonded, the cement-bone interface deformed in a nonhomogeneous manner. For example, during application of the tensile load, the cement and bone remained in contact at some locations, while at other locations gaps occurred (Figure 3). The normal morphology model with a friction coefficient of 0.3 resulted in a micro-mechanical response at the cement-bone interface that was similar to the experiment (Figure 4). In all models, the majority of the deformation took place at the contact interface, both in tension (90%) and compression (87%); this was consistent with the experimental results. In addition, the cement-bone interface was found to be more

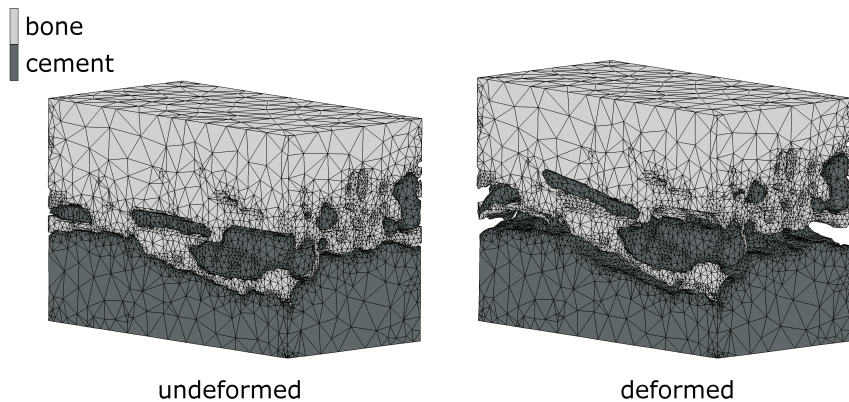


Figure 3: FEA model in the unloaded (left) situation, and under full tension load (right). Notice that in the deformed state, gaps occurred between the cement and bone at some locations, while at other locations the cement remained in contact with the bone. In this particular case, a friction coefficient of 0.3 was modeled. The deformations are 50 times magnified for illustrative purposes.

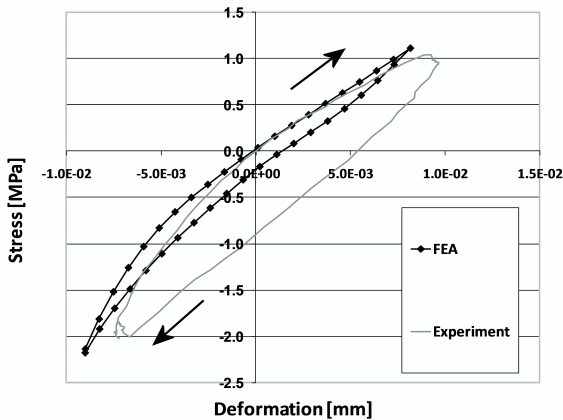


Figure 4: Micromechanical response of the cement-bone interface from experimental results and as simulated with an FEA model with a friction coefficient of 0.3 and a normal interface morphology. The loading direction is indicated by the arrows.

compliant in tension than in compression.

The mechanical response of the parametric studies is presented in terms of interface deformation (Table 1), interface stiffness in tension and compression (Figure 5), and horizontal span (Figure 6).

Increasing the friction coefficient generally decreased the deformation at the interface and increased the interfacial stiffness, both in compression and tension. The horizontal span decreased with increasing friction coefficient. An ideally bonded contact interface decreased the interface deformation and the horizontal span, and furthermore resulted in a response that was much stiffer than the unbonded cases. The results of the unbonded models with relatively low friction coefficient values (0.0–0.7) more closely approximated the experimental values than those of models with a relatively high friction coefficient (1.0 and 3.0), or with a bonded interface.

Changes in morphology at the contact interface had a dramatic effect on the interface deformation. Introduction of interface gaps increased interface motion, decreased stiffness and increased the horizontal span when compared to the normal morphology case. Filling gaps with cement had the opposite effect.

Compared to the frictional and morphological variations, reducing the cement stiffness had only a modest, but somewhat predictable effect on the mechanical response. Application of low modulus cement (with a cement stiffness decrease of 33%) decreased the tensile interface stiffness by 27% relative to the high stiffness cement. Decreasing the cement stiffness led to an increased interface deformation, reduced interface stiffness and increased horizontal span.

Discussion

In the current study, we analyzed the effect of parametric variations of frictional, morphological and material properties on the mechanical response of a cement-bone interface.

Our results show that when an ideally bonded contact interface was assumed, the deformation at the

interface was underestimated with respect to the experimental values. Furthermore, interface stiffness was overestimated in tension and compression, and hysteresis was underestimated. These results suggest the micro-mechanical behavior of the cement-bone interface is caused by frictional phenomena rather than by adhesive properties of the cement. Previously, authors have reported on the limited adhesive properties of cement relative to bone.^{14,21} Considering the presence of fluids in the bone (blood, fat, marrow) at the time of cement insertion, the assumption that cement does not adhere to the bone seems very plausible.

Morphological variations had a substantial effect on the micromechanical response of the cement-bone interface. Simulating additional interface gaps reduced the interface stiffness and resulted in large interface deformations. The interface gap led to a span of approximately 12 μm , which can be attributed to the additional erosion process. In contrast, a maximal cement fill increased the cement-bone interface stiffness and decreased the deformation. Previously, it has been shown that maximizing bone–cement interdigitation increases the strength of the interface.^{2,11,15} These findings stress the importance of cement pressurization during the preparation of a cemented total hip reconstruction.

Compared to the frictional and morphological properties of the interface, the effect of cement stiffness was

Table 1: Deformation of the cement-bone interface in full tension (1.04 MPa) and compression (-2.03 MPa).

Component	Interface deformation [μm]	
	Tension	Compression
$\mu = 0.0$	8.10	11.95
$\mu = 0.3$	8.05	12.03
$\mu = 0.7$	7.10	10.98
$\mu = 1.0$	7.05	10.11
$\mu = 3.0$	5.13	9.04
Glued interface	2.22	6.15
Interface gaps	31.90	17.01
Normal morphology	8.05	12.03
Maximal fill	4.98	6.98
Low cement stiffness	10.73	14.34
Medium cement stiffness	8.95	12.77
High cement stiffness	8.05	12.03
<i>Experimental results</i>	8.08	11.51

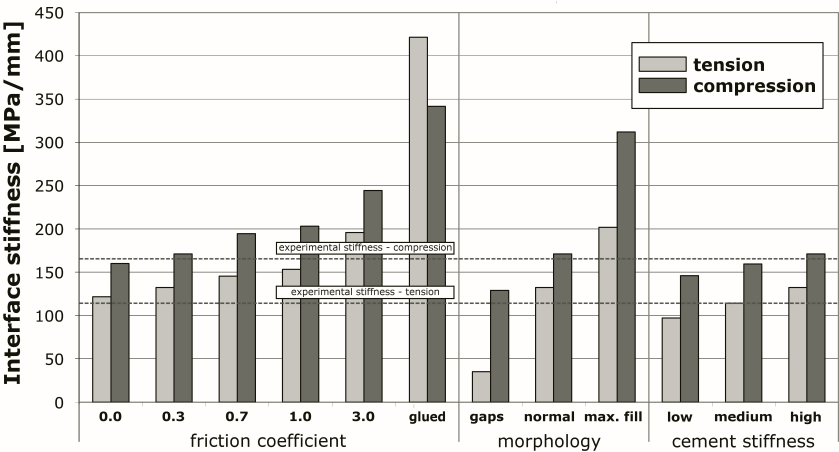


Figure 5: Stiffness response of the cement-bone interface in tension and compression for the parametric studies.

rather small. In our models, increasing the cement stiffness increased the stiffness and reduced hysteresis. The stiffness reduction was proportional to the cement stiffness reduction. Funk and Litsky⁶ showed a 50% interface shear stiffness reduction with low-stiffness PBMMA (polybutyl methyl methacrylate) cement compared to normal PMMA (polymethyl methacrylate) cement. However, the Young's modulus of the low-stiffness PBMMA cement was almost 8 times lower than that of normal cement. The discrepancy between that study and current findings may be attributed to differences in the loading, material properties or method of preparation of the experimental specimens.

Our study was limited by the fact that a single cement-bone interface specimen was used for the parametric variations. The specimen was chosen from a batch of 21 specimens used previously for experimental testing.¹⁶ That study showed the stiffness of the cement-bone interface is proportional to the level of cement interdigitation, with values ranging from 61.7 to 630.3 MPa/mm. This large range indicates the substantial effect of morphological variations on the micromechanical behavior; variations that were not included in the current study. In a separate study we modeled ten of the experimental specimens with frictional contact at the contact interface (friction coefficient of 0.3). The results of that study indicated that using frictional contact did not lead to an underprediction of the stiffness that was measured experimentally, which further confirms our assumption that the cement does not adhere to the bone.

In order to limit the number of elements, the μ CT data was reduced prior to surface meshing. Subsequently, the surface models were remeshed to improve the mesh quality and to further reduce the number of elements. These operations may have introduced errors in some parts of the models. Consequentially, smaller cement parts penetrating into the bone may have been lost or underrepresented due to the meshing process. Despite the errors the current models were able to approximate the micro-mechanical

behavior of the experimental cement-bone interface specimen. This suggests that the micro-mechanical behavior depends mainly on the interlock of the larger structures present at the interface. Increasing the μ CT resolution and the number of elements in the models should, however, result in a more accurate prediction of the interface micro-mechanics.

In order to prevent interpenetration between the cement and bone we applied a one-voxel erosion operation on the cement. Initial models in which this operation was not applied showed that interpenetration caused artificial stiffening of the contact interface. It was not possible to resolve this by adjusting the contact procedure (for instance by simulating initial stress-free contact). Projection of the mesh on the initial μ CT-data indicated that the application of the erosion process led to a more accurate morphological description of the specimen. Furthermore, our results indicated that the eroded model gave a better prediction of the micro-mechanical behavior as shown experimentally. The effect of the erosion process is reflected best by the comparison between the span produced by our “normal” and “gaps” models. While the standard 12 μ m erosion process led to only a relatively small span (approx. 3mm), the additional erosion process applied to the “gaps” model produced much more play (approx. 12 μ m). This illustrates that, as intended, our standard one-pixel erosion process removed the mesh interpenetration without introducing excessive play at the interface, whereas introducing an additional gap resulted in a substantial increase of the span. When assigning bone material properties based upon CT grayscale, it is common to use a power law relating the bone density to a certain Young’s modulus.^{3,9,26} In case of models based upon μ CT data sometimes a constant tissue modulus is used.^{8,23} In the current study, a linear relationship between the bone density and the Young’s modulus was assumed.³³ Preliminary analyses with models using a number of different modulus–density relationships for bone showed that the material law had only a minor effect

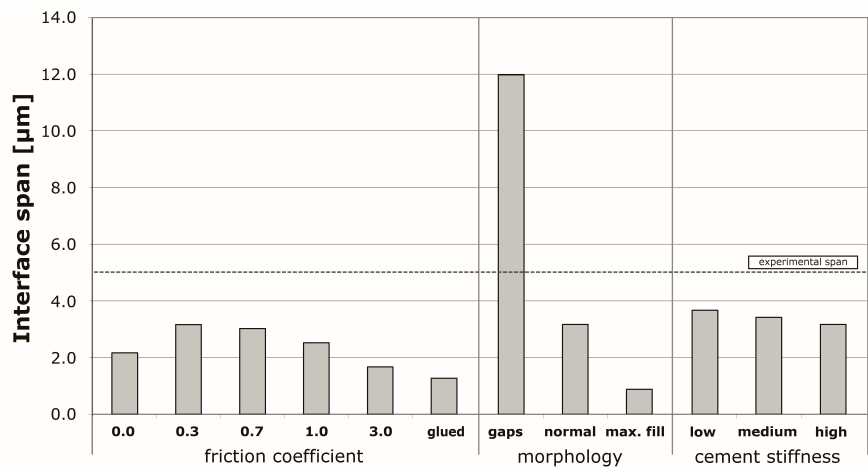


Figure 6: Horizontal span at the cement-bone interface from the various models.

on the mechanical behavior of the cement-bone interface.

Since linear elastic isotropic material properties were used for the cement and bone, the FEA models were unable to simulate viscoelastic material behavior that may have occurred in the experiments. This difference may explain why hysteresis (horizontal span in the stress-displacement curves) was generally underestimated by the current models. In addition, no damage was simulated at the cement-bone contact interface, although in some small parts rather high Von Mises stress levels (>150 MPa) were found, both in the cement and bone. This may provide an additional explanation for the discrepancy between the numerical and experimental findings.

To our knowledge, this is the first publication reporting a simulation of the micro-mechanical behavior of the cement-bone interface. Previously, authors have modeled debonding processes of the stem–cement interface.^{18,19,24,25} Furthermore, research has been conducted on the micromotions and osseointegration of the implant–bone interface in case of uncemented implants.^{17,20,22} The current study provides information that may help to better understand the load transfer mechanisms taking place at the cement-bone interface.

In conclusion, the results of this study indicate that in the current model: (1) the mechanical properties of the cement-bone interface were caused by frictional phenomena at the shape-closed mechanical interlock rather than by adhesive properties of the cement, (2) our findings furthermore showed that in the current model maximizing cement penetration and local apposition increased the cement-bone interface stiffness, while interface gaps had a detrimental effect on its micromechanical behavior, (3) relative to the frictional and morphological variations, variations in the cement stiffness had only a modest effect on the micro-mechanical behavior of the cement-bone interface.

Acknowledgements

This work was funded by the NIH grant AR42017.

References

1. Arola D, Stoffel KA, Yang DT (2006). Fatigue of the cement/bone interface: the surface texture of bone and loosening. *J Biomed Mater Res B Appl Biomater* 76(2):287-297.
2. Bean DJ, Convery FR, Woo SL, Lieber RL (1987). Regional variation in shear strength of the bone-polymethylmethacrylate interface. *J Arthroplasty* 2(4):293-298.
3. Carter DR, Hayes WC (1977). The compressive behavior of bone as a two-phase porous structure. *J Bone Joint Surg [Am]* 59(7):954-962.
4. Davies JP, Harris WH (1995). Comparison of diametral shrinkage of centrifuged and uncentrifuged Simplex P bone cement. *J Appl Biomater* 6(3):209-211.
5. Dohmae Y, Bechtold JE, Sherman RE, Puno RM, Gustilo RB (1988). Reduction in cement-bone interface shear strength between primary and revision arthroplasty. *Clin Orthop Relat Res* 236:214-220.
6. Funk MJ, Litsky AS (1998). Effect of cement modulus on the shear properties of the bone-cement interface. *Biomaterials* 19(17):1561-1567.
7. Hamilton HW, Cooper DF, Fels M (1988). Shrinkage of centrifuged cement. *Orthop Rev* 17(1):48-54.
8. Hou FJ, Lang SM, Hoshaw SJ, Reimann DA, Fyhrie DP (1998). Human vertebral body apparent and hard tissue stiffness. *J Biomech* 31(11):1009-1015.
9. Keller TS (1994). Predicting the compressive mechanical behavior of bone. *J Biomech* 27(9):1159-1168.
10. Kim DG, Miller MA, Mann KA (2004). Creep dominates tensile fatigue damage of the cement-bone interface. *J Orthop Res* 22(3):633-640.
11. Krause WR, Krug W, Miller J (1982). Strength of the cement-bone interface. *Clin Orthop Relat Res* 163:290-299.
12. Lewis G (1997). Properties of acrylic bone cement: state of the art review. *J Biomed Mater Res* 38(2):155-182.
13. Lotz JC, Gerhart TN, Hayes WC (1991). Mechanical properties of metaphyseal bone in the proximal femur. *J Biomech* 24(5):317-329.
14. Lucksanasombool P, Higgs WA, Ignat M, Higgs RJ, Swain MV (2003). Comparison of failure characteristics of a range of cancellous bone-bone cement composites. *J Biomed Mater Res A* 64(1):93-104.
15. Mann KA, Ayers DC, Werner FW, Nicoletta RJ, Fortino MD (1997). Tensile strength of the cement-bone interface depends on the amount of bone interdigitated with PMMA cement. *J Biomech* 30(4):339-346.
16. Mann KA, Miller MA, Cleary RJ, Janssen D, Verdonschot N (2008). Experimental micromechanics of the cement-bone interface. *J Orthop Res* 26(6):872-879.
17. Moreo P, Perez MA, Garcia-Aznar JM, Doblare M (2007). Modelling the mechanical behaviour of living bony interfaces. *Comput Methods in Appl Mech Engrg* 196(35-36):3300-3314.
18. Perez MA, Garcia-Aznar JM, Doblare M, Seral B, Seral F (2006). A comparative FEA of the debonding process in different concepts of cemented hip implants. *Med Eng Phys* 28(6):525-533.
19. Perez MA, Grasa J, Garcia-Aznar JM, Bea JA, Doblare M (2006). Probabilistic analysis of the influence of the bonding degree of the stem-cement interface in the performance of cemented hip prostheses. *J Biomech* 39(10):1859-1872.
20. Rubin PJ, Rakotomanana RL, Leyvraz PF, Zysset PK, Curnier A, Heegaard JH (1993). Frictional interface micromotions and anisotropic stress distribution in a femoral total hip component. *J Biomech* 26(6):725-739.
21. Skripitz R, Aspenberg P (1999). Attachment of PMMA cement to bone: force measurements in rats. *Biomaterials* 20(4):351-356.

22. Spears IR, Pfeleiderer M, Schneider E, Hille E, Morlock MM (2001). The effect of interfacial parameters on cup-bone relative micromotions. A finite element investigation. *J Biomech* 34(1):113-120.
23. Van Rietbergen B, Weinans H, Huiskes R, Odgaard A (1995). A new method to determine trabecular bone elastic properties and loading using micromechanical finite-element models. *J Biomech* 28(1):69-81.
24. Verdonschot N, Huiskes R (1997). Cement debonding process of total hip arthroplasty stems. *Clin Orthop Relat Res* 336:297-307.
25. Verdonschot N, Huiskes R (1997). The effects of cement-stem debonding in THA on the long-term failure probability of cement. *J Biomech* 30(8):795-802.
26. Wirtz DC, Schiffers N, Pandorf T, Radermacher K, Weichert D, Forst R (2000). Critical evaluation of known bone material properties to realize anisotropic FE-simulation of the proximal femur. *J Biomech* 33(10):1325-1330.

ement

rights girl

Chapter 9

Summary and general discussion

In this thesis a number of fundamental and clinical aspects of cemented total hip arthroplasty (THA) reconstructions and their effect on failure were investigated, using finite element analysis (FEA) and experimental techniques. The goal was to contribute to an improved understanding of the complex interactions of mechanical processes playing a role in failure of cemented femoral components.

Implant design (Chapter 2)

In Chapter 2 we analyzed the effect of implant design variations on cement mantle failure by modeling the various designs of the Capital Hip system (3M Health Care Ltd, Loughborough, UK). The Capital Hip system was introduced in 1991, and included two different implant shapes (roundback vs. flanged) made of two different materials (titanium vs. stainless steel). The designs were assumed to be very similar to the well-performing Charnley implants (DePuy International, Leeds, UK), but it soon became clear that the Capital Hip implants produced inferior clinical results.^{20,24} Interestingly, an investigation of the Royal College of Surgeons of England showed differences between the clinical outcome of the various Capital Hip designs that were sold on the orthopaedic market.²⁹ We therefore simulated cement crack formation in reconstructions with the Capital Hip stems with the objective to investigate whether the various designs of the Capital Hip produced different crack patterns in the cement mantle.

Consistent with the findings of the Royal College of Surgeons of England,²⁹ our simulations demonstrated that the flanged Capital Hip design was inferior to the roundback design, and that the titanium-alloy

implants were inferior to the stainless-steel implants. Our analysis furthermore showed that the flanged Capital Hip designs had an inferior rotational stability, which was also found clinically.²⁴ These findings provide further validation for the custom-written FEA-based cement creep-damage algorithm that has been developed by our group.^{28,32}

Cementing philosophy (Chapter 3)

In Chapter 3 we investigated the effect of cementing philosophy on fatigue crack formation in the cement mantle. The research was initiated by reports on the so-called “French paradox”.^{13,14,26} The “French paradox” describes the phenomenon that two seemingly contradictory cementing philosophies can both lead to excellent clinical results. The first philosophy is based on the recommendations made by Charnley,^{3,5} and comprises the use of an undersized stem to obtain an intact cement mantle with a thickness of at least 2 mm. The second philosophy was developed by Kerboul, and comprises the use of a canal filling stem that is in contact with the surrounding bone, leading to a thin cement mantle with multiple defects.²⁶ In our FEA simulations we varied the cement mantle thickness and type of bone surrounding the cement mantle and analyzed the effect of these variations on implant stability and on fatigue crack formation in the cement. Consistent with Kerboul’s philosophy, we found that implant-bone contact of the large canal-filling stems ‘protects’ the cement and reduces fatigue crack formation, and that the use of a large stem improved the rotational stability of the reconstruction. Our simulations furthermore showed that a cement mantle supported by trabecular bone was inferior to a cement mantle supported by cortical bone. In the “French” technique this is achieved by removing most of the trabecular bone.^{23,27} When using an undersized stem, this can be achieved by applying cement pressurization during and after insertion of the femoral component^{6,7} and pressure lavage of the bone prior to cement insertion.^{2,12}

Cement porosity (Chapters 4 and 5)

Experimental investigations have shown that pores reduce the fatigue resistance of bone cement,^{10,15,22} caused by an elevated stress level near pores.³⁰ These findings have led to the general idea that cement porosity is detrimental for the longevity of cemented THA. Therefore, methods were developed to reduce bone cement porosity, such as vacuum mixing systems.^{16,18,33} However, the beneficial effect of vacuum mixing on the actual clinical outcome of THA has been questioned by several authors.^{8,17} In Chapter 4 of this thesis we tried to address this discrepancy by simulating fatigue failure in models of an experimental specimen and of a transversal slice of a cemented reconstruction with various levels of cement porosity. Our results showed that the introduction of pores caused elevated stress levels in experimental specimens, leading to early fatigue failure. In contrast, our simulations of the cemented reconstruction showed that the stress concentrations around pores in the cement mantle were small compared to the stress intensity at the crack tip. Consequently, pores had only a minor effect on the fatigue crack formation in the cemented reconstruction.

Although cement porosity is generally regarded as being detrimental for the fatigue resistance of bone cement, the actual effect of pores on fatigue crack formation in the cement mantle still remains unclear. For instance, microscopic fractographic analyses has revealed that pores may act both as crack initiators^{11,31} and as crack stoppers.^{25,31} In order to further elucidate the mechanical effect of pores on fatigue crack formation, FEA simulations were performed with models of cement mantles with different levels of microporosity and with a single large pore at different locations in the cement (Chapter 5).

Our simulations revealed that the effect of a pore on crack propagation was dependent on the location of the pore with respect to the stress concentration at the crack tip. When a pore was located directly on the crack path, it would accelerate the crack formation. When a pore was located a little further away from the crack, it could deviate the crack from its projected path. Located even further away, a pore would initiate a secondary crack and simultaneously decelerate the primary crack by dispersion of the crack propagating energy.

Although the findings of our simulations suggest that pores can also be beneficial under certain circumstances, in general the survival of cemented THA will be improved by minimizing the cement mantle porosity. Nonetheless, the various effects of pores on fatigue crack formation may further explain why the effect of pores is less clear in clinical studies than in laboratory experiments.

Cement-bone interface (Chapter 6 to 8)

Relatively little is known about anchorage of the cement mantle in the femoral bone. Research on the cement-bone interface has mainly been focused on the strength of the interface at a macroscopic, apparent level.^{1,12,19} In Chapter 6, the micro-mechanical behavior of the interface was investigated in laboratory experiments to establish the stiffness response of the cement-bone interface in tension and compression, and to gain insight in failure of the interface under a tensile load.

The results of the experimental study showed that both under tension and compression the cement-bone interface had a much lower stiffness than the cement or the bone. Previous studies have already shown that increasing the amount of cement-bone interdigitation improves the strength of the interface.^{9,19,21} The current study showed that also the stiffness of the interface is proportional to the cement-bone contact area. In addition, analysis of failure of the interface revealed that more damage occurred to the cement than to the bone.

In Chapter 7 an attempt was made to simulate the micro-mechanical response of the cement-bone interface using FEA. Ten models were created of specimens tested in Chapter 6, based on micro-computed tomography (μ CT) images. The FEA models included the morphology of the cement-bone interface and frictional contact surfaces at the interface.

The results of our simulations indicated that the μ FEA models of the cement-bone interface specimens

were able to reproduce stiffness values similar to those found in the experiments. There was, however, a weak correlation between the experimental and computational stiffness values in tension and compression. This was attributed to the fact that the FEA models were relatively coarse compared to the applied displacements.

In Chapter 8 we used a parametric approach to further investigate the micro-mechanical behavior of the interface. We analyzed the effect of frictional properties and adhesion on the micro-mechanical behavior of the cement-bone interface. We furthermore varied the cement-bone interface morphology, simulating inferior and optimal cement pressurization techniques, and investigated the effect of variations in cement stiffness.

Our results indicated that the micro-mechanical behavior is caused by a shape-closed interlock of cement and bone, rather than by adhesive properties of the cement. We furthermore found that the micro-mechanical behavior of the interface is extremely sensitive to interface morphology. Interface gaps resulted in a more compliant response, while increased cement penetration increased the cement-bone interface stiffness substantially. The interface stiffness was proportional to the cement stiffness, although variations of the cement stiffness had a much smaller effect than variations of the interface morphology.

References

1. Arola D, Stoffel KA, Yang DT (2006). Fatigue of the cement/bone interface: the surface texture of bone and loosening. *J Biomed Mater Res B Appl Biomater* 76(2):287-297.
2. Breusch SJ, Norman TL, Schneider U, Reitzel T, Blaha JD, Lukoschek M (2000). Lavage technique in total hip arthroplasty: jet lavage produces better cement penetration than syringe lavage in the proximal femur. *J Arthroplasty* 15(7):921-927.
3. Charnley J (1960). Anchorage of the femoral head prosthesis to the shaft of the femur. *J Bone Joint Surg [Br]* 42-B:28-30.
4. Charnley J (1961). Arthroplasty of the hip. A new operation. *Lancet* 1(7187):1129-1132.
5. Charnley J (1964). The bonding of prostheses to bone by cement. *J Bone Joint Surg [Br]* 46:518-529.
6. Davies JP, Harris WH (1993). In vitro and in vivo studies of pressurization of femoral cement in total hip arthroplasty. *J Arthroplasty* 8(6):585-591.
7. Dozier JK, Harrigan T, Kurtz WH, Hawkins C, Hill R (2000). Does increased cement pressure produce superior femoral component fixation? *J Arthroplasty* 15(4):488-495.
8. Geiger MH, Keating EM, Ritter MA, Ginther JA, Faris PM, Meding JB (2001). The clinical significance of vacuum mixing bone cement. *Clin Orthop Relat Res* 382:258-266.
9. Graham J, Ries M, Pruitt L (2003). Effect of bone porosity on the mechanical integrity of the bone-cement interface. *J Bone Joint Surg [Am]* 85(10):1901-1908.
10. Jasty M, Davies JP, O'Connor DO, Burke DW, Harrigan TP, Harris WH (1990). Porosity of various preparations of acrylic bone cements. *Clin Orthop Relat Res* 259:122-129.
11. Jasty M, Maloney WJ, Bragdon CR, O'Connor DO, Haire T, Harris WH (1991). The initiation of failure in cemented femoral components of hip arthroplasties. *J Bone Joint Surg [Br]* 73(4):551-558.
12. Krause WR, Krug W, Miller J (1982). Strength of the cement-bone interface. *Clin Orthop Relat Res* 163:290-299.
13. Langlais F, Howell JR, Lee AJ, Ling RS (2002). The "French paradox". *Hip International* 12(2):166-168.
14. Langlais F, Kerboul M, Sedel L, Ling RS (2003). The 'French paradox'. *J Bone Joint Surg [Br]* 85(1):17-20.
15. Lewis G (2003). Fatigue testing and performance of acrylic bone-cement materials: state-of-the-art review. *J Biomed Mater Res* 66B(1):457-486.
16. Lewis G, Nyman JS, Trieu HH (1997). Effect of mixing method on selected properties of acrylic bone cement. *J Biomed Mater Res* 38(3):221-228.
17. Ling RS, Lee AJ (1998). Porosity reduction in acrylic cement is clinically irrelevant. *Clin Orthop Relat Res* 355:249-253.
18. Macaulay W, DiGiovanni CW, Restrepo A, Saleh KJ, Walsh H, Crossett LS, Peterson MG, Li S, Salvati EA (2002). Differences in bone-cement porosity by vacuum mixing, centrifugation, and hand mixing. *J Arthroplasty* 17(5):569-575.
19. Mann KA, Ayers DC, Werner FW, Nicoletta RJ, Fortino MD (1997). Tensile strength of the cement-bone interface depends on the amount of bone interdigitated with PMMA cement. *J Biomech* 30(4):339-346.
20. Massoud SN, Hunter JB, Holdsworth BJ, Wallace WA, Juliusson R (1997). Early femoral loosening in one design of cemented hip replacement. *J Bone Joint Surg [Br]* 79(4):603-608.
21. Miller MA, Race A, Gupta S, Higham P, Clarke MT, Mann KA (2007). The role of cement viscosity on cement-

- bone apposition and strength: an in vitro model with medullary bleeding. *J Arthroplasty* 22(1):109-116.
22. Murphy BP, Prendergast PJ (2002). The relationship between stress, porosity, and nonlinear damage accumulation in acrylic bone cement. *J Biomed Mater Res* 59(4):646-654.
23. Postel M (1987). The routine operation. In: Postel M, Kerboull M, Evrard J, Courpied JP. Total hip replacement. Berlin, Germany: Springer Verlag; 26-33.
24. Ramamohan N, Grigoris P, Schmolz W, Chapell AM, Hamblen DL (2000). Early failure of stainless steel 3M Capital femoral stem. *J Bone Joint Surg [Br]* 82 (Suppl. 1):71.
25. Rimnac CM, Wright TM, McGill DL (1986). The effect of centrifugation on the fracture properties of acrylic bone cements. *J Bone Joint Surg [Am]* 68(2):281-287.
26. Scheerlinck T, de Mey J, Deklerck R, Noble PC (2006). CT analysis of defects of the cement mantle and alignment of the stem: in vitro comparison of Charnley-Kerboul femoral hip implants inserted line-to-line and undersized in paired femora. *J Bone Joint Surg [Br]* 88(1):19-25.
27. Scott G, Freeman MA, Kerboull M (2005). Femoral Components: The French Paradox. In: Breusch SJ, Malchau H. The Well-Cemented Total Hip Arthroplasty - Theory and Practice. Heidelberg, Germany: Springer Medizin Verlag; 249-253.
28. Stolk J, Verdonchot N, Murphy BP, Prendergast PJ, Huiskes R (2004). Finite element simulation of anisotropic damage accumulation and creep in acrylic bone cement. *Eng Fract Mech* 71:513-528.
29. The Royal College of Surgeons of England (2001). 3M Capital Hip system. The lessons learned from an investigation. The Royal College of Surgeons of England, London.
30. Timoshenko, S. P. and Goodier, J. N. (1970). Theory of elasticity. McGraw-Hill, New York.
31. Topoleski LD, Ducheyne P, Cuckler JM (1993). Microstructural pathway of fracture in poly(methyl methacrylate) bone cement. *Biomaterials* 14(15):1165-1172.
32. Verdonchot N, Huiskes R (1997). The effects of cement-stem debonding in THA on the long-term failure probability of cement. *J Biomech* 30(8):795-802.
33. Wang JS, Franzen H, Jonsson E, Lidgren L (1993). Porosity of bone cement reduced by mixing and collecting under vacuum. *Acta Orthop Scand* 64(2):143-146.

of - O's

to zcina

Chapter 10

Samenvatting en algemene discussie

Dit proefschrift beschrijft onderzoek naar een aantal fundamentele en klinische aspecten van de gecementeerde totale heupvervanging, waarbij gebruik gemaakt is van de eindige elementen methode (EEM) en experimentele technieken. Het doel van dit proefschrift was om meer inzicht te krijgen in de complexe interacties van mechanische processen die een rol spelen in het falen van gecementeerde implantaten.

Implantaat ontwerp (Hoofdstuk 2)

In Hoofdstuk 2 is onderzoek gedaan naar het effect van het ontwerp van een implantaat op het mechanisch falen van de cement mantel van een totale heupvervanging. Hiervoor zijn de verschillende ontwerpen van het Capital Hip Systeem (3M Health Care Ltd, Loughborough, UK) gemodelleerd. Het Capital Hip Systeem is in 1991 op de markt gekomen en bestond uit een serie implantaten met twee verschillende geometrieën ("roundback" en "flanged"), gemaakt van titanium of roestvrij staal. De ontwerpen leken sterk op de goed functionerende Charnley prothese (DePuy International, Leeds, UK), maar al snel werd duidelijk dat de Capital Hip implantaten klinisch inferieur waren.^{20,24} Een onderzoek van het Royal College of Surgeons of England toonde aan dat er onderlinge verschillen waren tussen de verschillende uitvoeringen van het Capital Hip systeem.²⁹ In Hoofdstuk 2 is in EEM modellen onderzocht of de verschillende ontwerpen tot verschillende scheurpatronen in het cement zouden leiden.

Overeenkomstig met de bevindingen van het Royal College of Surgeons of England²⁹ toonden onze

simulaties aan dat de “flanged” Capital Hip slechter presteerde dan het “roundback” ontwerp en dat de titanium implantaten tot slechtere resultaten leidden dan de implantaten van roestvrij staal. Daarnaast toonden onze resultaten aan dat het “flanged” ontwerp een slechtere rotatiestabiliteit had, wat eerder ook gevonden was een klinische studie.²⁴ De resultaten van deze studie bevestigen de validiteit van de cement-faalsimulatie die ontwikkeld is op het Orthopaedic Research Laboratory van het Universitair Medisch Centrum Sint Radboud.^{28,32}

Cementeringstechniek (Hoofdstuk 3)

In Hoofdstuk 3 is onderzoek gedaan naar het effect van cementeringstechniek op falen van de cement mantel. De studie is opgezet naar aanleiding van eerder onderzoek naar de zogenaamde “French paradox”.^{13,14,26} De “French paradox” beschrijft het fenomeen dat twee schijnbaar tegengestelde cementeringstechnieken beide kunnen leiden tot goede klinische resultaten. De eerste techniek is gebaseerd op de aanbevelingen van Charnley³⁻⁵ om een “undersized” implantaat te gebruiken, met het doel een intacte cement mantel met een minimale dikte van 2 mm te verkrijgen. De tweede techniek is ontwikkeld door Kerboull, waarbij gebruik gemaakt wordt van een kanaal-vullende steel die in contact is met het omliggende bot, wat juist leidt tot een dunne cementmantel met meerdere defecten.²⁶ In EEM simulaties is de dikte van de cement mantel en het type bot rondom de mantel gevarieerd, waarbij het effect op de implantaat stabiliteit en falen van de cement mantel is onderzocht.

Overeenkomstig met het concept van Kerboull vonden we dat het contact tussen implantaat en bot de cement mantel beschermd, wat leidde tot een vermindering van de scheurvorming in het cement en een verbeterde rotatie stabiliteit. Onze resultaten toonden verder aan dat een cement mantel ondersteund door trabeculair bot inferieur was aan een cement mantel ondersteund door corticaal bot. In de techniek ontwikkeld door Kerboull wordt hiervoor gezorgd door het trabeculair bot te verwijderen.^{23,27} Wanneer gebruik gemaakt wordt van een “undersized” implantaat kan dit bereikt worden door het bot schoon te spoelen^{2,12} en door het cement tijdens en na het inbrengen van het implantaat onder druk te zetten.^{6,7}

Cement porositeit (Hoofdstuk 4 en 5)

Experimentele studies hebben aangetoond dat poriën de sterkte van botcement verminderen,^{10,15,22} veroorzaakt door een verhoogd spanningsniveau rondom de poriën.³⁰ Deze bevindingen hebben geleid tot de algemene aanname dat cement porositeit nadelig is voor de levensduur van gecementeerde heupprothesen. Verschillende methoden zijn ontwikkeld om porositeit te reduceren, bijvoorbeeld door het mengen van cement onder een vacuüm.^{16,18,33} Sommige onderzoekers hebben echter vraagtekens gezet bij het voordeel van vacuümmengsystemen.^{8,17} In Hoofdstuk 4 van dit proefschrift zijn de verschillen tussen experimentele en klinische bevindingen onderzocht door falen van cement te simuleren in modellen van experimentele test specimens en in een model van een transversale schijf van een gecementeerde heupreconstructie. In deze modellen is de cementporositeit gevarieerd.

De resultaten toonden aan dat poriën verhoogde spanningen in experimentele test specimens veroorzaken, wat tot vervroegd falen leidt. In de modellen van een gecementeerde reconstructie waren de verhoogde spanningen rondom de poriën echter laag vergeleken met de belasting die de prothese op het cement uitoefende. Hierdoor hadden poriën een minimale invloed op de vorming van vermoeiingsscheuren in het cement.

Hoewel algemeen aangenomen wordt dat cement porositeit nadelig is voor de sterkte van botcement is het daadwerkelijke effect van poriën op de cement scheurvorming onduidelijk. Onderzoek op microscopisch niveau heeft aangetoond dat poriën kunnen functioneren als scheur initiators,^{11,31} maar dat ze er ook voor kunnen zorgen dat een scheur gestopt wordt.^{25,31} Om het effect van poriën op de scheurvorming in botcement verder te onderzoeken zijn EEM simulaties uitgevoerd in modellen van cement mantels met verschillende concentraties van microporiën en modellen met een enkele, grote porie op verschillende locaties in de cement mantel (Hoofdstuk 5).

De simulaties lieten zien dat het effect van een porie op de cement scheurvorming afhankelijk was van de locatie van de porie ten opzichte van spanningsconcentraties die veroorzaakt worden door scheuren in het cement. Wanneer een porie precies op het pad van de scheur lag, versnelde deze de scheurvorming. Wanneer een porie een stukje verwijderd was van de scheur, zorgde deze ervoor dat de loop van de scheur veranderd werd. Nog verder weg van de scheur initieerde een porie een tweede scheur en vertraagde tegelijkertijd de primaire scheur, door dispersie van de energie die benodigd is voor scheurvorming.

Hoewel deze bevindingen aantonen dat poriën onder sommige omstandigheden een positief effect kunnen hebben op de sterkte van botcement, zal in het algemeen de levensduur van gecementeerde heupreconstructies verbeteren door cement porositeit te minimaliseren. De resultaten van deze studie geven echter een mogelijke verklaring waarom het effect van porositeitreductie meer uitgesproken is in experimentele dan in klinische studies.

Cement-bot verbinding (Hoofdstuk 6 tot en met 8)

Er is relatief weinig bekend over de hechting van de cement mantel aan het omliggende bot. Onderzoek naar de sterkte van de cement-bot verbinding heeft zich met name gericht op de sterkte van de verbinding op een macroscopisch niveau.^{3,12,29} In Hoofdstuk 6 is experimenteel onderzoek gedaan naar het micro-mechanische gedrag van de cement-bot verbinding. Het doel was om de stijfheid te bepalen van de verbinding onder trek en druk en om inzicht te krijgen in het faalproces van de verbinding onder een trekbelasting.

De resultaten van de experimenten toonden aan dat zowel onder trek als druk de cement-bot verbinding een veel lagere stijfheid heeft dan het cement of het bot op zich. Eerdere studies hebben aangetoond dat het verhogen van penetratie van het cement in het bot de verbinding sterker maakt.^{9,19,21} De huidige studie heeft daarnaast aangetoond dat ook de stijfheid van de verbinding proportioneel is aan de mate

van cement penetratie in het bot. Ten slotte toonde analyse van specimens aan dat er bij falen van de verbinding meer schade optreedt in het cement dan in het bot.

In Hoofdstuk 7 is het micro-mechanische gedrag van de cement-bot verbinding gesimuleerd in EEM analyses. Hiervoor zijn tien modellen gemaakt van specimens die getest zijn in Hoofdstuk 6, gebruik makende van micro-computed tomography (μ CT) scans. In de modellen is de lokale morfologie van de cement-bot verbinding gemodelleerd, waarbij wrijving op de verbinding tussen cement en bot is gesimuleerd.

De resultaten wezen uit dat de EEM modellen in staat waren om een stijfheid te reproduceren die gelijk was aan de experimentele waarden. De correlatie tussen de experimentele en EEM waarden onder trek en druk was echter zwak, waarschijnlijk veroorzaakt doordat de modellen relatief grof waren in vergelijking tot de opgelegde verplaatsingen.

In Hoofdstuk 8 is door middel van een parametrische aanpak het micro-mechanische gedrag van de cement-bot verbinding verder onderzocht. In EEM modellen is het effect van wrijving, adhesie en variaties van morfologie en cement materiaaleigenschappen op de stijfheid van de verbinding bestudeerd.

De resultaten toonden aan dat het micro-mechanische gedrag van de cement-bot verbinding veroorzaakt wordt door een vormgesloten verbinding van cement en bot, in plaats van adhesie van het cement aan het bot. Het micro-mechanische gedrag van de verbinding bleek gevoelig te zijn voor variaties in de morfologie. Het simuleren van spleten in de verbinding resulteerde in een reductie van de stijfheid, terwijl bij een verhoogde penetratie van het cement in het bot de stijfheid substantieel toenam. De stijfheid van de verbinding was proportioneel met de stijfheid van het cement, hoewel variaties van de materiaaleigenschappen van het cement een veel kleinere invloed hadden dan variaties van de morfologie.

References

1. Arola D, Stoffel KA, Yang DT (2006). Fatigue of the cement/bone interface: the surface texture of bone and loosening. *J Biomed Mater Res B Appl Biomater* 76(2):287-297.
2. Breusch SJ, Norman TL, Schneider U, Reitzel T, Blaha JD, Lukoschek M (2000). Lavage technique in total hip arthroplasty: jet lavage produces better cement penetration than syringe lavage in the proximal femur. *J Arthroplasty* 15(7):921-927.
3. Charnley J (1960). Anchorage of the femoral head prosthesis to the shaft of the femur. *J Bone Joint Surg [Br]* 42-B:28-30.
4. Charnley J (1961). Arthroplasty of the hip. A new operation. *Lancet* 1(7187):1129-1132.
5. Charnley J (1964). The bonding of prostheses to bone by cement. *J Bone Joint Surg [Br]* 46:518-529.
6. Davies JP, Harris WH (1993). In vitro and in vivo studies of pressurization of femoral cement in total hip arthroplasty. *J Arthroplasty* 8(6):585-591.
7. Dozier JK, Harrigan T, Kurtz WH, Hawkins C, Hill R (2000). Does increased cement pressure produce superior femoral component fixation? *J Arthroplasty* 15(4):488-495.
8. Geiger MH, Keating EM, Ritter MA, Ginther JA, Faris PM, Meding JB (2001). The clinical significance of vacuum mixing bone cement. *Clin Orthop Relat Res* 382:258-266.
9. Graham J, Ries M, Pruitt L (2003). Effect of bone porosity on the mechanical integrity of the bone-cement interface. *J Bone Joint Surg [Am]* 85(10):1901-1908.
10. Jasty M, Davies JP, O'Connor DO, Burke DW, Harrigan TP, Harris WH (1990). Porosity of various preparations of acrylic bone cements. *Clin Orthop Relat Res* 259:122-129.
11. Jasty M, Maloney WJ, Bragdon CR, O'Connor DO, Haire T, Harris WH (1991). The initiation of failure in cemented femoral components of hip arthroplasties. *J Bone Joint Surg [Br]* 73(4):551-558.
12. Krause WR, Krug W, Miller J (1982). Strength of the cement-bone interface. *Clin Orthop Relat Res* 163:290-299.
13. Langlais F, Howell JR, Lee AJ, Ling RS (2002). The "French paradox". *Hip International* 12(2):166-168.
14. Langlais F, Kerboull M, Sedel L, Ling RS (2003). The 'French paradox'. *J Bone Joint Surg [Br]* 85(1):17-20.
15. Lewis G (2003). Fatigue testing and performance of acrylic bone-cement materials: state-of-the-art review. *J Biomed Mater Res* 66B(1):457-486.
16. Lewis G, Nyman JS, Trieu HH (1997). Effect of mixing method on selected properties of acrylic bone cement. *J Biomed Mater Res* 38(3):221-228.
17. Ling RS, Lee AJ (1998). Porosity reduction in acrylic cement is clinically irrelevant. *Clin Orthop Relat Res* 355:249-253.
18. Macaulay W, DiGiovanni CW, Restrepo A, Saleh KJ, Walsh H, Crossett LS, Peterson MG, Li S, Salvati EA (2002). Differences in bone-cement porosity by vacuum mixing, centrifugation, and hand mixing. *J Arthroplasty* 17(5):569-575.
19. Mann KA, Ayers DC, Werner FW, Nicoletta RJ, Fortino MD (1997). Tensile strength of the cement-bone interface depends on the amount of bone interdigitated with PMMA cement. *J Biomech* 30(4):339-346.
20. Massoud SN, Hunter JB, Holdsworth BJ, Wallace WA, Juliusson R (1997). Early femoral loosening in one design of cemented hip replacement. *J Bone Joint Surg [Br]* 79(4):603-608.
21. Miller MA, Race A, Gupta S, Higham P, Clarke MT, Mann KA (2007). The role of cement viscosity on cement-

- bone apposition and strength: an in vitro model with medullary bleeding. *J Arthroplasty* 22(1):109-116.
22. Murphy BP, Prendergast PJ (2002). The relationship between stress, porosity, and nonlinear damage accumulation in acrylic bone cement. *J Biomed Mater Res* 59(4):646-654.
23. Postel M (1987). The routine operation. In: Postel M, Kerboull M, Evrard J, Courpied JP. Total hip replacement. Berlin, Germany: Springer Verlag; 26-33.
24. Ramamohan N, Grigoris P, Schmolz W, Chapell AM, Hamblen DL (2000). Early failure of stainless steel 3M Capital femoral stem. *J Bone Joint Surg [Br]* 82 (Suppl. 1):71.
25. Rimnac CM, Wright TM, McGill DL (1986). The effect of centrifugation on the fracture properties of acrylic bone cements. *J Bone Joint Surg [Am]* 68(2):281-287.
26. Scheerlinck T, de Mey J, Deklerck R, Noble PC (2006). CT analysis of defects of the cement mantle and alignment of the stem: in vitro comparison of Charnley-Kerboul femoral hip implants inserted line-to-line and undersized in paired femora. *J Bone Joint Surg [Br]* 88(1):19-25.
27. Scott G, Freeman MA, Kerboull M (2005). Femoral Components: The French Paradox. In: Breusch SJ, Malchau H. The Well-Cemented Total Hip Arthroplasty - Theory and Practice. Heidelberg, Germany: Springer Medizin Verlag; 249-253.
28. Stolk J, Verdonchot N, Murphy BP, Prendergast PJ, Huiskes R (2004). Finite element simulation of anisotropic damage accumulation and creep in acrylic bone cement. *Eng Fract Mech* 71:513-528.
29. The Royal College of Surgeons of England (2001). 3M Capital Hip system. The lessons learned from an investigation. The Royal College of Surgeons of England, London.
30. Timoshenko, S. P. and Goodier, J. N. (1970). Theory of elasticity. McGraw-Hill, New York.
31. Topoleski LD, Ducheyne P, Cuckler JM (1993). Microstructural pathway of fracture in poly(methyl methacrylate) bone cement. *Biomaterials* 14(15):1165-1172.
32. Verdonchot N, Huiskes R (1997). The effects of cement-stem debonding in THA on the long-term failure probability of cement. *J Biomech* 30(8):795-802.
33. Wang JS, Franzen H, Jonsson E, Lidgren L (1993). Porosity of bone cement reduced by mixing and collecting under vacuum. *Acta Orthop Scand* 64(2):143-146.

across

mechanical

Chapter 11

Computational modeling of total hip arthroplasty: past, present and future

In this thesis computational modeling techniques based on finite element analysis (FEA) were employed to investigate several aspects of cemented total hip arthroplasty (THA). FEA has been introduced into orthopaedic research several decades ago to investigate the mechanics of THA, and has been applied to study a wide range of mechanical aspects. At our group, the Orthopaedic Research Laboratory of the Radboud University Nijmegen Medical Centre, FEA techniques have been introduced in the early 1980's, when Rik Huiskes started investigating stress distributions of joint reconstructions through linear elastic analyses.^{14,16,17} Gradually, the FEA models became more complex. In the field of cemented THA, Nico Verdonschot started investigating the effect of cement creep and debonding of the implant-cement interface in the early 1990's,^{55,56,60} followed by the simulation of cement creep and fatigue damage in THA.^{57,59} The FEA-based creep-damage simulation was further developed by Jan Stolk,^{52,57} and validated against experimental tests.⁵⁰ Further validation of the simulation against clinical data has shown that the algorithm was also able to differentiate between the clinical survival of various implant designs.⁴⁹

One can ask the question whether there is still a need for computational pre-clinical research, considering the excellent survival rates of current THA procedures.^{12,34,43} Unfortunately, not all implants that are being introduced to the orthopaedic market are as successful.^{2,53} Furthermore, patients are undergoing THA at an increasingly younger age, and the patient population is becoming more active. These factors increase the likelihood of revision surgery,^{3,7,31,35} and stress the need for implants with a superior survival. Research on the mechanics of THA in younger, more active patients may increase the life-span of cemented hip

reconstructions, thereby reducing the need for revision surgery. In addition, recently more conservative implants have been developed, such as hip resurfacing^{19,46,48} and metaphyseal implants.^{23,45} These conservative implants have the aim to preserve bone stock to improve the survival of subsequent revision surgery using a standard hip implant, after failure of the primary reconstruction. However, as these implants have a much smaller fixation area, their factor of safety against mechanical failure is relatively small. Since currently there is a lack of long-term survival data on these new conservative implants, they need to be tested extensively in a pre-clinical phase to ensure that the desired improvements are achieved and that the implants introduce no additional adverse effects. In this phase numerical simulations provide excellent tools to test these implants against known failure scenarios.

There is often discussion about the added value of computational analysis in the field of orthopaedic research. An important reason for this is that biomechanical aspects of cemented reconstructions are usually studied in simplified, rather abstract models, while *in vivo* these aspects are interrelated with clinical and biological phenomena that are not or cannot be captured by the models. In addition, FEA models generally study a limited number of cases, making the results only valid for the specific situation that is analyzed. Of course with increased computational power, advancing numerical skills and improved input data FEA models could be upgraded to capture a wider variety of biological and clinical variables. However, the actual strength and beauty of numerical simulation lies in the fact that one can isolate and study the effect of one parameter, while keeping all other variables constant. In a clinical setting this is virtually impossible, which is the reason why clinical studies need to cover large patient populations and require long follow-up times. And even then some variables that influence the lifetime of a reconstruction cannot be filtered out. On the other hand, numerical studies could not exist on their own, since they need clinical studies for validation purposes. So in fact, numerical and clinical studies complement each other, rather than that only one of them contains the truth.

Evidently, there is still room for improvement of the predictive power of FEA simulations in orthopaedic research, despite the highly sophisticated numerical techniques that exist nowadays. One of the main issues holding back the predictive power is a lack of data that serves as input for the models, or as validation for the outcomes of FEA analyses.

An example of a case where input data is lacking is the creep-damage simulation that was applied in several studies of the current thesis. The algorithm uses creep and fatigue data of only one type of bone cement, whereas other types of cement might have different properties, that may affect failure of a reconstruction differently. Furthermore, clinical validation is hard as little is known about how the cement failure process evolves over time in real reconstructions. Attempts have been made to follow failure of *in vitro* reconstructions, using for example acoustic techniques,²¹ translucent bone cement,²⁹ or by sectioning reconstructions at different moments in time.⁵⁰ However, data from *in vivo* reconstructions

is not available.

Another example of a case where input data is lacking is the simulation of implant-cement interface debonding. From clinical studies it is known that the implant-cement interface debonds over time.²⁴ FEA simulations have studied this debonding process,^{40,42,56,57} but several assumptions have to be made about the interface properties and how these degrade due to repetitive loading. Furthermore, validation of these predictions is hard as, like in the cement creep-damage simulation, clinical data is lacking about how the debonding process evolves over time. Only the end stage of a completely debonded stem is known from retrievals and post-mortem cases.

Conversely, in the current work we have tried to improve input data on one particular aspect: the micro-mechanical response of the bone-cement interface. Chapter 6 of this thesis presented experimental data on the micro-mechanics of the cement-bone interface. Such information is extremely valuable for computational modeling of cemented THA, since until recently research on the cement-bone interface was mostly performed to determine the strength on a more apparent, macroscopic level.^{1,5,8,9,25} The micro-mechanical model as described in this thesis has highlighted the appearance of a thin compliant layer between the cement and bone, thereby making the interface not solidly bonded as generally assumed in FEA studies.^{20,49} We are currently expanding the experimental work on the cement-bone interface to characterize its micro-mechanical response to shear and fatigue loading. This information can subsequently be implemented in FEA models of cemented femoral reconstructions, in order to further improve the quality of the analyses.

In judging the value of FEA predictions it is important to note that FEA studies only test implants against the failure scenario that is implemented in the simulation. The simulations are based on known failure scenarios that are observed clinically. This directly implies that an FEA simulation will never capture new failure scenarios or ones that arise unforeseen. An implant may be optimized against one failure scenario by FEA techniques, but it may still introduce new failure scenarios *in vivo*.^{18,24} However, an elaborate pre-clinical testing phase using FEA-based techniques will dramatically reduce the risks involved in marketing a new implant, and may provide information that otherwise could not be obtained.

The analysis of the Capital Hip case (Chapter 2) provides an excellent example of how FEA simulations could have reduced the risk of marketing a new implant design, but also that FEA is not able to capture all failure scenarios. By means of FEA pre-clinical testing we showed that changing the implant material from steel to titanium and updating the flange design would increase the risk of inferior *in vivo* behavior. It would clearly have been worthwhile to have this information in a pre-clinical stage. However, an additional feature of the titanium Capital Hip stems was that these had a higher surface roughness than the stainless steel stems,⁵³ and produced more bone cement particles. Therefore, reconstructions with these implants may have been more sensitive to failure due to inflammatory, osteolytic reactions to these particles, causing mechanical degradation of the femoral bone.²⁵ The particulate reaction failure scenario was,

however, not included in the simulation. A simulation of abrasive wear of the cement mantle would enable further differentiation between the various Capital Hip designs than was already achieved in this work. However, no algorithm currently exists for simulating this failure scenario.

Another example is presented by Chapter 4, in which the effect of vacuum mixing on cement fatigue resistance was investigated in an experimental and clinical setting. Our study focused on differences in the cement stress distribution to explain why the benefit of vacuum mixing is difficult to demonstrate in clinical studies.³² Consequently, our analyses demonstrated that a local stress intensity overruled the effect of a higher level of porosity in the clinical situation, explaining why vacuum mixing did not postpone fatigue failure. However, we assumed that vacuum mixing led to cement porosity reduction, which may be a questionable assumption. Experiments have shown that when cement is forced to polymerize in a constrained environment, polymerization shrinkage induces the formation of cement pores.¹⁰ Since cement test specimens are usually allowed to polymerize in an unconstrained manner, vacuum mixing leads to extremely low porosity in such specimens.^{30,33,62} In contrast, the *in vivo* polymerizing cement mantle is constrained by the implant and the femoral bone surrounding the cement mantle. Consequently, the *in vivo* level of porosity is not reduced as effectively as expected by vacuum mixing,³⁶ which may provide an alternative explanation why the beneficial effect of vacuum mixing is more difficult to demonstrate clinically.

Despite its shortcomings, FEA has contributed tremendously to expanding the knowledge in orthopaedics. For example, FEA studies have attributed to the basic understanding of total hip replacement, they have provided guidelines for prosthetic design and have led to introduction of surgical techniques that were shown to improve the survival of cemented femoral hip reconstructions.

An example of the contributions to the basic understanding of THA is the development of algorithms that simulate failure scenarios. Such algorithms have provided insight in failure of THA by simulating the actual process of mechanical degradation of the reconstruction; processes that could not be studied otherwise. Studies utilizing these algorithms have provided information of the process of crack formation in the cement mantle,⁵² and have demonstrated the mechanisms of load transfer from the cement mantle to the bone (Chapter 8). In addition, FEA simulations have provided knowledge on the failure processes of uncemented THA, and on how load transfer from prosthesis to bone takes place.^{54,63,64}

The added value of computational modeling for prosthetic design has been demonstrated in pre-clinical tests, in which it was shown why some designs are more prone to failure than others. For instance, such studies have shown that sharp edges should be avoided in prosthetic designs⁴⁹ and that rough surfaces should be avoided in subsiding implants.⁵⁸ Furthermore, this thesis and other studies^{22,38,47} showed that titanium implants that have a rather slim design are not suitable for cemented THA, and why a particular implant design that is very similar to a successful predecessor does not necessarily guarantee clinical success (Chapter 2). For uncemented implants FEA has provided information on the effect of implant design on

stress shielding and subsequent bone remodelling.^{63,64} These findings illustrate that computational studies are very suitable for evaluation of implant designs in a pre-clinical phase, before a clinical trial is started.

The value of FEA for the evaluation of surgical techniques was demonstrated in Chapter 3 of this thesis, in which it was investigated how cementing techniques affect cement fatigue and implant stability. In addition, Chapter 8 demonstrated the importance of cement pressurization for the fixation of the cement mantle within the femoral bone, and Chapter 4 provided an explanation why vacuum mixing is not as effective in the clinical situation. Others have reported on the effect of surgical technique (cemented or uncemented) on peri-prosthetic remodelling,⁶ and on the effect of the implant positioning on bone and cement stresses.²⁶ Similar to the implant design, the mechanical consequences of an alternative surgical technique can be evaluated using FEA.

Finally, FEA has identified patient factors that may affect the mechanical behavior of total hip reconstructions. For instance, it has been demonstrated that inferior bone quality may lead to more cement mantle damage⁵⁷ and increased implant migration.^{13,57} In addition, variations in patient activity patterns also affect cement mantle failure⁵¹ and the primary stability of uncemented implants.³⁹

Several recent developments may contribute to improve the predictive power of current models even further. These include developments in computational hardware, but also the development of new numerical techniques, such as so-called probabilistic and patient-specific models.

Throughout history, FEA simulations have explored the boundaries of computational hardware to optimize calculations. These boundaries have shifted gradually with the development of newer, faster and smaller workstations. One of the first FEA studies investigating the intramedullary fixation of THA (1976) consisted of 42 elements.⁴ Around this time, workstations such as the CRAY-1 that were used to perform calculations were enormous machines that weighed 5,500 kg and were equipped with a separate cooling system. In comparison, the largest model in this thesis consisted of approximately 800,000 elements, and was run on a workstation not much larger than a standard personal computer. In order to further illustrate the advances in computational power, currently, the fastest machine in the world is about four million times faster than the CRAY-1 system of the early 1970's. Hence, further developments of computational hardware hold major potential for the field of computational biomechanics.

A computational approach that is relatively new to orthopaedics is the use of probabilistic models. Probabilistic models offer the possibility to include variations of several aspects such as bone quality and anatomy, sizing, orientation and position of the implant in the femoral cavity, degree of implant-cement bonding and the loading configuration.^{11,37,42,61} Inclusion of parametric variations of several aspects affecting failure of cemented hip reconstructions should make the FEA predictions more comprehensive, robust and reliable. However, one should realize that the quality of predictions does not improve by including a wider range of variables when the validity of the underlying model is poor. In addition, despite the promising results of probabilistic analyses, it is still necessary to validate these techniques through experimental and

clinical studies.

Another development in the area of FEA-based pre-clinical testing of THA is the introduction of patient-specific models. The objective of patient-specific modeling is to choose a type and size of implant that would lead to the best clinical performance for a specific patient, based on FEA predictions. Results of one particular study²⁸ showed that patient-specific FEA models were able to differentiate between migration patterns of THA reconstructions of well-functioning patients and patients who had revision surgery. It was furthermore shown that in reconstructions of patients who underwent revision surgery more fatigue crack formation was predicted compared to non-revised patients. These findings illustrate the predictive power of FEA for patient-specific pre-clinical testing. A similar approach has also been used for the development of a patient-specific pre-clinical tests for uncemented hip reconstructions, based on the primary stability of the implant within the bone.^{27,44}

An advantage of patient-specific models is that with the development of navigation systems for orthopaedic surgery the findings of such simulations theoretically could be implemented directly in the operating theatre. In computer assisted surgery (CAS) the patient, instruments and implant are equipped with markers that are tracked by a navigation system. During the operation the surgeon is instructed such that the desired implant position is obtained. Thus, by using CAS, besides the optimal implant type and size, also the optimal position would be ensured in the operating theatre, which eventually should lead to an optimal implant survival. The application of this technology may become more relevant in the future for the implantation of smaller implants that have a reduced factor of (mechanical) safety, and are therefore more sensitive to inadequate placement.

Over the past decades, computational biomechanical analysis has proven itself as a valuable tool for investigation of the effects of issues related to implant design, surgical technique and patient characteristics on the mechanical behavior of cemented femoral reconstructions. A few of such studies have been presented in this thesis. Promising developments in various fields of computational biomechanics may further improve the predictive power and applicability of current computational modeling techniques.

References

1. Arola D, Stoffel KA, Yang DT (2006). Fatigue of the cement/bone interface: the surface texture of bone and loosening. *J Biomed Mater Res B Appl Biomater* 76(2):287-297.
2. Barrack RL (2000). Early failure of modern cemented stems. *J Arthroplasty* 15(8):1036-1050.
3. Barrack RL, Mulroy RD, Jr., Harris WH (1992). Improved cementing techniques and femoral component loosening in young patients with hip arthroplasty. A 12-year radiographic review. *J Bone Joint Surg [Br]* 74(3):385-389.
4. Bartel DL (1977). The calculation of stresses in bone-prosthesis structures. In: Walker PS. *Human Joints and their Artificial Replacements*. Springfield, IL: Charles C. Thomas; 440-448.
5. Bean DJ, Convery FR, Woo SL, Lieber RL (1987). Regional variation in shear strength of the bone-polymethylmethacrylate interface. *J Arthroplasty* 2(4):293-298.
6. Behrens BA, Bougoucha A, Nolte I, Meyer-Lindenberg A, Stukenborg-Colsman C, Pressel T (2008). Strain adaptive bone remodelling: influence of the implantation technique. *Stud Health Technol Inform* 133:33-44.
7. Bizot P, Banallec L, Sedel L, Nizard R (2000). Alumina-on-alumina total hip prostheses in patients 40 years of age or younger. *Clin Orthop Relat Res* 379:68-76.
8. Dohmae Y, Bechtold JE, Sherman RE, Puno RM, Gustilo RB (1988). Reduction in cement-bone interface shear strength between primary and revision arthroplasty. *Clin Orthop Relat Res* 236:214-220.
9. Funk MJ, Litsky AS (1998). Effect of cement modulus on the shear properties of the bone-cement interface. *Biomaterials* 19(17):1561-1567.
10. Gilbert JL, Hasenwinkel JM, Wixson RL, Lautenschlager EP (2000). A theoretical and experimental analysis of polymerization shrinkage of bone cement: A potential major source of porosity. *J Biomed Mater Res* 52(1):210-218.
11. Grasa J, Perez MA, Bea JA, Garcia-Aznar JM, Doblare M (2005). A probabilistic damage model for acrylic cements. Application to the life prediction of cemented hip implants. *Int J Fatigue* 27(8):891-904.
12. Havelin LI, Engesaeter LB, Espehaug B, Furnes O, Lie SA, Vollset SE (2000). The Norwegian Arthroplasty Register: 11 years and 73,000 arthroplasties. *Acta Orthop Scand* 71(4):337-353.
13. Hsu JT, Chang CH, Huang HL, Zobitz ME, Chen WP, Lai KA, An KN (2007). The number of screws, bone quality, and friction coefficient affect acetabular cup stability. *Med Eng Phys* 29(10):1089-1095.
14. Huiskes R (1980). Stress analyses of implanted orthopaedic joint prostheses for optimal design and fixation. *Acta Orthop Belg* 46(6):711-727.
15. Huiskes R (1993). Failed innovation in total hip replacement. Diagnosis and proposals for a cure. *Acta Orthop Scand* 64(6):699-716.
16. Huiskes R, Chao EY (1983). A survey of finite element analysis in orthopedic biomechanics: the first decade. *J Biomech* 16(6):385-409.
17. Huiskes R, Nunamaker D (1984). Local stresses and bone adaption around orthopedic implants. *Calcif Tissue Int* 36 Suppl 1:S110-S117.
18. Huiskes R, Verdonschot N, Nivbrant B (1998). Migration, stem shape, and surface finish in cemented total hip arthroplasty. *Clin Orthop Relat Res* 355:103-112.
19. Itayem R, Arndt A, Nistor L, McMin D, Lundberg A (2005). Stability of the Birmingham hip resurfacing arthroplasty at two years. A radiostereophotogrammetric analysis study. *J Bone Joint Surg [Br]* 87(2):158-162.

20. Jeffers JR, Browne M, Lennon AB, Prendergast PJ, Taylor M (2007). Cement mantle fatigue failure in total hip replacement: experimental and computational testing. *J Biomech* 40(7):1525-1533.
21. Jeffers JR, Browne M, Taylor M (2005). Damage accumulation, fatigue and creep behaviour of vacuum mixed bone cement. *Biomaterials* 26(27):5532-5541.
22. Jergesen HE, Karlen JW (2002). Clinical outcome in total hip arthroplasty using a cemented titanium femoral prosthesis. *J Arthroplasty* 17(5):592-599.
23. Karatosun V, Unver B, Gunal I (2008). Hip arthroplasty with the thrust plate prosthesis in patients of 65 years of age or older: 67 patients followed 2-7 years. *Arch Orthop Trauma Surg* 128(4):377-381.
24. Karrholm J, Nivbrandt B, Thanner J, Anderberg C (2000). Radiostereometric evaluation of hip implant design and surface finish - Micromotion of cemented femoral stems. Transactions of the 67th annual meeting of the American Academy of Orthopaedic Surgeons, Orlando, FL, USA .
25. Kim DG, Miller MA, Mann KA (2004). Creep dominates tensile fatigue damage of the cement-bone interface. *J Orthop Res* 22(3):633-640.
26. Kleemann RU, Heller MO, Stoeckle U, Taylor WR, Duda GN (2003). THA loading arising from increased femoral anteversion and offset may lead to critical cement stresses. *J Orthop Res* 21(5):767-774.
27. Lengsfeld M, Burchard R, Gunther D, Pressel T, Schmitt J, Leppke R, Griss P (2005). Femoral strain changes after total hip arthroplasty--patient-specific finite element analyses 12 years after operation. *Med Eng Phys* 27(8):649-654.
28. Lennon AB, Britton JR, MacNiocaill RF, Byrne DP, Kenny PJ, Prendergast PJ (2007). Predicting revision risk for aseptic loosening of femoral components in total hip arthroplasty in individual patients--a finite element study. *J Orthop Res* 25(6):779-788.
29. Lennon AB, McCormack BAO, Prendergast PJ (2003). The relationship between cement fatigue damage and implant surface finish in proximal femoral prostheses. *Med Eng Phys* 25(10):833-841.
30. Lewis G, Nyman JS, Trieu HH (1997). Effect of mixing method on selected properties of acrylic bone cement. *J Biomed Mater Res* 38(3):221-228.
31. Lewthwaite SC, Squires B, Gie GA, Timperley AJ, Ling RS (2008). The Exeter Universal hip in patients 50 years or younger at 10-17 years' followup. *Clin Orthop Relat Res* 466:324-331.
32. Ling RS, Lee AJ (1998). Porosity reduction in acrylic cement is clinically irrelevant. *Clin Orthop Relat Res* 355:249-253.
33. Macaulay W, DiGiovanni CW, Restrepo A, Saleh KJ, Walsh H, Crossett LS, Peterson MG, Li S, Salvati EA (2002). Differences in bone-cement porosity by vacuum mixing, centrifugation, and hand mixing. *J Arthroplasty* 17(5):569-575.
34. Malchau H, Herberts P, Eisler T, Garellick G, Soderman P (2002). The Swedish Total Hip Replacement Register. *J Bone Joint Surg [Am]* 84 Suppl 2:2-20.
35. McAuley JP, Szuszczewicz ES, Young A, Engh CA, Sr. (2004). Total hip arthroplasty in patients 50 years and younger. *Clin Orthop Relat Res* 418:119-125.
36. Messick KJ, Miller MA, Damron LA, Race A, Clarke MT, Mann KA (2007). Vacuum-mixing cement does not decrease overall porosity in cemented femoral stems: an in vitro laboratory investigation. *J Bone Joint Surg [Br]* 89(8):1115-1121.
37. Nicoletta DP, Thacker BH, Katoozian H, Davy DT (2006). The effect of three-dimensional shape optimization on the probabilistic response of a cemented femoral hip

- prosthesis. *J Biomech* 39(7):1265-1278.
38. Pabinger C, Kroner A, Lange A, Eyb R (2004). Cemented titanium stems show high migration: transprosthetic drainage system has no advantage over third-generation cementation technique. *Arch Orthop Trauma Surg* 124(7):489-494.
39. Pancanti A, Bernakiewicz M, Viceconti M (2003). The primary stability of a cementless stem varies between subjects as much as between activities. *J Biomech* 36(6):777-785.
40. Perez MA, Garcia JM, Doblare GM (2005). Analysis of the debonding of the stem-cement interface in intramedullary fixation using a non-linear fracture mechanics approach. *Eng Fract Mech* 72(8):1125-1147.
41. Perez MA, Garcia-Aznar JM, Doblare M, Seral B, Seral F (2006). A comparative FEA of the debonding process in different concepts of cemented hip implants. *Med Eng Phys* 28(6):525-533.
42. Perez MA, Grasa J, Garcia-Aznar JM, Bea JA, Doblare M (2006). Probabilistic analysis of the influence of the bonding degree of the stem-cement interface in the performance of cemented hip prostheses. *J Biomech* 39(10):1859-1872.
43. Puolakka TJ, Pajamaki KJ, Halonen PJ, Pulkkinen PO, Paavolainen P, Nevalainen JK (2001). The Finnish Arthroplasty Register: report of the hip register. *Acta Orthop Scand* 72(5):433-441.
44. Reggiani B, Cristofolini L, Varini E, Viceconti M (2007). Predicting the subject-specific primary stability of cementless implants during pre-operative planning: preliminary validation of subject-specific finite-element models. *J Biomech* 40(11):2552-2558.
45. Rohrl SM, Li MG, Pedersen E, Ullmark G, Nivbrant B (2006). Migration pattern of a short femoral neck preserving stem. *Clin Orthop Relat Res* 448:73-78.
46. Schmalzried TP (2007). Why total hip resurfacing. *J Arthroplasty* 22(7 Suppl 3):57-60.
47. Scholl E, Eggli S, Ganz R (2000). Osteolysis in cemented titanium alloy hip prosthesis. *J Arthroplasty* 15(5):570-575.
48. Steffen RT, Pandit HP, Palan J, Beard DJ, Gundle R, Lardy-Smith P, Murray DW, Gill HS (2008). The five-year results of the Birmingham Hip Resurfacing arthroplasty: AN INDEPENDENT SERIES. *J Bone Joint Surg [Br]* 90(4):436-441.
49. Stolk J, Janssen D, Huiskes R, Verdonschot N (2007). Finite element-based preclinical testing of cemented total hip implants. *Clin Orthop Relat Res* 456:138-147.
50. Stolk J, Maher SA, Verdonschot N, Prendergast PJ, Huiskes R (2003). Can finite element models detect clinically inferior cemented hip implants? *Clin Orthop Relat Res* 409:138-150.
51. Stolk J, Verdonschot N, Huiskes R (2002). Stair Climbing is More Detrimental to the Cement in Hip Replacement than Walking. *Clin Orthop Relat Res* 405:294-305.
52. Stolk J, Verdonschot N, Murphy BP, Prendergast PJ, Huiskes R (2004). Finite element simulation of anisotropic damage accumulation and creep in acrylic bone cement. *Eng Fract Mech* 71:513-528.
53. The Royal College of Surgeons of England (2001). 3M Capital Hip system. The lessons learned from an investigation. The Royal College of Surgeons of England, London.
54. Turner AW, Gillies RM, Sekel R, Morris P, Bruce W, Walsh WR (2005). Computational bone remodelling simulations and comparisons with DEXA results. *J Orthop Res* 23(4):705-712.
55. Verdonschot N, Huiskes R (1995). Dynamic creep behavior of acrylic bone cement. *J Biomed Mater Res* 29(5):575-581.

56. Verdonschot N, Huiskes R (1997). Cement debonding process of total hip arthroplasty stems. *Clin Orthop Relat Res* 336:297-307.
57. Verdonschot N, Huiskes R (1997). The effects of cement-stem debonding in THA on the long-term failure probability of cement. *J Biomech* 30(8):795-802.
58. Verdonschot N, Huiskes R (1998). Surface roughness of debonded straight-tapered stems in cemented THA reduces subsidence but not cement damage. *Biomaterials* 19(19):1773-1779.
59. Verdonschot N, Tanck E, Huiskes R (1998). Effects of prosthesis surface roughness on the failure process of cemented hip implants after stem-cement debonding. *J Biomed Mater Res* 42(4):554-559.
60. Verdonschot NJ, Huiskes R, Freeman MA (1993). Pre-clinical testing of hip prosthetic designs: a comparison of finite element calculations and laboratory tests. *Proc Inst Mech Eng [H]* 207(3):149-154.
61. Viceconti M, Brusi G, Pancanti A, Cristofolini L (2006). Primary stability of an anatomical cementless hip stem: a statistical analysis. *J Biomech* 39(7):1169-1179.
62. Wang JS, Franzen H, Jonsson E, Lidgren L (1993). Porosity of bone cement reduced by mixing and collecting under vacuum. *Acta Orthop Scand* 64(2):143-146.
63. Weinans H, Huiskes R, Grootenboer HJ (1992). Effects of material properties of femoral hip components on bone remodeling. *J Orthop Res* 10(6):845-853.
64. Weinans H, Huiskes R, Grootenboer HJ (1994). Effects of fit and bonding characteristics of femoral stems on adaptive bone remodeling. *J Biomech Eng* 116(4):393-400.

Acknowledgements

Een groot aantal mensen heeft bijgedragen aan de totstandkoming van dit proefschrift. Deze mensen wil ik daarvoor graag bedanken.

Allereerst mijn promotor. Beste Nico, ik beschouw het als een eer om als eerste bij je te mogen promoveren. Het is ondertussen meer dan 10 jaar geleden dat ik voor het eerst bij je stage kwam lopen, toen ik nog op de HTS zat. Tijdens die stage is mijn interesse voor biomedische werktuigbouwkunde gewekt. Jouw aanstekelijke enthousiasme heeft eraan bijgedragen dat ik uiteindelijk besloot verder te studeren aan de UT, om uiteindelijk weer terug te keren bij het ORL.

Ik kan me iedere keer weer verbazen over je analytisch vermogen. Wanneer we bijvoorbeeld tijdens een congres naar een praatje zitten te luisteren, weet jij altijd wel een vraag te verzinnen, die vervolgens ook nog eens ergens op slaat ook. Die scherpe analytische blik heeft mij erg geholpen om er zelf ook een te ontwikkelen.

Nico, ik denk dat je samen met Pieter een mooi lab op poten gezet hebt, waar werk van hoogwaardige kwaliteit afgeleverd wordt en waar tegelijkertijd een geweldige werksfeer heerst. Ik denk dat die sfeer voor een groot gedeelte te danken is aan jullie instelling en inzet. Bedankt.

Jan, jij was vooral betrokken bij het begin van mijn promotietraject. Tijdens mijn stage bij jou heb ik veel geleerd over biomechanisch onderzoek en je hebt me wegwijs gemaakt in de eindige elementen wereld van MARC. Toen ik begon met onderzoek naar gecementeerde heupprothesen kwam daar ook nog eens het programmeren in Fortran bij; iets waarmee ik eigenlijk tijdens mijn hele opleiding bijna niets te maken had gehad. Jouw gestructureerde werkwijze heeft me enorm geholpen om dit allemaal snel onder de knie te krijgen. Daarnaast heb ik erg veel van je geleerd over het schrijven van een wetenschappelijke publicatie: "...ik snap wel wat je hier probeert te vertellen, maar zo staat het er niet...". Bedankt voor al je hulp en adviezen.

Dear Ken, I will never forget the time Judith, Stef and I spent in Syracuse. I learned more from that experience than I ever could have imagined. The collaboration between our departments has resulted in great research, and I'm pleased some parts of the project were included in this thesis. On a more linguistic note, you introduced me to the world of colloquialisms, vocabulary and Alabama speech (which I will never master, I'm afraid...).

We want to thank you, Marcie and Caroline for your hospitality and generosity. Moving to another country, even only for a short time, is quite an experience, especially with a three-months old Stef. Nonetheless, you made us feel at home right from the start. Even when I managed to get my bike stolen on the first day in Syracuse (which is quite an accomplishment for someone Dutch). Thank you.

Graag wil ik alle leden van de manuscriptcommissie, Stan Gielen, Stefaan Bergé, Ruud Geesink, Timo Meinders en Dick Stegeman, bedanken voor het beoordelen van mijn manuscript.

Geachte Dr. Scheerlinck, beste Thierry. Ik had nooit eerder een orthopedisch chirurg ontmoet die kon programmeren in MatLab! Onze samenwerking heeft uiteindelijk geleid tot twee artikelen, waarvan er één opgenomen is in dit proefschrift. De combinatie van jouw klinische blik en onze biomechanische instelling levert iedere keer weer verfrissende ideeën op. Ik ben daarom ook erg blij dat we onze samenwerking nog voort kunnen zetten. Bedankt!

Willem, ik geloof niet dat er in dit proefschrift onderzoek beschreven staat waaraan we samen gewerkt hebben. Dat wil echter niet zeggen dat ik de uurtjes die we samen in de kelder doorgebracht hebben niet waardeer! Het lijkt wel of er met jou in de buurt geen technische problemen zijn die niet opgelost kunnen worden. Bedankt voor je hulp bij experimenten en voor de gezellige gesprekken!

René, bedankt voor het draaiende houden van workstations die op het punt staan om te crashen, en voor de vele programma's die ik gebruik heb tijdens het 'ouderwets' bouwen van een mesh.

Ineke, ik heb nog steeds een brief in de la liggen die je me ooit geschreven hebt omdat je het zo sneu voor me vond dat ik nooit post kreeg. Bedankt voor je betrokkenheid, je inzet, maar vooral voor de gezelligheid.

Ik wil mijn huidige en ex-kamergenoten, Gerjon, René, Esther en Miranda bedanken voor alle gesprekken over onderzoek, statistiek en schrijven in een 'second language', maar ook over muziek en muzieksmaak (of het gebrek eraan), kinderen en opvoeding (of het gebrek eraan), sport en sportiviteit (of het gebrek eraan), films en quotes. Daarnaast wil ik jullie bedanken voor het aanhoren van mijn grappen, of ze nou goed waren of niet (en of jullie nou wilden of niet). Ik beloof aan de kwaliteit (en kwantiteit) te werken.

Ook wil ik graag alle overige (ex)collega's van het ORL bedanken: Chantal, Chris, Daan, Eric, Erwin, Huub, Jantien, Jasper, Jorrit, Leon, Liesbeth, Loes, Luc, Marco, Maria, Marieke, Marloes, Maud en Natasja.

Uiteraard wil ik ook alle stagiairs bedanken die ik de afgelopen jaren heb mogen begeleiden: Mark, René (Hoofdstukken 2 en 5!), Martijn & Ruud, Patrick, Roland, Pieter, Jantien (Hoofdstuk 3!), Loes, Daan, Sylvain en Jeroen. Het was iedere keer weer een bijzondere ervaring om jullie te mogen begeleiden.

Thanks to Mark , Amos, Fred, Levi, Nat, Joe, Matthew and all at the orthopedic department of SUNY Upstate Medical University for their hospitality during my time at the lab. I very much enjoyed the lab barbecue and game of volleyball!

And a special word of thanks to the lady who arranged practically everything for our trip to the USA. Stephanie, I never knew there was so much that has to be taken care of when visiting another country, especially when you are travelling with your wife and son. Thank you for all your help!

Martine en Freek, Marjolein, Ronald, Marjan en Cas, Koos en Kathelijne, Jeroen, Teun en Iris: bedankt voor jullie vriendschap.

En dan de paranimfen, Gerjon en Wibo. Ik ben blij en trots dat jullie als paranimfen naast me willen staan op deze bijzondere dag. Bedankt.

Pap, mam, Erwin en Martine, Tiny en Leonne, Karin en Luuk. Bedankt voor jullie interesse. Ik hoop dat het allemaal een beetje duidelijk geworden is waar ik nou de afgelopen 6-7 jaar mee bezig ben geweest. Nu is het tijd voor het langverwachte feestje!

Judith, Stef en....? Werk is leuk, maar thuiskomen is nog veel leuker. Ik kan er soms met mijn pet niet bij hoe geweldig ik het heb met jullie, en hoeveel ik van jullie hou. Bedankt.

About the author

Dennis Janssen was born on April 7 1977 in 's-Hertogenbosch. He grew up in Schijndel, were attended secondary school at the "Skinle College". After getting his VWO certificate, he started studying mechanical engineering at the "Hogeschool 's-Hertogenbosch" in 1995. During this study he did a traineeship at the Orthopaedic Research Laboratory, in those days known as the "Sectie Biomechanica" of the orthopaedics department of the Radboud University Nijmegen Medical Centre. His supervisor during this traineeship was Nico Verdonshot. The assignment was to explore the possibility to measure acetabular cup wear from radiographs, which entailed spending many hours staring at a video screen in a small, dark room (next to the copier). Nonetheless, he became interested in biomechanics. Therefore, after obtaining his bachelor degree he decided to go to the Twente University for a master study of mechanical engineering, with a specialization in biomedical engineering. During his final year he did a masters assignment, again at the Orthopaedic Research Lab, under supervision of Jan Stolk and Nico Verdonshot. The assignment was to simulate the capsule surrounding the human hip joint in a finite element model. After finishing the assignment and obtaining his masters degree, he was offered a PhD position at the Orthopaedic Research Lab in 2002. His research focused on failure mechanisms of cemented total hip arthroplasty. In 2007 he was given the opportunity to visit the lab of Kenneth Mann at the SUNY Upstate Medical University in Syracuse, with whom a collaboration was started funded by the US National Institutes of Health. Eventually, about 7 years of research resulted in several scientific publications, presentations at national and international conferences, and this thesis. Dennis is currently working as a postdoctoral researcher at the Orthopaedic Research Laboratory. He lives in Nijmegen with his wife Judith and son Stef, and is expecting an additional family member in June 2009.

macro- and

micro-mechanics of

total cemented

hip arthroplasty

Benjamin J. van